Experimental Effects of Low Octane Primary Reference Fuels on Burn Rates and Phasing Limits in a Homogeneous Charge Compression Ignition Engine with Negative Valve Overlap

by

Luke Monroe Hagen

A dissertation submitted in partial fulfillment
of the requirements for the degree of
Doctor of Philosophy
(Mechanical Engineering)
in The University of Michigan
2014

Doctoral Committee:

Provost Dionissios N. Assanis, Co-Chair, Stony Brook University
Professor Margaret S. Wooldridge, Co-Chair
Professor Andre L. Boehman
Associate Research Scientist Stani V. Bohac
Professor James F. Driscoll
Research Scientist George A. Lavoie

Time is one of the few things man cannot influence. We all have

a desire to create something that will show we were here. That

we did something of value.

— Ferry Porsche

Acknowledgments

The number of people who have contributed this work are too numerous to list without omission, but I wish to specifically thank the following people for their significant involement.

I would first like to thank Dennis Assanis, for it was he who convinced me to pursue a Ph.D. here at the University of Michigan. Later, both George Lavoie and Margaret Wooldridge took an active role in my work and I am thankful for their support and guidance.

Throughout the entire duration of my time at the UM Autolab, I have been thankful for the support and camaraderie of all my co-workers here in the UM Autolab. This has truly been the best group of graduate students and research scientists at the University of Michigan.

I would like to thank my family for their support ever since I moved to Michgan to pursue my Ph.D. It's been a long journey, and I'm thankful they have alway been there.

Last, but most certainly not least, I want to thank my fiancée and soon to be wife, Heather, for her unfailing support and patience during this incredibly busy time. This degree is truly not just mine, but ours.

Preface

The following work was supported in part by the U.S. Department of Energy under contract DOE-EE0000203, "A University Consortium on Efficient and Clean High Pressure Lean Burn (HPLB) Engines."

Table of Contents

List of Tables

List of Figures

List of Abbreviations

η_{th} thermal efficiency

γ ratio of specific heats

ϕ 'fuel-to-air' equivalence ratio

ϕ' 'fuel-to-charge' equivalence ratio

10_M–90   CA10 main event to CA90 burn duration

10–90   CA10 to CA90 burn duration

CA   crank angle

CA10   10% MFB crank angle location

$CA10_M$ CA10 for main event w/o LTHR

CA50   50% MFB crank angle location

CA90   90% MFB crank angle location

CAD   crank angle degree

COV   coefficient of variation

DAQ   data acquisition system

EGR   exhaust gas recirculation

EVO/EVC   exhaust valve opening/closing

FFVA   fully-flexible valve actuation

HC   hydrocarbon emissions

HCCI   homogeneous charge compression ignition

$IMEP_g$ gross indicated mean effective pressure

$IMEP_n$ net indicated mean effective pressure

IVO/IVC   intake valve opening/closing

LHV   Lower Heating Value

MFB   mass fraction burned

NH40   Fuel blend, gasoline with 40% (by mass) n-heptane

NO_x oxides of nitrogen

NVO   negative valve overlap

PID   Proportional Integral Derivative

PRF   Primary Reference Fuel

PRF40   PRF, 40% iso-octane, 60% n-heptane

PRF60   PRF, 60% iso-octane, 40% n-heptane

PRR   pressure rise rate

RGF   residual gas fraction

RI   ringing intensity

RoHR   rate of heat release

SACI   spark assisted compression ignition

SCTE   Single cylinder test engine

SI   spark ignition

TDC   top dead center

TWC   three-way catalyst

c_p constant pressure specific heat capacity

eEGR external EGR

iEGR internal EGR

ATDC after top dead center

BTDC before top dead center

Abstract

Homogeneous charge compression ignition (HCCI) remains an active area of engine research, promising to deliver high thermal efficiency while producing low levels of nitrogen oxides (NOx) and particulate emissions. The pre-mixed auto-ignition nature of HCCI allows the use of a wide variety of fuels, including fuels with lower octane number (ON) than traditional gasoline spark-ignited engines. A method to achieve HCCI traps high levels of internal exhaust gas residuals (iEGR) which introduce thermal and compositional gradients. The contributions in this work compare fuel effects on burn rates and phasing limits of low ON primary reference fuels (PRFs) to gasoline, separating the effects of fuel from iEGR effects.

Specifically, in this study, increased load limits were demonstrated for a low ON fuel, but changes in composition obfuscated fuel effects. A new experimental method was therefore developed which isolated composition effects across wide levels of iEGR. Using this method, gasoline at fixed combustion phasing was shown to exhibit sensitivity to increasing iEGR with burn rates decreasing by 15% compared to the lowest iEGR case. Examining the effect of iEGR on stability limits demonstrated iEGR increased cyclic variability due to cyclic feedback.

Further experiments showed burn rates of the primary reference fuel PRF40 were 35% faster than gasoline at equal iEGR, but PRF40 showed no dependence on iEGR. PRF40 required a reduced IVC temperature compared to gasoline, which could reduce thermal gradients and increase burn rates. Increased phasing limits were consistently demonstrated for PRF60 compared to gasoline as iEGR was reduced. Both PRF40 and PRF60 demonstrated increasing levels of low temperature heat release (LTHR) as engine speed was reduced, and at 1000 rpm PRF60 showed no phasing dependence on iEGR.

Compared to gasoline, observed differences in behavior for the low ON PRFs are attributed to enhanced non-Arrhenius ignition delay behavior which is understood to reduce sensitivity to thermal gradients (or iEGR) and cyclic variations in temperature.

The results of this study are the first to isolate charge composition effects during HCCI operation, and the results provide important quantitative insight into the relative importance of thermal stratification and chemical effects of fuels and iEGR.

Chapter 1

Introduction

1.1 Motivation for Engine Research

On September 27, 1908 the first Model T left Henry Ford's factory, to be followed by 15 million more. An unassuming car with a 20 hp 4 cylinder engine, its low price and durability revolutionized how people and goods were transported not just in America, but the world over. Until the success of the Model T, the "Horseless Carriage" was a mere curiosity; the horse-drawn carriage was the means by which people, goods and mail were transported. Propelled in part on the success of the Model T, the automobile has transitioned from a novelty for the rich to become a necessity of modern living — with some 250 million automobiles on American roads as of 2010 [1]. While many great societal advances can be attributed to the advent of the automobile, perhaps its greatest contribution has been the freedom of personal mobility, as noted by David E. Davis, Jr. [2]:

> We drive cars because they make us free. With cars, we need not wait in airline terminals, or travel only where the railway tracks go. Governments detest our cars: they give us too much freedom. How do you control people who can climb into a car at any hour of the day or night and drive to who knows where?

Over 100 years following the Model T's auspicious debut, that freedom is still predominately powered, like the Model T, by the internal combustion engine (ICE). The continued reliance of the automobile on the ICE has brought with it many unintended consequences. The most significant of these are exhaust emissions and fuel consumption concerns, both of which are discussed below in more detail. The predominance of IC engines is due to many factors, notably the high energy density of liquid fuels allowing for

1

long vehicle range and fast refills, and the fact that ICEs are a mature technology and cost significantly less than the latest battery electric technology. Hybrid vehicles (e.g. Toyota Prius) have improved drive cycle efficiently by coupling an internal combustion engine with an electric drivetrain, but pure electric vehicles have yet to gain widespread acceptance; battery technology has yet to develop to the point where range and cost are competitive with the internal combustion engine.

In the 2011 State of the Union Address President Obama had decreed for there to be one million electric vehicles on the road by 2015 [3], but less than a year later had already backed off of this goal. The current goal for electric vehicles was outlined by the Department of Energy in 2013 [4] and focuses on making electric vehicles as affordable as average gasoline cars today, highlighting again the primary hurdle to EV implementation - the cost of an EV that can match an ICE powered vehicle in range and performance.

The automobile and its freedoms are now firmly established in our modern living, and the ICE remains an integral part of the automobile. While improvements in automobile efficiency are being investigated in every aspect, from aerodynamics to gear friction, the challenge approached herein is to mitigate the drawbacks of the ICE while maintaining the functionality that has enabled its success over the last 100 years.

1.1.1 Regulated Tailpipe Emissions

Two thousand miles away from Detroit and the Model T's birthplace, the city of Los Angeles was by the late 1940s suffering the consequences of large-scale automobile adoption and facing significant air quality concerns. The so-called "smog" problem was becoming a significant health concern: respiratory problems and burning eyes were the most obvious symptoms stemming from exposure to the brown haze hanging over the city. In the early post-war period, the causes of smog were not immediately known; the moniker smog itself is a portmanteau of "smoke" and "fog" as it was once assumed the combination of the two produced the haze. Two separate air control districts were established (the South Coast Air

Quality Management District in 1946 and the Los Angeles County Air Pollution Control District in 1947) and aimed regulation at the petroleum industry and banned outside burning — no regulation was sought for automobiles and consequently little progress was made in air quality improvement [5].

Gradually, scientific study of the problem determined that smog constituted neither smoke nor fog, but corresponded to the production of ozone, formed by the photochemical reaction of oxides of nitrogen in the presence of hydrocarbons. This was first reported by Haagen-Smit in 1952 [6]. The discovery originated due to the fact that the presence of ozone was known to lead to cracking in vulcanized rubber and a study noted the accelerated deterioration of rubber in the Los Angeles area. Haagen-Smit further noted that

> Estimates, as well as actual measurements, have shown that from 1000 to 2000 tons of hydrocarbons are released daily into the Los Angeles atmosphere through evaporative losses in manufacture and distribution of petroleum products and through incomplete combustion, chiefly from automobiles. Combustion processes add nitrogen oxides at a rate of 200 to 300 tons daily to the air.

Thus, the first direct link had been made between automobile exhaust emissions and smog, or air pollution. Armed with this knowledge, the California government began to directly approach the concerns of automobile exhaust, with the Bureau of Air Sanitation formed in 1955 and the Motor Vehicle Pollution Control Board in 1960. The latter was responsible for emissions control devices and mandated the first emissions control device in the U.S. with the requirement of Positive Crankcase Ventilation in 1961 (implemented in 1963). Then in 1966 the Motor Vehicle Pollution Control Board mandated, for all vehicles sold in California, allowable hydrocarbon and carbon monoxide limits over a defined driving cycle — the first instance of regulation on allowable tailpipe emissions. The two aforementioned agencies were combined in 1968 to form the Air Resources Board, now the California Air Resources Board (CARB).

Along a parallel path, the Federal Government signed into effect in 1963 the Clean Air Act. This was amended in 1965 to include in its scope the regulation of automobile

Table 1.1 Historical U.S. Passenger Car Tailpipe Emissions Standards

Species[g/mi]	1970	1975	1981	Tier 2 Bin 5
NO_X	4.1	3.1	1.0	0.05
CO	34	15	9.0	3.4
NMOG/HC	4.1	1.5	0.41	0.075

emissions. Following the lead of California, the Federal Government essentially adopted the 1966 California emissions requirements and mandated them for the remaining 49 states starting with the 1968 model year [5]. In part to enforce the Clean Air Act amended again in 1970, the Environmental Protection Agency was officially formed on December 1, 1970. From this point forward the EPA would develop Federal Emissions standards that would vary from (and were usually less stringent) CARB regulation. The fact that CARB regulated tailpipe emissions before the Federal Government has given them a legal precedence that allows them to petition for waivers and apply their own standards separate from the Federal Government and the EPA.

Since emissions standards were first implemented, the allowable levels for all species have declined by at least an order of magnitude. The challenge moving forward is to maintain or reduce these allowed emissions while increasing efficiency. A comparison of emission level standards since 1970 are presented in Table 1.1, the data for 1970 and 1975 from Mondt [5], noting that 1975 marked the introduction of the catalytic converter to most automobiles in US, and 1981 marked the introduction of the three-way catalyst (TWC). Tier 2 Bin 5 [7] is representative of the fleet average for light duty vehicles as of the end of 2013, but even stricter Tier 3 proposals are forthcoming [8, 9] for 2017.

1.1.2 Fuel Economy and CO_2 Emissions

As a nation, the United States has developed a strong dependence on oil to meet its energy needs. According to the US Energy Information Administration [10], transportation in all forms accounts for 29% of the US energy consumption, and 94% of this energy is supplied

from petroleum based products. Nearly 20 million barrels of oil are consumed *per day*, with 71% (roughly 13 million barrels as of 2009) for transportation. This demand for oil, coupled with the increased demand of economically developing nations, specifically the BRIC (Brazil, India, Russia and China) countries, has seen a significant increase in the price of fuel over the past few years.

Prior to 1973, the price of gasoline in the United States had remained, inflation adjusted, relatively low throughout most of the post-war period [11]. During this period of post-war boom, both vehicle size and engine displacement had continued to increase. The OAPEC oil embargo of 1973 suddenly constrained the supply of gasoline, resulting in a shortage that immediately brought about desires of smaller, more fuel efficient vehicles. American automakers in particular were hit hardest by this sudden shift in demand, with General Motors responding by spending a then unprecedented 15 billion to downsize its entire car range, starting with the full-size models in 1977 and the intermediates in 1978 [12]. The second oil crisis, brought about by the Iranian revolution of 1979 continued the trend of downsized automobiles that continued into the 1980s by all of the Big Three. Following the second oil crisis, gasoline prices then demonstrated a 20 year gradual decline after the second oil crisis. In fact, the average price of gasoline in the U.S. in 1998 was, adjusted for inflation, the historical low [11]. During this period, consumers gradually shifted back to larger vehicles, brought about largely with the increase in popularity of SUVs in the 1990s.

The concept of peak oil — the time at which daily production of oil is maximizes and will only continue to then decline — was thought to have been reached by the end of the first decade of the 21st century. By 2005 the continued demand from the developed world, coupled with dramatic increases from developing nations such as China and India had driven oil prices to record highs and the supply in the middle east as maximum capacity [13]. However, instead of the panic that was anticipated, increased oil prices led the oil industry to heavily invest in hydraulic fracturing, commonly known as "fracking" in the United States, bringing U.S. petroleum production to its highest level since 1989 [14]. At the same time,

with memories of high gas prices still recent, and ever increasing fuel economy standards reducing consumption, consumer oil consumption decreased to a 16 year low in 2012 [15]. The combined effect of increased production and reduced consumer consumption have projections that predict the U.S. could be a net oil exporter by 2025 [16].

While supply of oil, at least as far as the U.S. is concerned, is not an immediate problem, the environmental ramifications of fracking are still unknown, so a reduction in consumption of oil is of great environmental consequence in terms of the production of oil and as well as consumption. Concerns over consumption relate, in addition to regulated tailpipe emissions, to the impact of green house gases (GHGs) on climate change, specifically as it relates to CO_2 and global warming. In the past decade the majority of the science community has accepted the position of the Intergovernmental Panel on Climate Change, as reiterated in the Bali Action Plan from the 13th session of the United Nations Framework Convention on Climate Change [17], that "warming of the climate system is unequivocal, and that delay in reducing emissions significantly constrains opportunities to achieve lower stabilization levels and increases the risk of more severe climate change."

Related to the goals of the IPCC, the United States, under the Obama administration [18], has for the first time taken direct action to regulate CO_2 emissions. The National Highway and Traffic Safety Administration (NHTSA), which administers Corporate Average Fuel Economy (CAFE) standards, and the EPA have passed regulation for the 2017 - 2025 model years (MY), jointly regulating to harmonize fuel economy and GHG emissions standards [19]. The collaboration is due to the fact that the NHTSA regulates CAFE standards while the EPA regulates emission standards, which in this case is CO_2 and now considered a GHG by the EPA. As CO_2 is a direct by-product of complete combustion of fossil fuels, the CAFE and GHG standards must be harmonized such that the allowed fuel consumption matches the allowed GHG emissions. The EPA's new regulation states that "over the lifetimes of the vehicles sold in MYs 2017-2025 standards, this program is projected to save approximately 4 billion barrels of oil and reduce GHG emissions by

6

2 billion metric tons" [19]. Furthermore, the EPA states "car CO_2 emission levels are projected to increase in stringency from 212 to 143 grams per mile (g/mi) between MYs 2017 and 2025. Similarly, fleet-wide CO_2 emission levels for trucks are projected to increase in stringency from 295 in MY 2017 to 203 g/mi in MY 2025. EPA projects that the average light vehicle (combined car and truck) tailpipe CO_2 compliance level in MY 2017 will be 243 g/mi, phasing down by MY 2025 to 163 g/mi, corresponding to 54.5 mpg in MY 2025 if all reductions were made through fuel economy improvements". While CAFE credits are explicitly given to hybridization in the new standards, the increase in overall vehicle efficiency required dictates that improvements in ICE efficiency will play a major role in meeting the challenge.

It has become readily apparent that the world faces a future that will be significantly more frugal with regards to petroleum consumption, due both to the environmental impacts of new methods of extracting the remaining oil reserves, and concerns over the potentially negative impact that the production of CO_2, via burning fossil fuels, has on the environment. Yet future legislation pending in the U.S. and abroad is requiring even higher fuel efficiency and lower emissions. The challenge then, for automobiles, is improving the efficiency of the ICE to reduce both fuel consumption and CO_2 emissions while maintaining the size and features consumers will purchase.

1.2 Combustion Modes and Fuels

Historically, ICEs have fallen into two distinct categories: spark-ignited (SI) gasoline fueled engines, and compression-ignited (CI) diesel fueled engines. Each have utilized fuels optimized for the specific mode of combustion. Low Temperature Combustion (LTC) is a concept for a mode of combustion that seeks to couple the benefits of both SI and CI engines, and it has been approached with both modified SI and CI engines. LTC engines can operate with a wide range of fuels depending on the specific application, and this document

will further investigate fuel chemistry effects on LTC performance.

1.2.1 Spark Ignited Engines and Fuels

A spark ignited engine utilizes a spark plug to generate a spark, at a prescribed timing, in a flammable mixture of fuel and air. The spark creates a flame kernel which expands and ideally consumes the entire charge of air and fuel, leaving products of combustion. The fuel and air are premixed, either in the intake runner port or in-cylinder (via early direct injection). To control load, the intake charge is throttled at low and part loads, reducing the amount of energy inducted in each cycle. Throttling losses are one of the primary inefficiencies of SI engines, as most of the time SI engines are operated at part load and suffer the pumping losses of the throttle.

Since the ignition control method for SI engines is the timing of the spark, preignition of the mixture (ignition prior to spark) can lead to excessive pressure rise rates and end gas knock, both of which are potentially detrimental to engine components. A consequence of this is that the compression ratios of SI engines have historically been significantly lower than those of CI engines to prevent preignition and knock. While this is necessary for practical SI engines, it comes at the cost of thermal efficiency.

To control emissions, as mentioned in Section 1.1.1, the primary emissions control device on SI engines is the three way catalyst (TWC). The TWC, combined with electronic closed-loop engine control, has proven a commercial success in reducing reducing SI exhaust emissions to regulated levels. A TWC derives its name from the fact that it simultaneously reduces the three primary pollution constituents: NO_X, CO, and HC. A requirement to successful TWC operation is the air/fuel ratio (A/F) remaining within ± 0.2 of stoichiometric [5]. Operation lean of stoichiometric provides efficiency gains (further discussed in Section 1.2.3) but control and/or reduction of NO_X emissions requires dedicated NO_X devices.

The predominant fuel for SI engines since their widespread adoption in the early 20th

Century has been gasoline. Most gasolines are a mixture of aromatics, olefins, naphthenes, oxygenates (in regions where ethanol is blended with gasoline) and paraffins [20]. The Model T previously mentioned had a compression ratio (CR) of 4:1 to ensure safe operation on the low anti-knock quality gasoline of the day. Improving the anti-knock quality of the gasoline to improve compression ratio and efficiency was desirable almost immediately, and in 1929 the octane scale and octane number for rating gasoline anti-knock quality were introduced [20].

The gasoline octane rating is based on two tests: the Research Octane Number (RON) and Motor Octane Number (MON). These tests are performed on a Cooperative Fuel Research (CFR) engine, which is a port fuel injected single cylinder engine with variable compression ratio. The RON test is performed at 600 rpm with an intake temp of 52°C [21], while the MON is performed at 900 rpm with an intake temperature of 149°C [22]. For each test, a fuel is operated at a prescribed spark timing and the CR adjusted until the onset of knock. The blend of iso-octane and n-heptane that has the same compression ratio for onset of knock of the test fuel prescribes the RON or MON of the fuel with 100% iso-octane being 100 RON and/or MON and 100% n-heptane being 0 RON and/or MON. Due to this test, iso-octane and n-heptane are referred to as Primary Reference Fuels (PRFs). In the United States, the reported octane rating at fueling stations is the average of the RON and MON, also known as the Anti-Knock Index (AKI). For example, a fuel having a RON of 100 and a MON of 90 would have an AKI of 95. Typical standard grade gasoline in the U.S. has an AKI of 87.

As the conditions of the RON and MON test are not the same, practicals fuels exhibit a RON and MON that do not match the same PRF blend (e.g. an 87 AKI gasoline with a RON = 90 and a MON = 84). The arithmetic difference between RON and MON has historically been referred to as the octane sensitivity, S, of the fuel. Paraffin fuels, and n-heptane in particular, have well documented so-called negative temperature coefficient behavior [23]. Within the negative temperature coefficient region, a reduced temperature

9

leads to shortened ignition delay time. Leppard [24] demonstrated that the paraffinic nature and NTC behavior of n-heptane and iso-octane blends is the source of octane sensitivity for most refinery gasoline fuels, as these fuels contain olefins and aromatics which do not exhibit NTC behavior. There are other ramifications of the NTC behavior of paraffin PRF fuels, which are developed in Section 5.4.

1.2.2   Compression Ignition Engines and Fuels

Compression Ignition (CI) engines are commonly known as diesel engines due to the name of the inventor, Rudolf Diesel, and the class of petroleum fuels used for them also bear his name. CI engines operate by injecting a high pressure, highly ignitable fuel into the combustion chamber near top dead center, at which point the ambient conditions are at high pressure and temperature. The fuel ignites almost immediately upon injection, in a highly stratified manner, resulting in a diffusion burn. Combustion timing is controlled by the timing of the fuel injection event. Since autoignition of the fuel is required (unlike with SI engines), the compression ratio of typical CI engines is much higher than that of SI engines, providing a thermal efficiency benefit.

Compared to SI engines, CI engines operate unthrottled, or with very little throttle (some throttling is now employed to create a small pressure differential to help induct EGR), as the throttle is not required for load control; load is controlled solely by the amount of fuel injected. Due to this, CI engines operate lean of stoichiometric for most operating conditions. The lack of throttling at part load, coupled with higher compression ratios and lean operation gives diesel engines efficiency benefits over SI engines.

While CI engines exhibit greater efficiencies than SI engines, the primary drawbacks are particulate and NO_X emissions. The formation of particulates are a consequence of the stratified diffusion burning of the fuel in the combustion process, a problem not shared with SI engines due to their premixed nature. Secondly, CI engines suffer from high NO_X emissions due to high combustion temperatures. Whereas SI engines use a TWC

to successfully treat NO_X emissions, the lean equivalence ratio operation of CI engines precludes that option. Dedicated particulate and NO_X traps are being implemented, but add considerable cost to the powertrain as a whole compared to an SI engine with a TWC.

Fuels for CI engines, generally classified as diesel fuel, are comprised of the same general group of compounds as gasoline, but at different levels. In general, diesel fuels have higher aromatics and less paraffins compared to gasoline. The standard ignition quality test for diesel fuels is the Cetane Test [25], also performed in a CFR engine but modified for CI use with a precombustion chamber. The cetane number (CN) of a fuel is defined by the volume fraction of reference fuels n–cetane and heptamethyl nonane (HMN) whose ignition characteristics match those of the test fuel. The Cetane tests comprises the range of cetane number from 0 – 100, but practical fuels fall in the range of 30 – 65 [25].

It is worth noting that the octane scale for gasoline quantifies resistance to auto-ignition and as such a fuel of *lower* ignitability has a *higher* octane number. Conversely, the cetane scale for diesel fuel quantifies the ignitability of the fuel, and as such a fuel of *lower* ignitability has a *lower* cetane number. The scales are not directly inverted, but n-heptane (0 on the octane scale) has an approximate CN of 56 [26], while 87 AKI gasoline has an approximate cetane of 13 [27].

1.2.3   Low Temperature Combustion

Within the realm of engine research, the means of accomplishing the seemingly opposing tasks of both reducing emissions and improving fuel economy (thus reducing CO_2 emissions) is being approached by what is generally referred to as "low temperature combustion," or LTC. The hallmark characteristics of LTC are a mixture with globally lean equivalence ratio and peak cylinder temperatures that remain below that of thermal NO_X formation (i.e. 2000 K) [28]; the latter for reducing NO_X formation, and the former for high efficiency. LTC has been approached with CI engine hardware with Premixed Compression Ignition (PCI), and from gasoline engine hardware with Homogeneous Charge Compression Ignition (HCCI).

LTC Development and Background

In 1979, Onishi et al. published the groundbreaking paper on what he referred to as "Active Thermo-Atmosphere Combustion" (ATAC) [29]. In the paper, Onishi demonstrated the ability to operate a small gasoline two-stroke engine at part throttle with a fully pre-mixed charge without spark. The fact that combustion was premixed like a gasoline SI engine but auto-ignited like a diesel engine identified it as a new combustion mode. This combustion mode was able to operate at low load over a wide speed range with the two-stroke cycle. It was noted that large levels of residual were present due to the throttled operation and scavenging nature of the two-stroke engine. Important key characteristics identified regarding "ATAC" were significantly reduced specific fuel consumption and NO_X emissions.

Near the same time, Noguchi et al. from Toyota Motor Co. and Nippon Soken published a similar paper on what they referred to as "Toyota-Soken," or TS combustion [30]. Similar in approach to Onishi, a uniflow-scavenged two-stroke engine at lean part throttle operation was operated in a self-ignited (no spark) combustion mode. From physical and visual analysis of the combustion, Noguchi noted that combustion could start at lower temperatures and pressures than for traditional diesel combustion, and that the behavior was unlike that of either gasoline or diesel combustion.

Taking the concept of controlled auto-ignition from Onishi and Noguchi, Najt and Foster in 1983 [31] published work applying it to a four-stroke. Experimentally "Compression-Ignited Homogeneous Charge (CIHC)" combustion, as Najt referred to it, was achieved using a modified Cooperative Fuel Research engine with a pancake combustion chamber and shrouded valves. By tailoring engine operating parameters and employing large (~50%) quantities of EGR, the "proof-of-concept" for four-stroke HCCI was demonstrated. Following the work of Najt, Thring [32] undertook to explore the limits of Homogeneous-Charge Compression Ignition (establishing HCCI as the now accepted initalism) engines. Thring confirmed the findings of Najt in terms of operating four-stroke HCCI and the

12

requirements for high EGR rates. Using regular gasoline (Najt had used PRF blends), Thring established that four-stroke HCCI exhibited specific fuel consumption comparable to that of a diesel engine but was limited to low load and engine speed.

Ryan and Callahan [33] next promoted the concept of HCCI to operate on diesel fuel, demonstrating the ability to operate HCCI with 45 - 50% EGR at an 8:1 compression ratio; the fuel was conventional diesel and operated from lean to near stoichiometric equivalence ratios. Intake temperatures required significant heating to aid auto-ignition, but the compression ratio had to be lowered to keep engine knock at an acceptable level.

Alternative to the approach of Ryan and Callahan, significant research has been devoted to the simultaneous reduction of NO_X and particulates from diesel engines. This has led to the development of what is best called Premixed Diesel Combustion, or Premixed Compression Ignition (PCI). Various strategies have been suggested, such as Toyota's UNIBUS system [34], New ACE Institutes Premixed Diesel Combustion [35], Toyota's Smokeless Rich Diesel Combustion [36], Nissan's Modulated Kinetics (MK) method [37] and Jacob's work at The University of Michigan [38]. The approaches vary, with some employing early injection (i.e. UNIBUS) and others late injection (Nissan MK), and much has been looked into regarding the shape and number of injectors. In all approaches, the goal was to lower NO_X and soot emissions by shifting combustion into the lower temperature and equivalence ratio regions to avoid the so-called "islands" of NO_X and soot [39]. By utilizing high levels of cooled external EGR, the ignition delay of the charge was lengthened, allowing for better mixing and reduction of particulates. Additionally, the high levels of cooled EGR and premixed burn allowed for lower NO_X emissions by decreasing peak combustion temperatures.

A drawback to PCI combustion is that in practice the compression ratio of the engine is reduced to lower the thermodynamic state at the time of fuel injection, thereby lengthening the ignition delay [38] to get the mixing required to reduce particulate emissions. The penalty is reduced thermodynamic efficiency compared to a traditional CI engine. In recent years,

aftertreatment technologies for diesel engines have greatly improved, with current selective catalytic reduction (SCR) catalysts operating with DeNOx efficiencies of 95-96%, and developers are targeting 98% for future generations, at which point EGR could be removed from CI operation entirely, improving thermal efficiency [9]. With Diesel Particulate Filters (DPFs) now a mature technology and effective in meeting particulate regulations, both particulate and NO_X requirements are being met in CI engines with higher thermal efficiencies than previously possible. This poses a challenge for LTC PCI in competing with CI engines to offer reduces emissions while at least equaling their thermal efficiency at comparable cost.

Practical implementations of HCCI combustion based on an SI engine might utilize a recompression or rebreathing method to retain hot combustion product (exhaust) gases in cylinder for the purpose of heating the mixture of the next cycle to autoignite. A third method, so - called "pure HCCI," is to not use recycled hot gases but rather to preheat the pre-mixed charge via an intake heater. Such an approach may use a diesel engine with a higher compression ratio to reduce the amount of preheat required, but this limits the ability to operate as an SI engine at higher load. Recompression is accomplished by closing the exhaust valve early, trapping hot exhaust gases in cylinder. The intake valve is opened late, further retaining the hot exhaust gases, then mixing them with the fresh charge so the combined charge autoignites at the desired timing, as illustrated in Figure 1.1. With this approach, the intake and exhaust valves are both closed across top dead center of the gas exchange cycle, the period which is termed negative valve overlap (NVO), and illustrated in Figure 1.2. A rebreathing approach retains standard intake valve timing, but utilizes a second valve opening event, opening the exhaust valve during the intake process, inducting and mixing hot exhaust gases into the charge. A simulation-based study by Babajimopoulos [40] investigating the merits of recompression vs. rebreathing found that at lower loads recompression was more efficient due to less pumping losses. Additionally, from a practical perspective it is easier to "mode switch" from SI to HCCI with a recompression
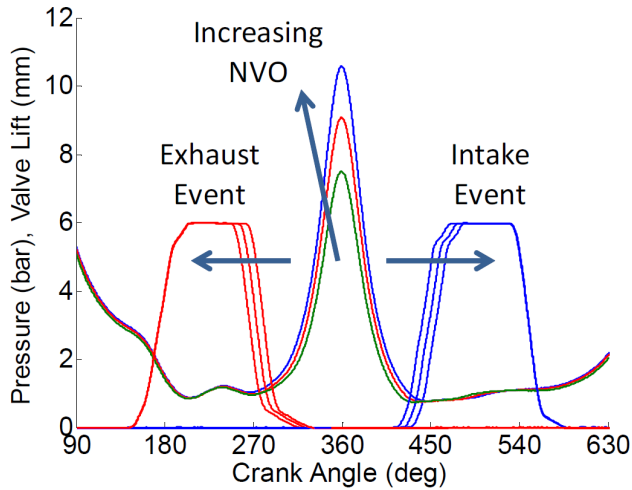
Figure 1.1 Characteristic cylinder pressure trace during a NVO event
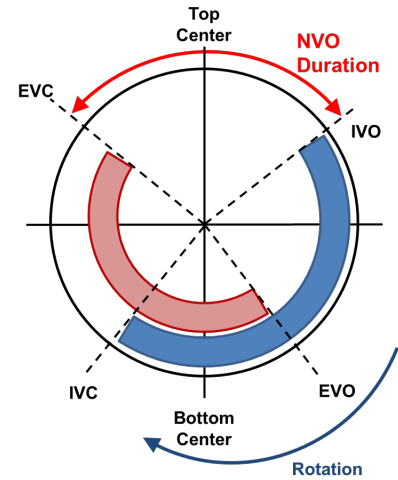
Figure 1.2 Characteristic timing chart for NVO HCCI operation

strategy, merely by phasing the cams via a hydraulically controlled cam phaser; rebreathing requires a two lobe camshaft that does not facilitate mode switches as easily. Based on this, recompression is the strategy most favored for HCCI implementation from an SI engine perspective.

The nature of recompression, or NVO, HCCI brings with it some unique thermal considerations. The process of trapping exhaust gases in cylinder and then mixing them with the fresh charge is a stochastic process with random distributions of composition and temperature that vary not only spatially but from cycle to cycle. Rothamer [41] has demonstrated this optically, comparing a "pure" HCCI engine with that of one employing NVO. This can be seen in Figure 1.3, as published in [41], which presents at 24°before top dead center the probability of both EGR mole fraction and temperature. The NVO engine demonstrates a significantly higher range of temperature and EGR mole fraction.

The potential of NVO HCCI operation to increase thermal and compositional stratification has ramifications on the combustion event. Fundamental flame studies with hydrogen demonstrate that increased thermal stratification will advance ignition and lengthen overall burn durations [42–45]. Similar results have been documented with simulations using PRF chemistries [46–48]. Experimental work by Dec and Sjöberg has used thermal

15
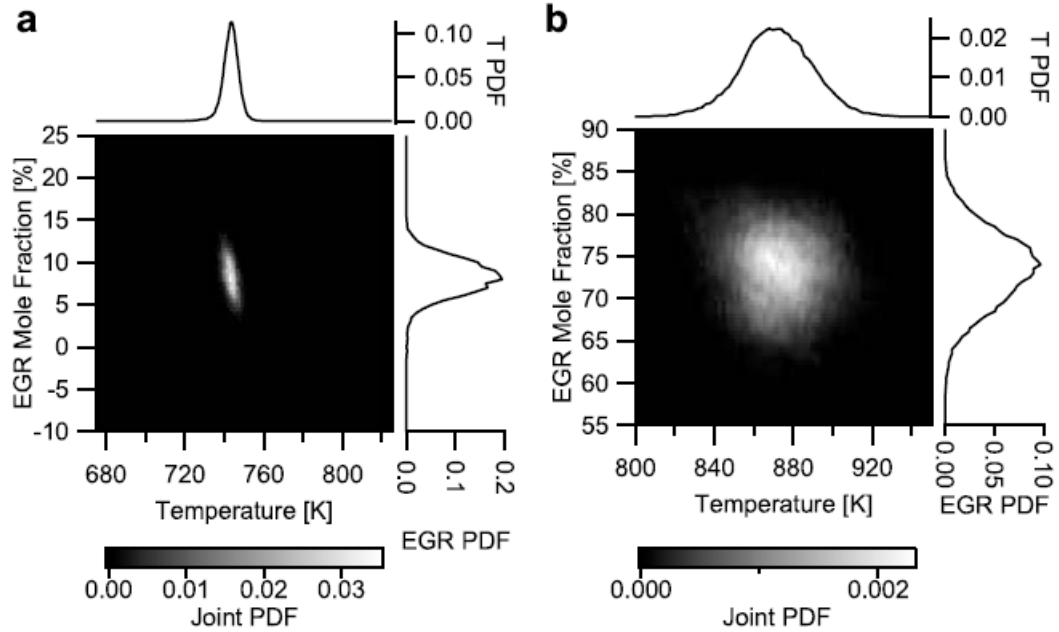
Figure 1.3 A joint probability distribution function (PDF) versus temperature and EGR mole fraction (a) pure HCCI operation and (b) NVO operation, highlighting the greater thermal and compositional distributions in NVO operation (Rothamer, 2009)

imaging with an optical engine to demonstrate that thermal and composition stratification could be used to slow burn rates for HCCI combustion [49], and they have also demonstrated this ability in another experiment by decreasing coolant temperature to increase thermal stratification and decrease burn rates [50]. However, the studies conducted by Dec and Sjöberg were performed with a "pure" HCCI engine[1] and the stratification employed was not by means of changing the amount of NVO or internal EGR. The impact of large changes in NVO and internal EGR on an NVO HCCI engine remain an open question, and is one of the main contributions of this work.

Another potential impact of NVO operation is on cycle to cycle stability. Studies with "pure" HCCI have demonstrated that HCCI is subject to cycle to cycle variability [51], which can be affected by intake temperature, ϕ, EGR rate and PRF number. A higher level of external EGR was observed to increase the cyclic variability, but it wasn't clear if this was

---

[1]Where "pure" here means the use of external inlet preheating to thermally control HCCI without the use of hot internal residual gas

16

also due to later phasing, as cyclic instability was shown to increase with retarded CA50. Both Xincai [52] and Shahbakhti [51] have observed that higher ON PRF fuels exhibit a lower COV of IMEP. Shahbakhti also noted that higher ON PRFs exhibited a higher cyclic variability in burn duration for a given condition compared to lower ON PRF blends.

Recently, Manofsky [53] demonstrated the use of spark to assist the HCCI auto-ignition event (known as SACI, spark assisted compression ignition) as a way to extend the load limits of HCCI combustion. The spark creates a flame which consumes a portion of the charge, so the main auto-ignition event has a lower peak HRR, allowing load extension over HCCI without spark assist. Manofsky demonstrated an increase in maximum load from ≈ 4 bar net mean indicated effective pressure $IMEP_n$ to 7.5 bar $IMEP_n$ [53]. Practical implementation of HCCI will most certainly use SACI operating modes to expand the HCCI operating range.

1.2.4   HCCI Combustion and Fuels Research

The fact that HCCI combustion ignites under different conditions than traditional CI and SI engines suggest that an ideal fuel for HCCI combustion might fall between traditional gasoline and diesel fuels in terms of ignitability. HCCI combustion may in fact benefit from a fuel with an octane rating in between that of typical gasoline and diesel fuels, as has been suggested by Hildingsson [54]. The use of low octane gasoline, or naptha - like, fuels may also offer environmental benefits. A low octane fuel requires less processing at the refinery; the octane rating of the gasoline at a refinery has to meet minimum octane requirements, and one way to do this is by the "cat cracking" process, cracking heavier oils into lighter (fewer carbons) hydrocarbons to be used to increase the octane rating of the gasoline [55]. A by-product of the cat cracking process is CO_2, a greenhouse gas. So, from a well to wheel perspective, a lower octane fuel may be more ecologically desirable.

HCCI Ignition Rating Correlation to RON and MON

The applicability of lower octane gasoline-like fuels for HCCI combustion has become a new focus in HCCI literature in recent years, for the reasons outlined above. To date, much of the research with fuels and HCCI has focused on relating auto-ignition in an HCCI engine to the RON and MON tests. The goal has been to characterize the ignition characteristics required for HCCI combustion to aid in fuel selection. The primary proponent of this type of method has been Kalghatgi [56] with his Octane Index (OI). The OI is a linear correlation between the RON and MON (via octane sensitivity) of a fuel, and the location of 50% mass fraction burn, or CA50. As an extension of the work of Kalghatgi, Shibata [57] developed the HCCI Fuel index which uses only the RON and fuel components (n-paraffins, iso-paraffins, olefins, aromatics, and oxygenates) to characterize the auto-ignition requirements of a fuel for HCCI.

However, recent work by Perez and Boehman [58] has shown that the correlation between OI and HCCI index with CA50 across fuels and engine conditions is not strong, and Perez demonstrated that using an ignition quality tester (IQT) to measure ignition quality gave better results than OI or HCCI Index. Additionally Rapp [59] recently demonstrated that while they achieved good correlation between the OI and HCCI Index for primary reference fuels, these correlations poorly predicted the performance of gasoline fuel blends. Given that the MON test does not even accurately predict modern engine knock characteristics [60], it is not surprising that attempts to relate RON and MON with HCCI conditions have been unsuccessful. Rather than attempt to determine empirical ignition correlations, other research has focused on characterizing different fuels operating under HCCI conditions in a CFR type engine.

Low PRF number fuels and Low Temperature Heat Release

A characteristic of paraffin based fuels is the two stage ignition process, where ignition first starts with at lower temperature, followed by the main ignition event. Paraffin fuels also

possess what is known as negative temperature coefficient (NTC) behavior with regards to the ignition behavior, where there exists a temperature range in which an increase in temperature will decrease the ignition delay time. This has been demonstrated in fundamental shock-tube experiments for n-heptane-air mixtures at pressures relevant to engine combustion [23,61]. At pressures and equivalence ratios relevant to engine combustion, n-heptane has pronounced NTC behavior, as shown by Fieweger [23] and shown in the Arrhenius plots in Figure 1.4. NTC behavior is a form of non-Arrhenius behavior, in that it is a deviation from a true Arrhenius plot which would be a line of constant slope in Figure 1.4. Depending on the operating conditions, a paraffin fuel may be operating in a non-Arrhenius region, where the slope is reduced as temperature decreases. To be true NTC behavior, the ignition delay must be decrease as temperature decreases within a temperature range, before then again increasing with decreasing temperature, as shown for 100% n-heptane in Figure 1.4.

The octane sensitivity of gasoline fuels (that is, non-equality between RON and MON) has been attributed to the lack of non-Arrhenius and NTC behavior of gasoline when compared to paraffin based PRFs [24]. HCCI combustion can operate in with low PRF number fuels at non-Arrhenius conditions, a consequence of which is low temperature heat release (LTHR) — a distinct heat release event prior to main ignition event. This unique behavior has been investigated, as reported by the following studies.

Truedsson [62] investigated the pressure sensitivity of auto-ignition temperature under HCCI conditions with nine PRFs, ranging from PRF 0 to 100. Engine speed was maintained at 600 rpm, CA50 was fixed at $3°$ ATDC with $\phi = 0.33$ and no external EGR was used. Ignition temperatures (defined as the temperature at the location of 0.2 J/CAD RoHR) are shown for inlet temperature sweeps, but the compression ratio was also changed to fix phasing, and as such compression pressures were changing as well making it difficult to draw conclusions on fuel specific effects. The behavior of PRF85 and above, in terms of ignition temperature, was different than for low PRF blends; lower PRF blends showed a fairly constant (slight reduction) auto ignition temperature with increased pressure (from
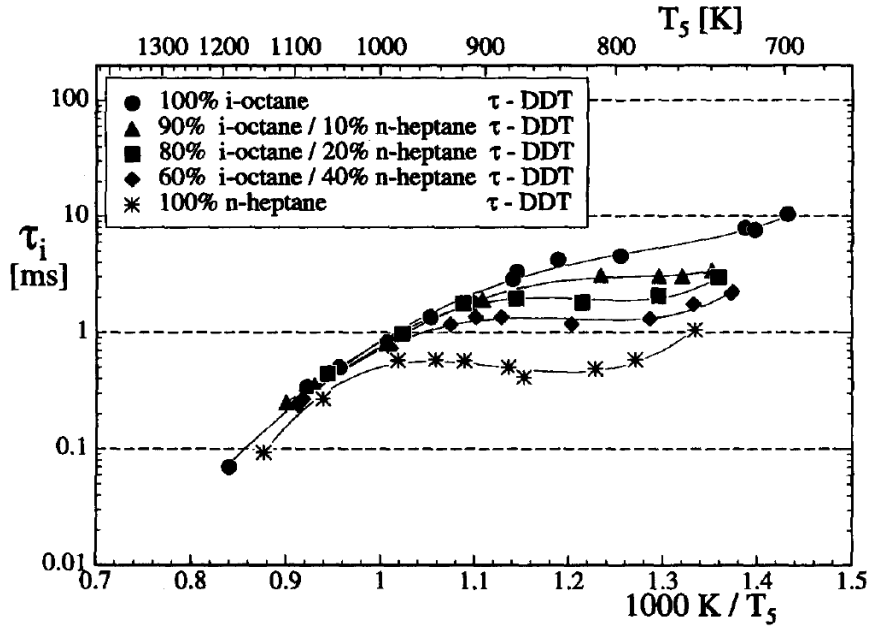
Figure 1.4 Ignition delay time of PRF fuels for $\phi = 1.0$, $p = 40 \pm 2$ bar (Fieweger, 1997)

higher CR), whereas the higher PRF blends show an increase in auto-ignition temperature with increased pressure. It was shown that the lower PRF fuels which exhibited (LTHR) required a lower auto-ignition temperature due to the LTHR. However, no discussion was made of the length of the combustion burn duration, so the impact of non-Arrhenius fuel characteristics on operability remain unknown.

Fixing compression ratio, Hosseini [63] used a CFR engine to compare ultra low sulfur diesel (ULSD), n-heptane and iso-octane with engine speeds from 900 to 1700 rpm at a constant ϕ. LTHR was demonstrated for all fuels except iso-octane. When engine speed was changed, the main combustion event was retarded, but the LTHR portion maintained the same phasing, as the LTHR reactions are dependent on the temperature history during compression and these temperature time histories remain mostly fixed as a function of engine speed. But as speed was increased, less time was spent at the temperatures where LTHR occurs so the magnitude of the LTHR decreased. When LTHR was plotted in the time domain, the peak RoHR in time remained constant across the speeds studied. Boosting with increased speed was shown to keep the amount of LTHR constant, and was the primary

conclusion of the work; boosting was an effective means to control LTHR and combustion phasing for diesel fuel in an HCCI environment.

John Dec's group at Sandia has performed multiple investigations utilizing a production Cummins CI engine modified to run on one cylinder. The engine utilizes either port fuel injection (PFI) or direct injection (DI), but uses no NVO, just external EGR, if any EGR is required or desired. Sjöberg [64] demonstrated increased LTHR for PRF60 and PRF80 as engine speed was reduced. The onset of LTHR with PRF60 and PRF80 required significantly more intake temperature adjustment for combustion phasing compared to gasoline or iso-octane. With regards to combustion phasing, Sjöberg [65] demonstrated that LTHR allowed PRF80 to operate at a later combustion phasing compared to iso-octane within the stability limits at a fixed speed of 1200 rpm. At a given CA50, the PRF80 had a faster 10-90 burn compared to the iso-octane, but since it was premixed combustion, the charge density (or load) of the PRF80 was higher than that of iso-octane, as the PRF80 was operated at a lower inlet air temperature. Additionally, the charge density was increased as combustion was retarded across the phasing range for the same reason, because the inlet air temperature was lowered to retard phasing. Increasing charge density will increase burn rates (decreasing 10-90 burn duration), so the actual effect of fuel chemistry (e.g. ignition delay) in the experiment is not clear with regards to burn rates.

Work by Shibata [66] compared different blends of similar low octane fuels in "pure HCCI" operating under a relatively high compression ratio (15.0:1) with conventional valve timing. Shibata compared PRF blends to those of n-heptane with other pure hydrocarbons. Comparing fuels at the same load and phasing it was noted that, compared to PRF85, a 75 RON blend of n-heptane and cyclopentane (NCP) exhibited a higher peak rate of heat release (RoHR). Conversely, a 70 RON blend of n-heptane and toluene (NTL) demonstrated a lower peak RoHR. The longer burn of the NTL (toluene blend) was attributed to a two-phase burning, characterized by separate and distinct heat release after the peak heat release, which enabled a lower peak pressure rise rate. The NTL was demonstrated to operate at

approximately 20% higher peak load than a PRF of equivalent RON. The reason for the higher load limit for the NTL fuel was not explained in the study.

Intermediate Temperature Heat Release

After LTHR is completed, under certain conditions the intermediate oxidation of paraffinic fuels begins [67], and its benefits to HCCI combustion have been promoted by John Dec's group at Sandia [68–70]. Specifically at elevated pressures for gasoline, they have shown that gasoline and other two stage ignition fuels exhibit an intermediate temperature heat release (ITHR) prior to the main ignition event and after LTHR (if present). This ITHR acts to stabilize combustion, allowing more retarded operation, which in turn allows higher load. Dec [69] has demonstrated the pressure sensitivity of gasoline, with increasing ITHR at increasing pressures, and utilized this to achieve an $IMEP_g$ of 16 bar.

Very recently, Yang [70,71] extended the work of Dec [69] — boosted HCCI combustion with partial fuel stratification — and approached it with a low octane fuel, Hydrobate (a low octane — 69 RON — hydrocarbon distillate with volatility similar to gasoline). Using a "pure" HCCI setup, the experiments relied upon high compression ratio and intake preheating to enable HCCI combustion. The Hydrobate fuel exhibited a strong ϕ sensitivity and under naturally aspirated conditions offered higher thermal efficiency and load.

Fuels Work with NVO HCCI

Another approach to HCCI combustion, and one that may have the most promise for production implementation, is to utilize a more traditional gasoline type engine (e.g. premixed fueling, CR $\sim$ 12) and utilize NVO (as shown in Figures 1.1 and 1.2) to trap hot exhaust gases to auto-ignite the next cycle. Cedrone and Cheng [72] have employed such an approach in studying range of fuels including a base gasoline, high olefin and high olefin/aromatic fuel with a high and low RON gasoline, E10, E20, E85 and an iso-butanol blend. Speed and load maps were made varying speed from 1250 – 2500 rpm. High and low

limits were set by rate of maximum pressure rise and IMEP COV/misfire limits respectively. Small differences were observed in the high and low limits, but all of the fuels had a RON within the range of 89 – 97 (save for E85 which was 107). Burn rate comparisons at the high load limit were made at different combustion phasing and different EGR levels so it is not possible to parse the fuel chemistry effects.

Extending an NVO engine to Spark Assisted HCCI (SACI), Weall and Szybist [73] used a single cylinder engine with NVO operated by a Sturman Hydraulically actuated fully flexible valve system to compare gasoline with E85 and a 50/50 blend of gasoline and iso-butanol at a fixed engine speed of 2000 rpm under (SACI) conditions. A range of load sweeps were studied and CA50 was held approximately constant. IMEP of up to 6 – 7 bar was reported, a marked increase over HCCI maximum load. The thermal efficiency of E85 and a 50/50 iso-butanol/gasoline blend was shown to be higher than that of gasoline, but the reasons for this were not given. Comparison based purely on the fuels was difficult in most cases as the ringing limit and not the combustion phasing was matched. Furthermore CA50 and load were not maintained at constant values.

Surveying the literature, there are many experiments examining fuel effects on HCCI operation, but the results do not identify optimum fuel characteristics for HCCI. Successful implementation of HCCI will most likely be in an NVO engine, yet the majority of research has utilized either a CFR engine or modified CI engine without NVO. Using NVO has been documented to add complexity to the combustion process by means of thermal and compositional stratification, yet it is within the NVO framework HCCI combustion is likely to be employed. The purpose of this work is to fill the gap in the knowledge of the effects of fuel chemistry effects on NVO controlled HCCI combustion.
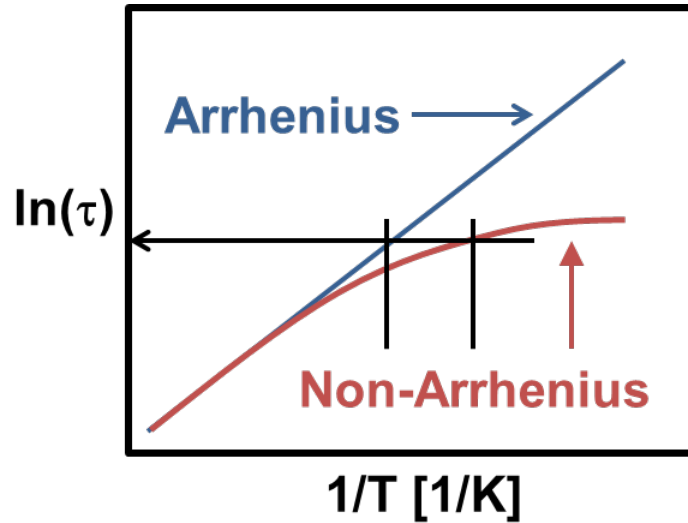
Figure 1.5   Conceptual ignition delay curves for an Arrhenius and non-Arrhenius fuel

1.3   Research Objectives

As the primary focus of this work is "fuel effects" in HCCI, some clarification is now made as to what the term "fuel effects" means within the scope of this document. Changing fuels can potentially impact the following: energy addition (changes in LHV), charge cooling (changes in heats of vaporization), spray and mixing effects (volatility, viscosity), and fuel chemistry. Of these, the parameter of focus is fuel chemistry. Changes in energy addition will be addressed, and other thermophysical properties are similar for the test fuels in question. By fuel chemistry, this investigation is focused on how fuels of different chemistry exhibit different ignition delay behavior, specifically non-Arrhenius behavior as shown below in Figure 1.5, where a non-Arrhenius fuel will require a lower temperature for a given ignition delay, and have a shallower slope.

With the above in mind, the following objectives, as detailed below, are addressed in this document.

HCCI Load Limits with a Low ON Fuel

The operating load limit of an NVO engine utilizing a low ON fuel is demonstrated,

24

extending load limits compared to gasoline. From this, the work will demonstrate fuel chemistry effects that may contribute to this load extension, independent of compositional effects due to the use of NVO.

Constant Charge Composition

In order for the fuel effects to be examined in an NVO HCCI engine, a method is developed to compare fuels of dramatically different ON rating, while maintaining constant composition. To the author's knowledge, no such previous method or study exists.

Fixed Combustion Phasing: Effects of NVO

The effect of changing iEGR (via NVO) on HCCI combustion burn rates, while maintaining constant phasing and load, has not been documented. It is clear that the use of NVO introduces thermal and compositional gradients to the charge, and the literature suggests that increased stratification will lengthen burn duration, but this has not been explicitly demonstrated experimentally. To do this will requires variation of a large range of NVO with fixed composition at fixed combustion phasing. The results will demonstrate the effects, if any, of thermal and compositional stratification inherent to NVO on the HCCI combustion process.

Fixed Combustion Phasing: Fuel Chemistry Effects

It has been demonstrated that low ON PRF fuels exhibit LTHR at conditions where higher ON PRF fuels do not, specifically lower engine speeds and higher pressures. Gasoline under certain conditions will exhibit ITHR, aiding combustion. The effects of fuel chemistry of a low PRF number fuel compared to gasoline are examined in this work at constant composition and combustion phasing. To compare the effect of fuel on HCCI combustion in the NVO engine environment requires that NVO (iEGR) is constant between fuels to remove the uncertainty of differences in composition and stratification inherent to changing NVO. No previous study has examined fuels of wide ON at constant composition and phasing

as a function of engine speed. These experiments answer the question: is the faster burn duration of the lower ON fuel at fixed load and phasing a function of fuel chemistry, or compositional/stratification differences?

Fixed Stability Limits: Effects of NVO

The work of Shahbakhti has noted increased cyclic variability for higher EGR levels. In the current work mapping engine load limits, lower ON fuel cases, which were phased later, also had less NVO compared to the gasoline. This suggested cyclic feedback of high iEGR levels could increase cyclic instability compared to lower iEGR operating conditions. To demonstrate this experimentally, iEGR was varied at a fixed COV of IMEP$_g$, with the hypothesis that lower iEGR cases would be able to operate within the set stability at a later CA50 timing.

Fixed Stability Limits: Fuel Effect

The work of Shahbakhti noted lower ON PRF blends had higher cyclic variability in burn duration than higher ON PRF blends, and that a shorter burn duration had less cyclic variability. In the current work mapping engine load limits, the low ON fuel was demonstrated to operate at a later phasing at a higher maximum load. To determine if this was a fuel chemistry effect or an iEGR effect, experiments are performed comparing phasing limits at a fixed COV of IMEP$_g$ and fixed iEGR between gasoline and a low ON PRF.

1.4   Overview of Document

This document is arranged into a total of seven chapters, including the current chapter. A brief description of the remaining chapters is as follows.

Chapter 2 details the experimental setup (engine hardware, data acquisition, etc.) and analysis methods used in the study, including heat release analysis and residual gas estimation methods. Experimental uncertainties and repeatability are quantified and

discussed.

Chapter 3 is a condensed version of the author's ASME paper [74] exploring the load and phasing limits of a low octane gasoline blend, NH40, compared to gasoline and iso-octane. Higher load limits are demonstrated for the NH40 at a later phasing, but differences in composition and internal EGR levels between fuels at a given phasing complicate interpretation of fuel chemistry effects. Chapters 5 and 6 revisit this work with controlled experiments designed to better isolate fuel effects.

Chapter 4 details the methods developed to maintain constant charge composition across wide ranges of NVO and engine speed. Methods employed include trading external EGR with internal, intake preheating, changing intake valve closing timing, and part throttle application.

Chapter 5 takes the methods presented in Chapter 4 and compares a low octane fuel, PRF40, with research grade gasoline at fixed phasing and fuel/air and fuel/charge composition to determine the effect of the fuel chemistry on combustion burn rates and overall combustion duration. Additionally, the sensitivity of combustion burn rates and overall burn duration to internal EGR levels is explored by varying the duration of NVO.

Chapter 6 expands upon the results of Chapter 5 to explore the effects of fuel chemistry and iEGR levels on phasing limits. Late phasing limits at fixed combustion stability (COV of IMEP) are compared for high and low iEGR conditions, and for PRF60 and gasoline at fixed iEGR conditions.

Chapter 7 presents a summary of the previous chapters, highlighting contributions of this work within the framework of the literature as well as the broader ramifications. A discussion of future work is included.

Chapter 2

Experimental Methods

All experiments within this document were conducted utilizing the University of Michigan Fully Flexible Valve Actuation (FFVA) engine. This chapter details the specifics of the FFVA engine, ancillary systems, and data acquisition as well as the analytical methods used for interpreting the results presented herein.

2.1 Experimental Hardware

The Fully Flexible Valve Actuation (FFVA) engine is a Single Cylinder Test Engine (SCTE) comprised of a Ricardo Hydra crankcase with a Sturman Industries Hydraulic Valve Actuation (HVA) unit. The following sections detail these main components and the relevant subsystems of the engine hardware. An image of the test cell is shown in Figure 2.1.

The capabilities of this test cell, notably the fully flexible valve system, exist in perhaps a half-dozen test cells in the world. As such it is both the benefit and burden of this work to utilize them to their fullest extent, extracting insight that is possible from few other experimental facilities.

2.1.1 Single Cylinder Test Engine

The Ricardo Hydra is a dedicated SCTE platform designed to be easily reconfigured for use with multiple cylinder heads. The engine details are summarized in Table 2.1. The crankcase is cast iron and utilizes a floating "jug" which contains the iron cylinder liner.

Table 2.1 FFVA engine specifications

Parameter	Value
Displaced volume [cm^3]	550
Cylinders	1
Stroke [mm]	94.6
Bore [mm]	86.0
Connecting rod length [mm]	156.5
Compression ratio	12.5:1
Number of valves	4
Piston shape	Shallow Bowl
Head design	Pent – roof
Fuel delivery	D.I. (wall guided)

The use of a custom jug allows for any head bolt pattern to be attached to the crankcase as well as multiple bore sizes.

For the UM FFVA engine, the cylinder is 0.55L displacement with a 86mm bore and 94.5mm stroke. It utilizes an aluminum cylinder head with four valves and pent roof geometry. The aluminum cylinder head was custom machined by Sturman Industries to accommodate the HVA system. There is a centrally located spark plug (which isn't used in these studies) and a side mounted direct fuel injector provides a wall guided fuel spray across a shallow bowl aluminum piston. An image of the crown of the piston is provided in Figure 2.2.

The engine is controlled by a combination of National Instruments and Drivven, Inc. hardware, with Labview software from Drivven developed for this particular application. The engine is connected to a Micro-Dyn 35 dynamometer manufactured by Electro-Mechanical Associates (EMA) of Ann Arbor, MI. The Micro-Dyn 35 is a low inertia hydraulic pump/motor dyamometer capable of absorbing up to 47 Nm (35 lb-ft) at speeds up to 4000 rpm.
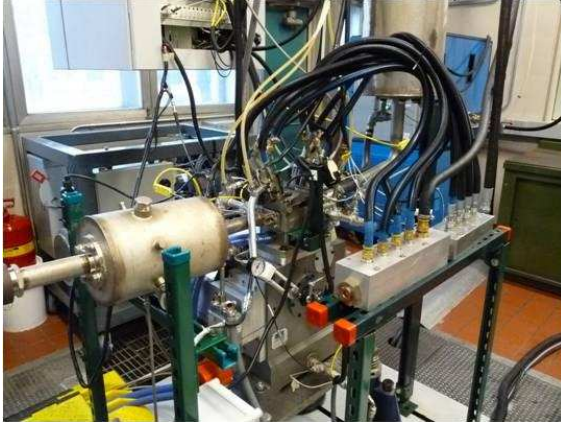
Figure 2.1   UM FFVA Experimental Test Cell   **Figure 2.2**   FFVA Engine Piston Crown
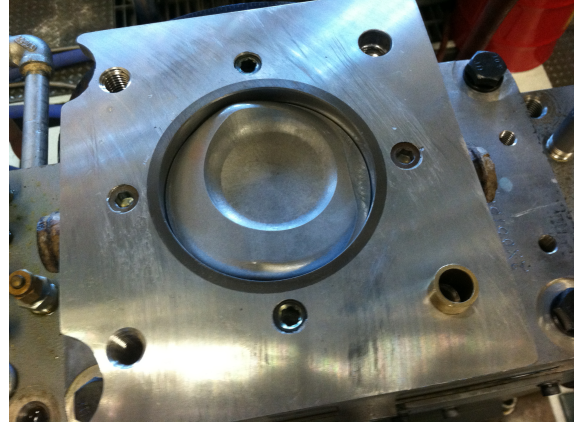
2.1.2   Fully Flexible Valve Actuation System

A key feature of the FFVA engine is the fully flexible hydraulic valve system. As installed in the FFVA engine, it is a modular variable lift system manufactured by Sturman Industries and marketed as the Hydraulic Valve Actuation (HVA) Combustion Research Module. An overall schematic of the HVA system is shown in Figure 2.3, highlighting the key components of the system: HVA drive units attached to the valves in the cylinder head; the hydraulic supply or "pump cart;" the electronic controller or "Condor;" and the the laptop PC for interface with the operator. Valve commands are sent from the laptop PC to the controller where they are stored in the ECU.

A schematic of the valve module system is provided in Figure 2.4, illustrating the valve, actuator, movable stop and hydraulic lines. The movable stop allows for variable lift. Not shown is a linear hall effect position encoder attached to the valve which records valve lift for each event. The system has a precision of $1°$ CA for valve event timing, necessitating the smallest incremental change in NVO be $2°$ ($1°$ for both EVC and IVO) if symmetrical NVO is utilized. The valve lash is set at 0.1mm and this is the criteria for determining valve opening and closing events.
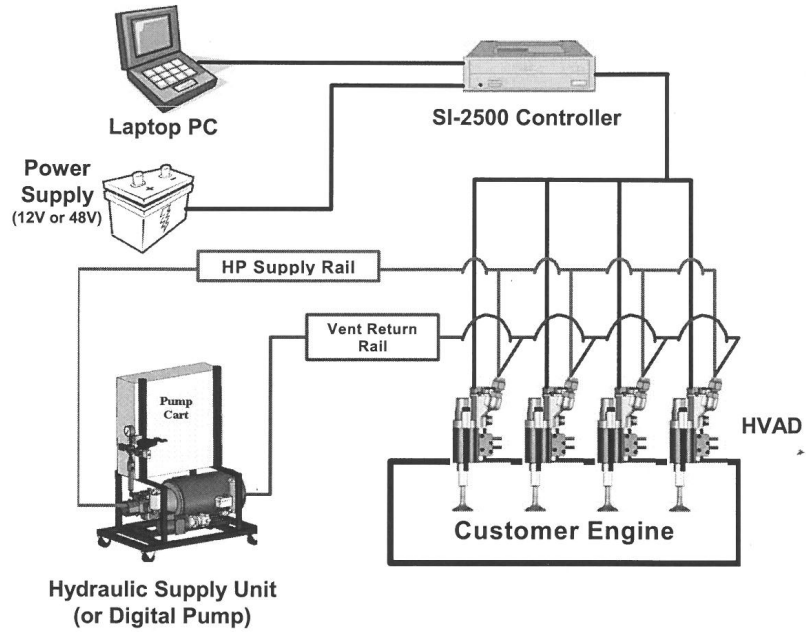
Figure 2.3   Schematic of the Sturman HVA Module System setup
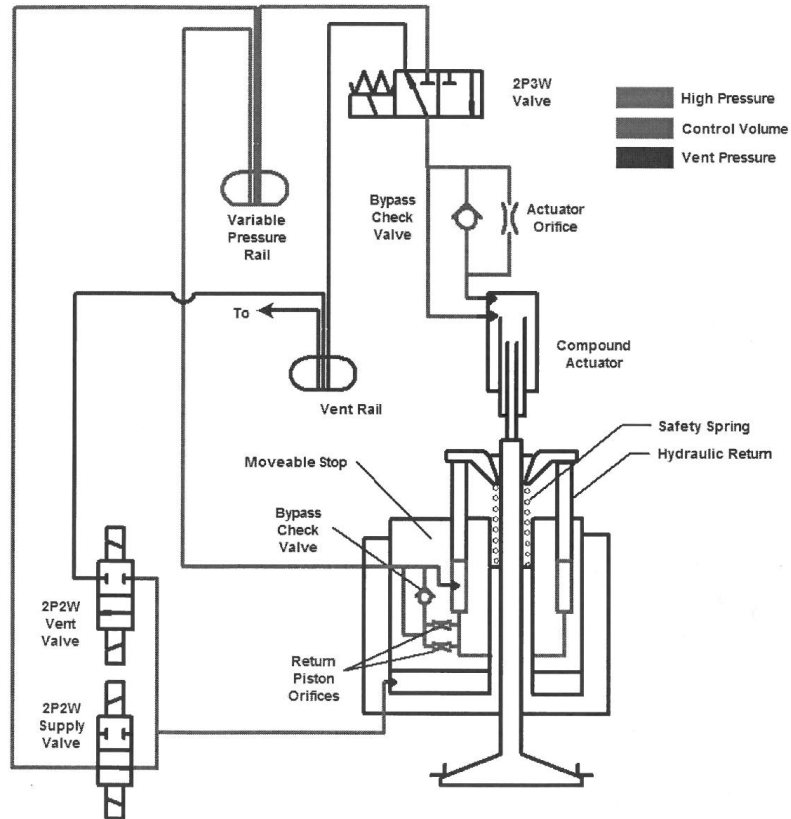
Figure 2.4   Schematic of the Sturman FFVA Valve Module
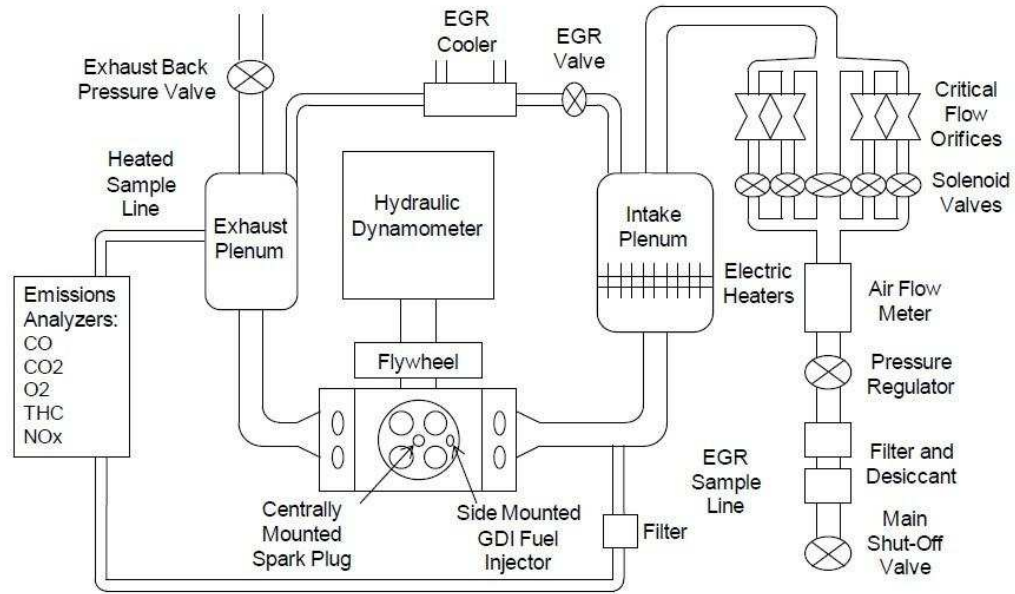
Figure 2.5 Schematic of the FFVA experimental setup

2.1.3 Ancillary Engine Systems

Supporting the primary engine hardware are the ancillary systems that provide air, coolant and oil to the engine. These systems are presented in the schematic of the test cell in Figure 2.5.

Air Delivery

Air is supplied to the engine from the compressed shop air lines in the Walter E. Lay Autolab facility. Compressed air is dried and filtered, and is metered through both critical flow orifices and a Fox Instruments hot wire anemometer for measurement redundancy. Air is supplied at atmospheric or partially throttled conditions; while the shop compressor could provide boosted conditions the intake plumbing is not presently capable of handling boosted conditions.

External EGR (eEGR) is introduced into the intake plenum through a line from the exhaust, and flow is controlled by a Hanbay MCM electrically actuated needle valve. The

eEGR is run through a heat exchanger that serves an EGR cooler. The heat exchanger has closed loop circulation of engine coolant set at 75°C to cool EGR prior to introduction in the inlet plenum.

For the experiments in Chapters 5 and 6, the intake heating capacity was increased to 5kW from the 3kW heating capacity used in the original study [74]. The entire intake plenum and runners have been wrapped with insulative fabric to enable inlet temperatures up to 200°C. These high inlet temperatures are required to operate NVO HCCI with small levels of NVO and high levels of external EGR, and is a unique capability of this test cell.

Standard K-type (nickel-chromium) thermocouples are used for measurement and control of inlet temperatures. Thermocouple placement exists at the end of the inlet runner approximately 1" before the port, and this is the reported value as well as the control value during operation. For this, a dual element thermocouple is used, with one thermocouple for recording the value and the second thermocouple for control with a PID controller. Additionally, a thermocouple is present immediately downstream of the inlet heater, and incorporated with a limit switch to ensure the heaters do not exceed a preset limit.

Fuel Delivery System

Fuel is direct injected into the cylinder as mentioned in Section 2.1.1. Supplying the fuel injector is a Parker/Greer Series BA bladder accumulator which is pressurized with purified nitrogen from a gas cylinder. The supply pressure is regulator controlled to 100 bar. From the bladder accumulator, fuel flows through a Max Machinery Model 213 piston driven flow meter to the injector.

The bladder accumulator, when full, holds approximately 3 gallons of fuel and allows for approximately one day of operation, depending on load. To refill the accumulator, the nitrogen supply is closed and pressure relieved from the pressurized side of the accumulator. Once depressurized, fuel is pumped into the accumulator from an external supply via a Mallory 12V electric fuel pump. Once filled, the external fuel supply is closed off and the

high pressure nitrogen supply gradually opened to re-pressurize the system.

As the primary focus of this work was with different fuels, fuel changeovers were frequent. When changing fuels, care must be taken to avoid cross contamination, which may occur if old fuel is not properly purged from the system. To accomplish this, high pressure drain valves were installed directly upstream of the fuel injector and immediately after the high pressure accumulator. Additionally, a compressed air line was attached, via a three way valve, to the high pressure drain valve after the accumulator. With this, the fuel changeover procedure is as follows:

1. Depressurize the accumulator
2. Drain the accumulator from the valve nearest the fuel injector. This is accomplished with slight residual pressure from the nitrogen line
3. Using the compressed air line blow out the entire fuel line, waiting for fuel spray vapors to no longer be present exiting the drain valve. The nature of the line plumbing allows the compressed air to move through the accumulator, vaporizing and purging the accumulator as well
4. Refill accumulator from external supply with new fuel until fuel flows from the drain directly in front of the fuel injector
5. Allow 1L of the new fuel to purge from the drain before closing
6. Re-pressurize the accumulator

Engine Oil and Coolant

Engine oil and coolant were both independently controlled through external pumps and dedicated closed systems. Both engine oil and coolant systems have dedicated electric tube in shell heaters that are kept at fixed setting. To regulate temperature, heat exchangers interfaced with cold city water are downstream of the heaters, and PID controlled valves adjust the amount of city water flowing through the heat exchangers. For both engine oil and coolant, the engine-out temperature is kept at 90°C.

2.2 Data Acquisition and Analysis

The data acquisition for the UM FFVA engine followed traditional engine dynamometer protocol and was separated into two distinct systems: a high speed and low speed system. The high speed system recorded data to a resolution of one tenth of a crank angle, which at 2000 rpm is a time domain sampling of 120kS/s and is reserved for crank angle quantities such a cylinder pressure. Low speed data acquisition was used for measurements such as intake temperature and is on the order of a sample per second.

2.2.1 High Speed Data Acquisition

High speed (crank angle resolved) engine data were collected at a resolution of 0.1 CAD using a Kistler model 2613B crank angle encoder and logged by an AVL combustion analysis system. Cylinder pressure was measured with a Kistler 6125A piezoelectric transducer using an AVL MICRO IFEM with integrated charge amplifier. For each data point 200 cycles are logged for analysis. Prior to recording a data point the engine is allowed to stabilize for several minutes to ensure a condition is steady-state.

In addition to cylinder pressure, high speed absolute intake and exhaust pressures were recorded with Kistler piezoresistive sensor models 4007B and 4045A, respectively. The high speed intake pressure sensor, model 4007B, is used for intake pressure pegging during the blowdown process, as the piezoelectric cylinder transducer is a relative pressure measurement.

2.2.2 Low Speed Data Acquisition

Low speed data acquisition was managed with National Instruments hardware and a Labview interface. The low speed data acquisition recorded all measured temperatures, such as intake, exhaust, engine oil, engine coolant, etc. As a redundancy to the high speed pressure measurements, there were low speed pressure sensors as well: a Kistler 4620A piezoresistive

sensor in the intake and an Omegadyne PX309 sensor in the exhaust.

Standard exhaust gas emissions were measured with a Horiba MEXA 7500D-EGR. The following measured exhaust emissions(and measurement principle) are as follows: total hydrocarbons (or THC) on a C1 basis (flame ionization detector or FID); oxides of nitrogen or NO_X (chemiluminescent analyzer); oxygen or O_2 (paramagnetic analyzer); carbon monoxide or CO(non-dispersive infrared analyzer, or NDIR); carbon dioxide or CO_2 (NDIR); and methane or CH_4 (FID); Additionally there was a second CO_2 NDIR analyzer to measure intake CO_2 for calculating the amount of intake EGR. The THC and NO_X were measured on a wet basis and all other emissions were taken on a dry basis. Dry emissions were converted back to a wet basis concentration by the method established by Stivender [75].

The Horiba MEXA emissions analyzer provides a calculation of exhaust equivalence ratio (ϕ) using the Brettschneider equation [76]. There were two additional redundant methods with which the exhaust ϕ was computed and those are with a Bosch LA4 wide band lambda sensor (LSU 4.9 revision) and by manual calculation using the measured fuel and air flow.

2.2.3 Heat Release Analysis

Heat Release was calculated based on first law approach [28]. The standard Woschni [77] heat transfer correlation was used in post processing for computation of cylinder pressure based heat release rates, but with a reduction in the pressure velocity term to account for the lack of flame propagation. This was based on the work of Chang [78] and Ortiz-Soto [79].

Residual Gas Estimation

Since a recompression strategy using NVO was used to facilitate HCCI combustion, it became necessary to know the level of internal residual for a given operating condition. As

this was not directly measured with the experimental setup, the residual gas fraction (RGF) was inferred using the Fitzgerald method [80] which has been developed specifically for HCCI conditions. The method models the in-cylinder temperature from EVO to EVC using the measured exhaust temperature and instantaneous cylinder pressure by accounting for heat loss during the exhaust process. This method was examined in detail by Ortiz-Soto [81] and found to provide the most accurate estimation of residual gas for HCCI conditions.

2.2.4 Experimental Repeatability

Due to the nature of experiments, uncertainties arise in the form of errors which could be due to offsets in the measured experiment (such as from a drift in calibration), intrinsic instrument uncertainty, and day to day variability. For the first two considerations, where possible there were redundancies built into the measurements. For example, the exhaust equivalence ratio was measured by the ETAS LA4 lambda sensor, the emissions bench, and was computed by the measured air and fuel flows. These three values were constantly checked to ensure measurement agreement.

For some quantities, reported values were from model based calculations, such as for the heat release analysis and the residual gas estimation method as discussed in Section 2.2.3. In the residual gas estimation, for example, there were inherent uncertainties with the assumptions in the model (e.g. the measured exhaust temperature is equal to the in-cylinder temperature during blowdown) in which actual experiments may deviate, and this deviation may change with different operating conditions. The model as well relies upon experimental measurements (exhaust temperature, cylinder pressure) which have inherent uncertainties. Carrying through a calculation for absolute total uncertainties for a quantity such as internal residual exhaust gas would give uncertainties much greater than encountered for the day to day operation of experiments. For this reason the experimental repeatability will be reported, and demonstrated by means of error bars when a quantity (such as iEGR fraction) is first introduced in a plot, but for the sake of graphical clarity will not be included on every plot.

Table 2.2 Experimental Repeatability of Gasoline Baseline Operating Condition

Experimental Parameter	Mean	Std. Deviation (1σ)
Fueling Rate [mg/cycle]	9.0	0.05
Maximum Pressure [bar]	45.9	0.72
Maximum Pressure Location [°ATDC]	6.2	0.49
$IMEP_g$ [bar]	3.1	0.04
NO_X, wet [ppm]	3.0	0.33
IVC Temperature [K]	492	5.1
IVC Pressure [bar]	1.2	0.01
Ringing Intensity [MW/m^2]	2.4	0.31
Total EGR fraction	0.53	0.01
CA10 [°ATDC]	-1.7	0.63
CA50 [°ATDC]	2.5	0.59
CA90 [°ATDC]	9.0	1.8
10 – 90 burn duration [°CA]	10.7	1.2

When error bars (either horizontal or vertical) are present on any data points in a plot, any data points without error bars (or lacking error bars for the opposing axis) are represented as such due to the fact the error bars are equal to or less than the size of the data markers.

For each fuel, a baseline condition for a given fueling rate, combustion phasing, and equivalence ratio was established and repeated each morning before conducting a complete set of experiments. The experimental repeatability reported here is calculated from the compilation of measured baseline conditions for gasoline conducted over the months during with this data was collected. Repeatability for engine relevant operation conditions are reported in Table 2.2, where the mean and standard deviation represent a 95% confidence level.

2.3   Operational Methods

2.3.1   Energy Matching of Fuels

Fuels specific to each set of experiments will be discussed in the chapter to which they pertain. However, each of the different test fuels have different lower heating values (LHV), so it was necessary to adjust fuel mass flow to maintain constant energy addition per cycle. In addition to maintaining energy per cycle constant, it was desirable that energy addition rates be comparable for engines of different displacement (looking to future work).

To this end a new quantity, energy mean effective pressure (EMEP) was defined (Equation 2.1), recognizing that energy per cycle divided by engine displacement has the units of pressure. This is equivalent to what Olsson termed FuelMEP [82] and is an effective pressure for the energy addition. The term FuelMEP lends itself to the abbreviation of FMEP, which could be easily confused with the standard abbreviation for Friction MEP [28, 83]. To avoid this confusion the term EMEP was chosen to represent, based on energy addition, the effective pressure that would be attained if there were no losses and 100% combustion efficiency. A convenient byproduct of this definition is that the indicated thermal efficiency is then simply the quotient of IMEP and EMEP.

$$
\text{EMEP [bar]} = \frac{Energy\ Addition\left[\dfrac{J}{cycle}\right]}{Displaced\ Volume[L]\cdot 100}
$$

(2.1)

$$
= \frac{LHV\left[\dfrac{J}{kg}\right]\cdot Fuel\ Flow\left[\dfrac{kg}{min}\right]\cdot\dfrac{2revs}{1cycle}\cdot\dfrac{1}{RPM}}{Displaced\ Volume\ [L]\cdot 100}
$$

As an example of how EMEP relates for fueling rate Table 2.3 provides a comparison of the required fueling rate in mg/cycle for the test fuels in this document at the 9.0 bar EMEP condition. The 9.0 bar EMEP condition is the primary load for comparison in this document.

39

Table 2.3 Fueling rates based on Lower Heating Value at 9.0 bar EMEP for the FFVA Engine

Fuel	PRF40	PRF60	NH40	Gasoline	Iso-Octane
LHV [kJ/kg]	44444	44401	43649	43043	44316
Energy Addition [J/cycle]	495	495	495	495	495
Fueling Rate [mg/cycle]	11.12	11.13	11.34	11.50	11.17

Given the similar LHV of the fuels, the difference in nominal mass fueling rate for the same EMEP is small (the largest percent difference in mass flow rate is 3% between gasoline and PRF40).

2.3.2 Combustion Constraints

Acceptable combustion limits for this study fell under three criteria: advanced combustion phasing limits, retarded combustion phasing limits, and acceptable emissions. The advanced combustion limit is termed the Ringing Intensity (RI) and was developed by Eng [84]. The equation for the correlation is given below in Equation 2.2. As a quantification of the intensity of pressure pulsations in-cylinder, the RI correlation has as inputs the pressure rise rate ($(dP/dt)_{max}$, where t is time), peak cylinder pressure (P_{max}), maximum in cylinder temperature (T_{max}), the ratio of specific heats of the mixture (γ), the gas constant (R). The scaling factor $\beta = 0.05$ ms relates the pressure pulsation amplitude to the maximum rate of pressure rise.

For these results, the RI was calculated for each cycle after applying a low pass 3.5 kHz filter. A study reported by Vavra [85] found that under HCCI conditions the use of a low pass filter provided the same slope for R.I. as a function of load, but resulted in a higher R.I. value compared to the high pass filter. The low pass filter is thus the more conservative method. The reported RI is the mean RI of the computed RI of the entire 200 recorded cycles. Applied to the average, an RI limit of 5 MW/m^2 was used as the advanced combustion limit for it coincided with the onset of audible knock and high frequency pressure oscillations. This combustion limit was applied to conditions in Chapter 3 in determining the advance

limit of combustion phasing. For the studies in Chapter 5 this limit was not enforced, as the requirement of fixed combustion phasing across wide variations in iEGR necessitated the lifting of this limit. Any production implementation with a lower octane fuel is however understood to fall within this constraint, as the data in Chapter 3 does. For the experiments in Chapter 6, the combustion was intentionally retarded to higher COV of $IMEP_g$ condition, at which all the cases had a RI less than 5 MW/m^2.

$$\text{Ringing Intensity} \approx \frac{1}{2\gamma} \cdot \frac{\left(0.05 \left(\frac{dP}{dt}\right)_{max}\right)^2}{P_{max}} \cdot \sqrt{\gamma R T_{max}} \tag{2.2}$$

The retard limit for HCCI is considered to be the point where combustion becomes unstable, with the instability criteria being a coefficient of variance (COV) of gross indicated mean effective pressure ($IMEP_g$) of 5%. This was the criteria used to determine the retarded phasing limit in Chapter 3. In Chapter 5 the CA50 is fixed at $6° ATDC$ where it is highly stable and all cases are well under the COV of $IMEP_g$ limit. For Chapter 6 the COV of $IMEP_g$ was intentionally fixed at 3%, a condition found to be operable across a wide range of engine speed and iEGR.

Chapter 3

Fuel Specific Load Limits in NVO HCCI Combustion

Low octane fuels have been demonstrated to achieve a higher load limit [66, 86] and benefit from increased ITHR [70], but these previous studies were performed in "pure" HCCI engines, utilizing high levels of intake preheat to accomplish autoignition. The purpose of this study is to investigate the effects of low octane fuels on HCCI load limits with an NVO engine utilizing high levels of internal residual (iEGR).

This study has been presented at the ASME Fall ICE Conference [87] and published in the ASME Journal for Gas, Turbines and Power [74].

3.1   Test Fuels

In this study, three fuels were utilized to compare the effect of octane number. The baseline fuel, henceforth referred to as "gasoline," is a research grade gasoline supplied by ChevronPhillips with an anti-knock index (AKI, equal to the average of the RON and MON) rating of 87. The RON and MON of the gasoline are controlled to 90.5 and 82.6, respectively, as listed in Table 3.1, such that both the fuel sensitivity and AKI are the same from batch to batch.

As noted earlier, low octane fuels have demonstrated benefits to HCCI combustion [66, 70, 71, 86]. The approach taken was to blend n-heptane with gasoline, as this made for a multi-component fuel which would potentially be more representative of an actual lower octane refinery fuel compared to a primary reference fuel. The blend chosen is comprised of 40% n-Heptane by mass (41.9% by volume). The RON and MON of the NH40 fuel are 58.1 and 56.4 respectively for an AKI of 57.2, which is more in line with a naphtha fuel

as proposed by Shibata [86]. An actual naphtha fuel would require less processing at the refinery.

To complete the fuel test matrix, iso-octane was included as a higher octane fuel. The difference in octane rating between iso-octane and gasoline was small compared to that of gasoline and n-heptane, so rather than using a higher octane blend (as was done for the NH40), pure iso-octane was selected for a higher octane fuel, completing the test fuel matrix and providing a range of octane above and below the gasoline baseline. For simplicity, from this point forward octane number (ON) will be used to denote the differences in octane rating between the fuels, with NH40 having the lowest ON and iso-octane the highest.

As the three test fuels have different lower heating values (LHV), it is necessary to adjust fuel mass flow to maintain constant energy addition per cycle. In addition to maintaining energy per cycle constant, it was desirable that energy addition rates be comparable for engines of different displacement (looking to future work). Hence a new quantity, energy mean effective pressure (EMEP) was defined (Equation 2.1), recognizing that energy per cycle divided by engine displacement has the units of pressure. This is equivalent to what Olsson termed FuelMEP [82] and is an effective pressure for the energy addition. The term FuelMEP lends itself to the abbreviation of FMEP, which could be easily confused with the standard abbreviation for Friction MEP. To avoid this confusion the term EMEP was chosen to represent, based on energy addition, the effective pressure that would be attained if there were no losses and 100% combustion efficiency. A convenient byproduct of this definition is that the indicated thermal efficiency is then simply the quotient of IMEP and EMEP.

3.2   Operational Procedure

The FFVA engine utilizes a higher compression ratio (12.5:1) than a typical SI engine, but less than a typical diesel. The higher compression ratio helps enable auto-ignition, however hot residual is still required for auto-ignition to occur. Thus HCCI operation in the FFVA is

43

Table 3.1   Test fuel properties

Property	iso-octane	Gasoline	NH40
LHV [kJ/kg]	44316	43043	43649
Density [g/mL]	0.692	0.736	0.721
MW [g/mol]	114.2	93.0	96.4
H/C [molar]	2.250	1.879	2.070
RON	100	90.5	58.1
MON	100	82.6	56.4
AKI [(R+M)/2]	100	87	57.2
Paraffins [% WGT]	0	8.1	44.9
Iso-Paraffins [% WGT]	100	37.5	22.5
Aromatics [% WGT]	0	32.3	19.4
Naphthenes [% WGT]	0	16.9	10.1
Olefins [% WGT]	0	4.5	2.8
Boiling Point [°C]	99	N/A	N/A
10% Evaporation [°C]	N/A	62	78
50% Evaporation [°C]	N/A	95	99
90% Evaporation [°C]	N/A	145	125

typically done through either recompression or rebreathing. A previous simulation-based study by Babajimopoulos [40] investigating the merits of recompression vs. rebreathing found that at lower loads recompression was more efficient due to less pumping losses. Additionally, the use of a fully flexible valve system allows variation of the duration of negative valve overlap without impacting IVC and EVO timings. Thus, for this work a recompression approach was taken to HCCI operation.

Utilizing an NVO enabled recompression strategy, the experimental procedure was to "map" the operational range of each of the test fuels by sweeping NVO at increasing EMEP levels. The general engine conditions are given in Table 3.2. For a given EMEP combustion phasing was advanced, via increasing the amount of NVO to increase the level of hot residual, until the ringing intensity (RI) limit was reached. The correlation for RI was developed by Eng [84] and the correlation is given below in Equation 2.2. As a quantification of the intensity of pressure pulsations in-cylinder, the RI correlation has as inputs the pressure rise rate ($(dP/dt)_{max}$, where t is time), peak cylinder pressure (P_{max}), maximum in cylinder

temperature (T_{max}), the ratio of specific heats of the mixture (γ), the gas constant (R). The scaling factor $\beta = 0.05$ ms relates the pressure pulsation amplitude to the maximum rate of pressure rise.

For these results, the RI was calculated for each cycle after applying a low pass 5 kHz filter. The average RI was then determined for the 200 recorded cycles, and this value is reported. Applied to the average, an RI limit of 5 MW/m^2 was used as the advanced combustion limit for it coincided with the onset of audible knock and high frequency pressure oscillations.

From the most advanced condition with a ringing intensity of 5 MW/m^2, the duration of NVO was decreased at increments of 2–4 degrees; for stable conditions 4° increments were used but lowered to 2° as combustion became more unstable. Eventually combustion would retard to a point where it became unstable, with the instability criteria being a coefficient of variance (COV) of gross indicated mean effective pressure (IMEP$_g$) of 5%. For some fueling rates, the most retarded point would have a COV of IMEP$_g$ lower than that of 5%, but further reduction of NVO by another 2° would lead to misfire.

After sweeping from the advanced (ringing intensity) limit to the retard (COV of IMEP$_g$) limit, the fueling rate was increased and the sweep was performed again. The sweep was continued for increasing EMEP levels until the sweep has only one point within the combustion limits, or the limits are separated by 2° of NVO.

3.3 Experimental Results

3.3.1 Operating Range

As described in the Operational Procedure, the operational "map" was obtained for each fuel. For gasoline this is shown in Figure 3.1, with a quadrilateral overlaid, highlighting the limits of load (IMEP$_g$) on the vertical axis, and the combustion phasing (CA50) on the horizontal

Table 3.2 Experimental parameters

Parameter	Value
Engine Speed [RPM]	2000
Fuel Injection Pressure [bar]	≈ 100
Fuel Start of Injection [° BTDC]	330
Intake Temperature [°C]	45
Abs. Intake Pressure [bar]	1.0
Abs. Exhaust Pressure [bar]	1.05
Coolant Temperature [°C]	90
Oil Temperature [°C]	90
Ringing Intensity Limit [MW/m^2]	5.0
COV of IMEP$_g$ Limit [%]	5.0
Emissions Index NO$_X$ [g/kg-fuel]	<1.0
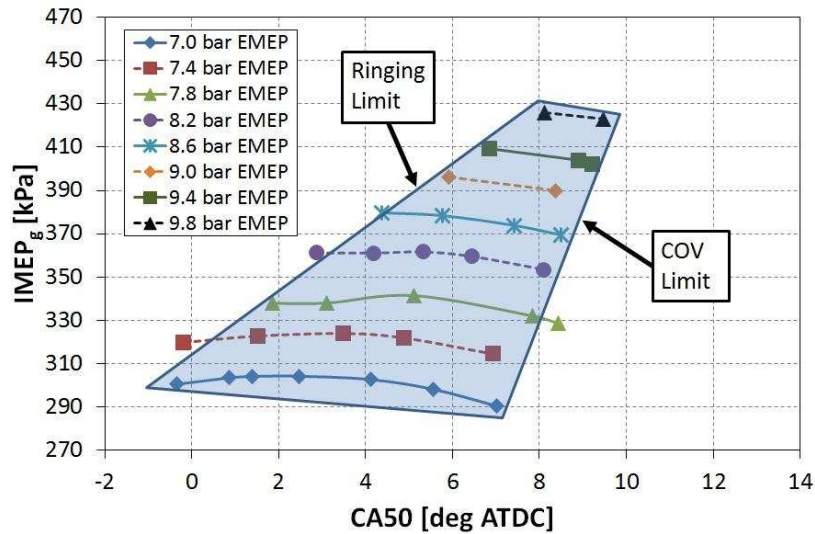
Figure 3.1 Operational range of the baseline gasoline

axis. It is observed that the ringing limit dictates the left side of the quadrilateral, and the COV limit the right. As the EMEP is increased, the operational range, in terms of attainable combustion phasing, decreases until a point is reached where there is a single operating point that is simultaneously at the ringing and COV limit. In practice, a single point that was simultaneously at both combustion limits was not always reached due to combustion instability. For the case with gasoline the highest attainable EMEP held two points that fell within the combustion limits, one at the ringing limit and the other at the COV limit.
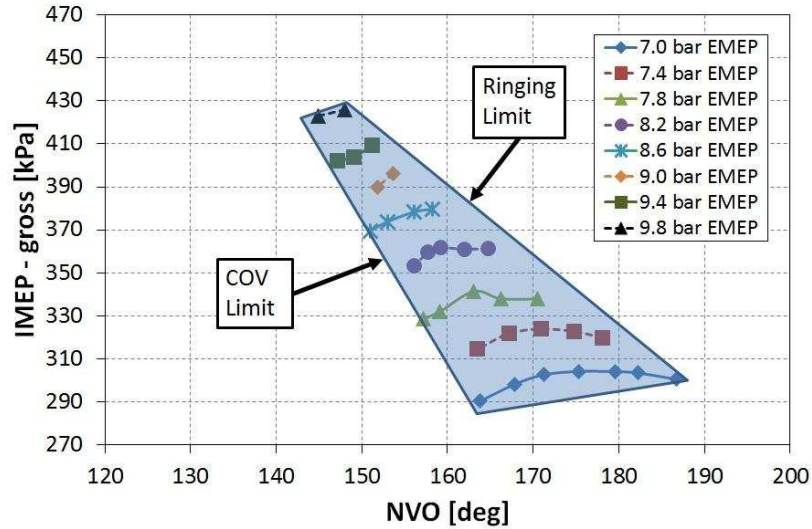
Figure 3.2 NVO range of the baseline gasoline

Starting from the most advanced point, each shift in CA50 in Figure 3.1 (at a given EMEP) corresponded to a reduction in the duration of NVO (Figure 3.2). Plotted in Figure 3.3 are the overlain operational maps for $IMEP_g$ as a function of NVO for the full sweep for each fuel. The required duration of NVO trends with the ON of the fuel; iso-octane requires the most NVO, followed by gasoline, and NH40 requires the least. A longer duration of NVO traps more hot residual in cylinder per cycle, advancing combustion. Iso-octane, with the highest ON, is least prone to autoignition and thus requires more hot internal residual to burn at a given combustion phasing than gasoline. Similarly, the NH40, with the lowest ON requires less NVO and thus less hot internal residual to match combustion phasing with the gasoline.

For the gasoline cases shown in Figure 3.1, the peak of the load range is in part dictated by the physical limitations of the hydraulic valve system. The difference in duration of NVO between the operating points at the maximum EMEP case (9.8 bar) for gasoline, as shown in Figure 3.2, is 4° but results from a 2° decrease in commanded NVO. This is due to the fact, as previously mentioned, that the commanded valve timing has an operational tolerance of ± 1°. While the absolute magnitude of the peak IMEPs might change for the fuels with less
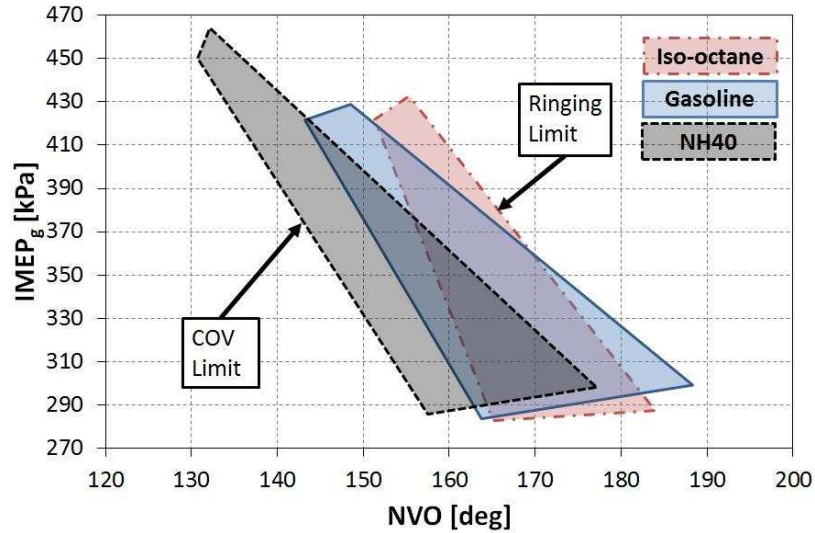
Figure 3.3 Comparison of required NVO for the three test fuels

variation in valve timing, the comparative ordering of maximum IMEP$_g$ for the fuels would not change; the instability merely shifts the upper limit.

3.3.2 Load Limits

The load range of all three test fuels are overlain in Figure 3.4. For clarity, most of the EMEP sweep points have been removed, leaving the representative quadrilaterals for each fuel. The data points for 9.0 bar EMEP for the three fuels, as well as the load limit points at 9.8, 10.0, and 10.2 EMEP have been included as they will be discussed in more detail. The most salient feature of Figure 3.4 is the load range of NH40 compared with iso-octane and gasoline. The iso-octane and gasoline fuels exhibit a nearly identical peak IMEP$_g$ of ~430 kPa, both occurring at an EMEP of 9.8 bar. The NH40 exhibits a higher peak load, an IMEP$_g$ of 460 kPa, or 7% increase over gasoline, at an EMEP of 10.2 bar. This higher load occurred for the NH40 at a markedly later CA50. In fact, the CA50 location of peak EMEP for each fuel retarded with decreasing ON. While both the iso-octane and gasoline fuels exhibited a similar peak IMEP$_g$, the actual peak occurred at a CA50 of 7.0° ATDC for iso-octane and at 8.1° ATDC for gasoline. For NH40, the peak load occurs even later, at
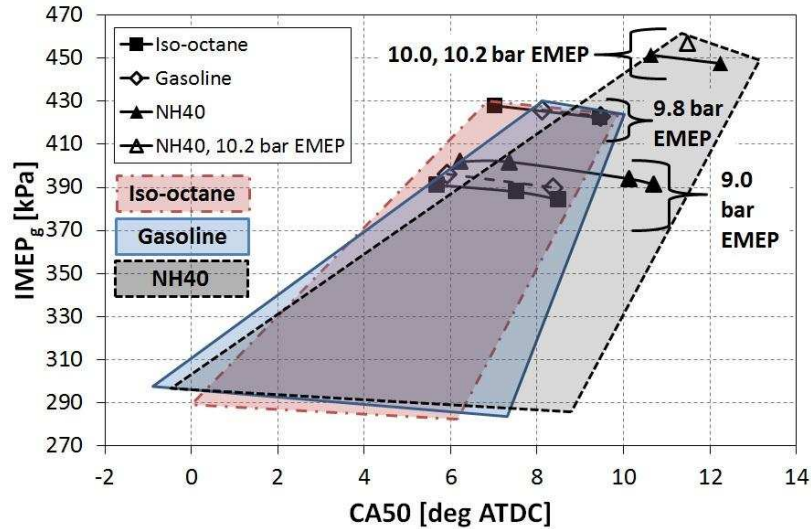
Figure 3.4 Overlaid operational range of the test fuels, highlighting the 9.0 bar EMEP and peak EMEP cases

11.5° ATDC.

An interesting observation is that for a given EMEP, the lower octane fuels exhibit a higher $IMEP_g$ across the sweep, as shown in Figure 3.5 for the 9.0 bar EMEP sweeps. To further understand this, pressure traces from the most advanced case for each fuel in Figure 3.5 are plotted in Figure 3.6. While all three fuels initially follow the same compression path, they start to diverge around 40°BTDC. At TDC the difference in cylinder pressure between iso-octane and NH40 is ∼1.5 bar. Compared to the higher ON fuels, the NH40 cases operate leaner, and at a lower temperature with less internal residual. From this, a reasonable explanation for the increase in compression pressure and $IMEP_g$ is due to a higher gamma (γ, the ratio of specific heats, C_P/C_V) for the NH40 cases, as the equivalence ratio is leaner for NH40 compared with the iso-octane and gasoline, as shown in Figure 3.5.

The NH40 has a higher $IMEP_g$ for a given EMEP, and from this a higher indicated thermal efficiency. As the EMEP is pushed higher, thermal efficiency continues to increase. This effect is shown in Figure 3.7 for NH40 at 10.0 bar EMEP and iso-octane and gasoline each at 9.8 bar EMEP. While peak $IMEP_g$ for the NH40 occurred at 10.2 bar EMEP, only one point was stable and within the combustion limits. Whereas at 10.0 EMEP the NH40
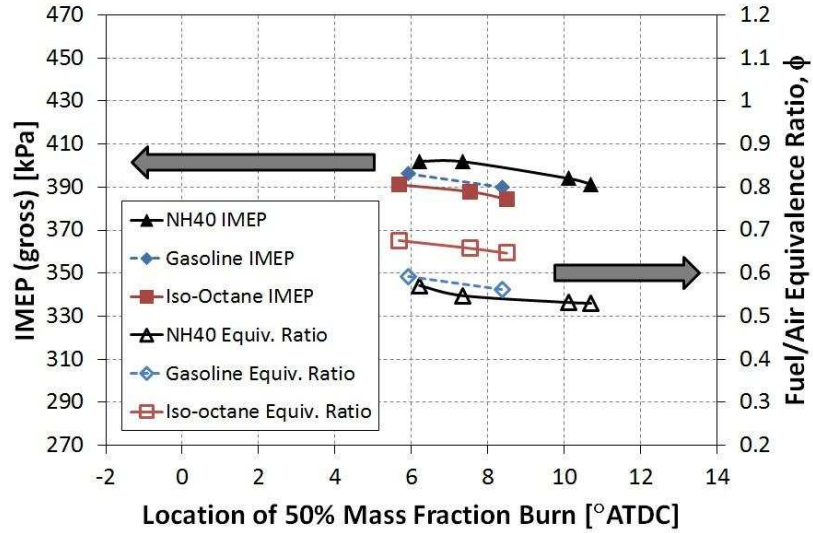
Figure 3.5 Comparison of IMEP$_g$ for sweeps at 9.0 bar EMEP
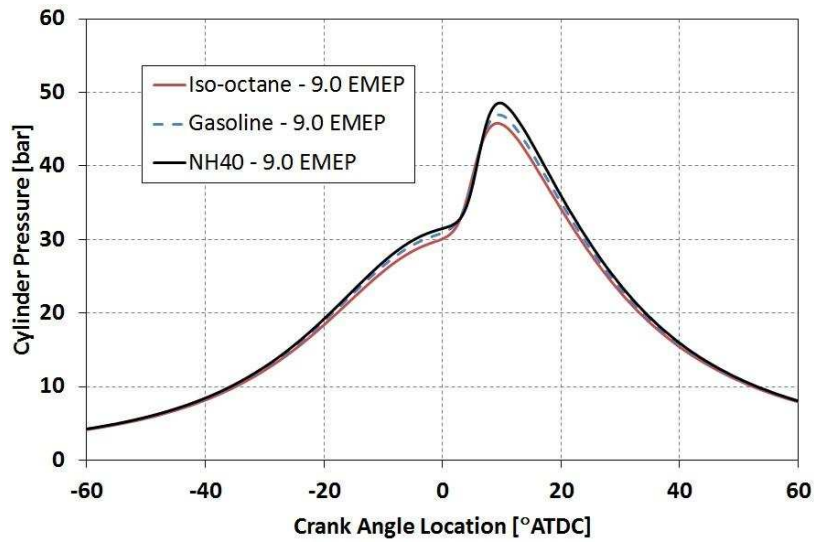
Figure 3.6 Cylinder pressure trace for the most advanced cases at 9.0 bar EMEP

operated with two stable points within the combustion limits. So for the sake of consistency, and identifying trends, plots at "peak IMEP$_g$" will use the 10.0 bar EMEP cases for NH40 and the 9.8 bar EMEP cases for iso-octane and gasoline.

Again highlighting Figure 3.7, there are several things to note. First, the 10.0 bar EMEP case at the earliest phasing for the NH40 fuel demonstrated the highest indicated thermal efficiency for all conditions in the experiment, 45% (the single point at 10.2 bar EMEP, not

shown, was 44%). As the duration of NVO is decreased for a given fuel and EMEP, thermal efficiency drops off. This is due to the resulting retarding of combustion further into the expansion stroke, and is evidenced by combustion efficiency decreasing $\sim$1% (from $\sim$ 96% to $\sim$ 95%) across the sweep for all fuels at these conditions.

Decreasing the duration of NVO at a fixed EMEP brings a corresponding decrease in equivalence ratio, ϕ, leaning the mixture as was noted for Figure 3.5. Since the EMEP remains constant for a given fuel in this test, the fuel/charge equivalence ratio, ϕ', remains constant. The fuel/charge equivalence ratio is defined in Equation 3.1 and is the traditional fuel/air equivalence ratio recast as a measure of the energy density of the charge [40, 88]. In Equation 3.1 the mass of fuel, air, and residual gas fraction are denoted by F, A, and RGF respectively with ϕ being the fuel/air equivalence ratio. The final approximation holds because the second term in the denominator is small compared to unity. Due to the resulting change in charge mass with varying NVO, ϕ' can be seen to vary slightly, but in general for a sweep at constant EMEP, ϕ' stays essentially constant.

$$\phi' \equiv \frac{Fuel/Charge}{(Fuel/Air)_{ST}} = \frac{F/(A+R)}{(F/A)_{ST}}$$

$$= \phi \cdot \frac{(1-RGF)}{(1+RGF \cdot \phi \cdot (F/A)_{ST})} \qquad (3.1)$$

$$\approx \phi \cdot (1-RGF)$$

3.3.3 Combustion Phasing Limits

Having demonstrated that the lower ON NH40 fuel can operate at a higher EMEP and $IMEP_g$ with a higher thermal efficiency, the question arises as to the exact enablers for
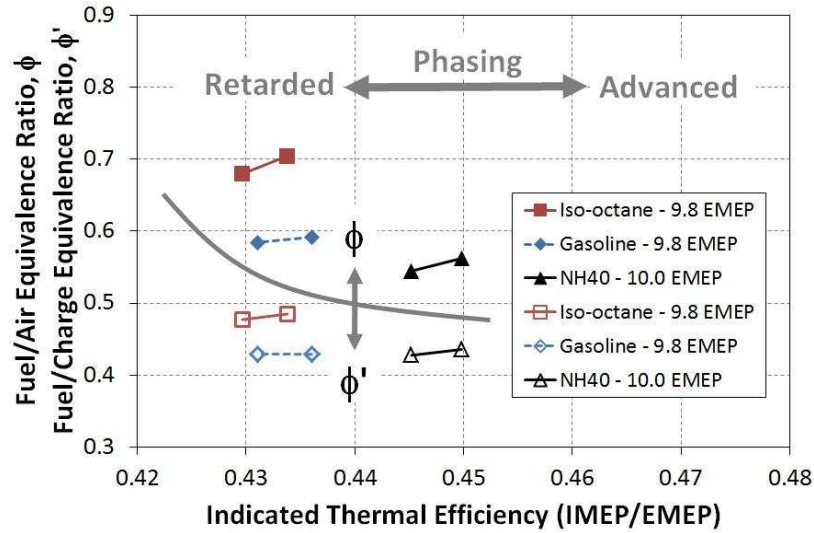
Figure 3.7 Comparing Fuel/Air (ϕ) and Fuel/Charge (ϕ') Equivalence Ratio with Thermal Efficiency

operating at a higher EMEP. To gain a better understanding of these enablers, the advanced and retarded combustion limits for a given EMEP sweep are examined. At the advanced side of the quadrilaterals in Figure 3.4, combustion is limited by the RI. To further examine this, the heat release rates (HRRs) corresponding to the pressure traces in Figure 3.6 are shown in Figure 3.8.

The HRRs for the most advanced combustion cases at 9.0 bar EMEP demonstrate that the NH40 has an absolute peak HRR that is higher than the higher ON fuels, which would correspond to a higher maximum pressure rise rate, which can be seen from Figure 3.6. For the most advanced case at 9.0 bar EMEP, the NH40 has a ringing intensity of 4.8 MW/m^2, as shown in Figure 3.10 comparing burn duration to combustion phasing. As expected based on the HRR, the RI of the NH40 is higher compared to iso-octane and gasoline which have ringing intensities of 3.4 and 3.9 MW/m^2, respectively. The gasoline and iso-octane are not at the limit of 5 MW/m^2 due to the fact that in some cases, a further addition of 2° of NVO would put combustion over the RI limit. So the higher HRR for the NH40 at the advanced limit is not necessarily a function of the fuel but a product of the RI limit imposed while performing the sweep.

Looking in Figure 3.10 at the two cases where both NH40 and iso-octane have a CA50 $\sim$7.5° ATDC, the NH40 has a RI of 3.7 MW/m^2 compared with 2.4 for iso-octane. So for a given EMEP and combustion phasing, the NH40 has a higher RI. Looked at another way, compared to higher ON fuels, the NH40 must be phased later to maintain the same RI (and thus HRR) for a given EMEP, and that the NH40 will be phased later than the iso-octane and gasoline at the advanced limit imposed by the RI constraint.

The average cylinder temperature (inferred from the heat release analysis) and HRR for the most retarded combustion points at the peak load EMEPs are plotted in Figure 3.9. The peak load points were selected for comparison because the differences in combustion phasing between the fuels is much more pronounced at the highest load.

The fact that the NH40 is burning at more retarded phasing is easily discerned from the heat release traces in Figure 3.9. Despite the later combustion phasing, the NH40 is still able to approach a peak cylinder temperature close to gasoline at just over 2000K, but at a later phasing. Work by Sjöberg [89] has demonstrated that the peak cylinder temperature correlates strongly with the ability to complete the burn in HCCI engines. Babajimopoulos [40] noted that for late cycle limits a failure to ignite dominated at higher loads, and a failure to burn (bulk quenching) at lower loads. The loads and phasing considered in this section are close to the boundary line between a failure to ignite and a failure to burn. The next section will examine the burn duration and phasing of the fuels in this study to better understand the nature of the late combustion phasing limits.

3.3.4 Burn Duration

For each fuel, the 9.0 bar EMEP sweep was selected to examine the effects of burn duration on the combustion phasing limits. Burn duration, defined as the time between the location of 10% mass fraction burned (CA10) and 90% mass fraction burned (CA90) is plotted against CA50 in Figure 3.10. The combustion limits (RI and COV) have been applied for convenient reference. In the figure, it is apparent that the operational range in terms of CA50 increases
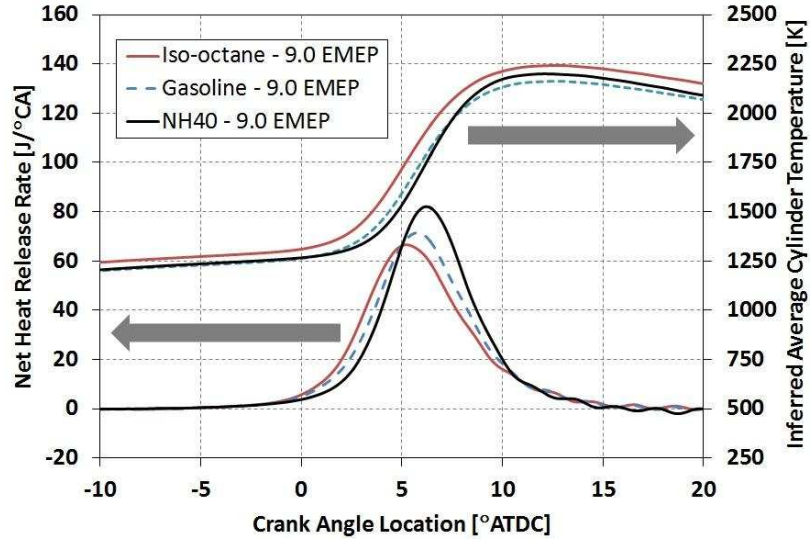
Figure 3.8 Heat release and inferred average cylinder temperature for the most advanced cases at 9.0 bar EMEP
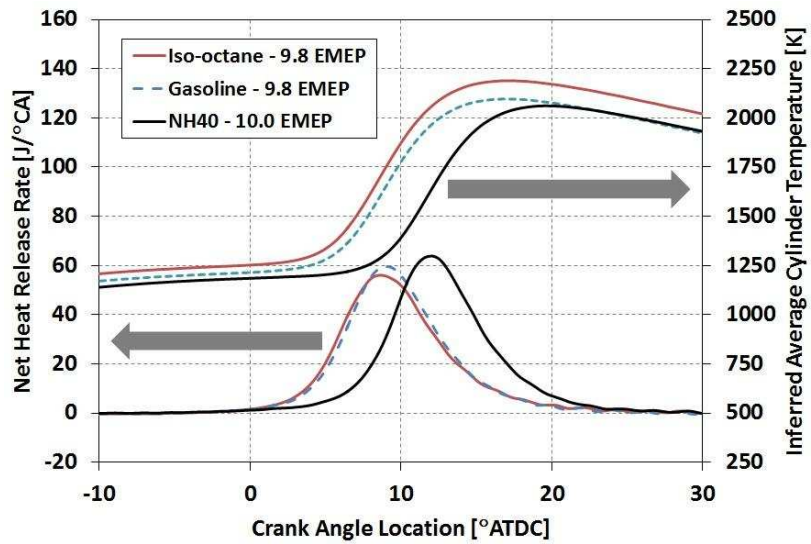
Figure 3.9 Heat release and inferred average cylinder temperature at the most retarded phasing at the highest EMEP

as ON decreases and that the spread in CA50 between the fuels for a given burn duration increases as combustion retards. As combustion is retarded for all three fuels (via reduced NVO), burn duration increases, as auto-ignition is occurring later into the expansion stroke, and the expansion process serves to counteract the pressure and temperature rise due to combustion.

Figure 3.10 also shows that lower ON fuels demonstrate shorter burn durations for a given CA50. The iso-octane requires the longest time, in CAD, to burn for a given phasing. The gasoline exhibits a slightly shorter burn duration, ~10% or ~1 CAD less across the sweep, compared with iso-octane. The NH40 more than doubles that difference, demonstrating a burn duration at least 20% less (~2 CAD) than iso-octane across the sweep.

Figure 3.11 compares iso-octane, gasoline, and NH40 at the highest attainable EMEP NVO sweep for each respective fuel (9.8 bar EMEP for iso-octane and gasoline, 10.0 bar EMEP for NH40). Here again, the iso-octane and gasoline are operated at the same EMEP (consistent with Figure 3.10) and gasoline demonstrates a shorter burn duration for a given combustion phasing. For the NH40, it is observed that there is no overlap in combustion phasing between this fuel and iso-octane and gasoline. The NH40, operated at a higher EMEP and $IMEP_g$ is phased significantly later, outside the CA50 range of the other fuels. However, it is noticed that the burn durations for the NH40 points closely match those for gasoline. For the advanced cases, both gasoline and NH40 have a 10-90 burn duration of ~9 CAD, and for the retarded cases a 10-90 burn duration of ~11 CAD.

From Figure 3.10, in addition to the NH40 having a shorter burn duration at a constant phasing, the most retarded phasing was later than that for the iso-octane and gasoline. Comparing the burn duration of the latest points of iso-octane and NH40 (the gasoline, as it was not as late with regards to the COV limit, was not used for this comparison) against both CA50 and CA90 in the lower graph of Figure 3.12 shows that while there is $\sim 2°$ spread between the CA50 of these two points, the difference in CA90 is only ~0.5°. This shows that combustion between the fuels is completed at close to the same location, but the faster burn of the NH40 allows the phasing to be later.

In the upper graph of Figure 3.12, the burn duration at the late CA50 phasing limit for the peak load cases is plotted against CA50 and CA90. Again, the spread in phasing noted for CA50 (~3°) is reduced for the CA90 (~1°). In this case the NH40, operating at a higher EMEP than this iso-octane, completed combustion at near the same time despite a later
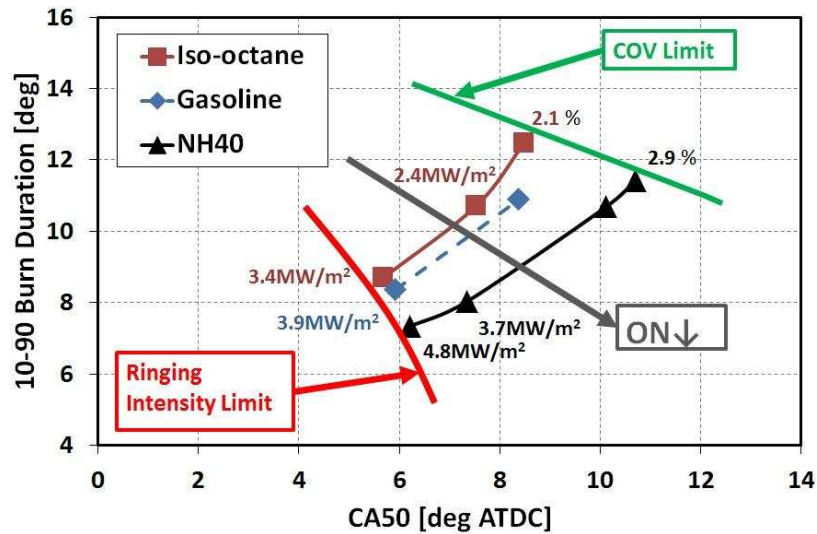
Figure 3.10   Decreasing burn duration with lower octane fuels at 9 bar EMEP

CA50 phasing due to a shorter burn duration compared with the iso-octane.

The fact that the CA90 values for the two fuels at both 9.0 EMEP and peak load are very similar suggests that the late cycle limit is dictated by a failure to burn. From Figure 3.12 at 9.0 bar EMEP that limit appears to be around 17° ATDC. Taken as the late cycle limit, combustion phased later than this would be quenched by the cylinder expansion and result in mis-fire.

For both the 9.0 bar EMEP and peak EMEP cases of Figure 3.12 (the lower and upper graphs, respectively), the NH40 had a CA90 slightly later than that of the iso-octane. Rather than a fuel effect, this is likely a function of the last stable point taken for each NVO sweep. Noting the COV of IMEP$_g$ values in Figures 3.10 and 3.11, the NH40 had a slightly higher COV of IMEP$_g$ for all the cases, which corresponds to the slightly later phasing of the NH40 compared with iso-octane.
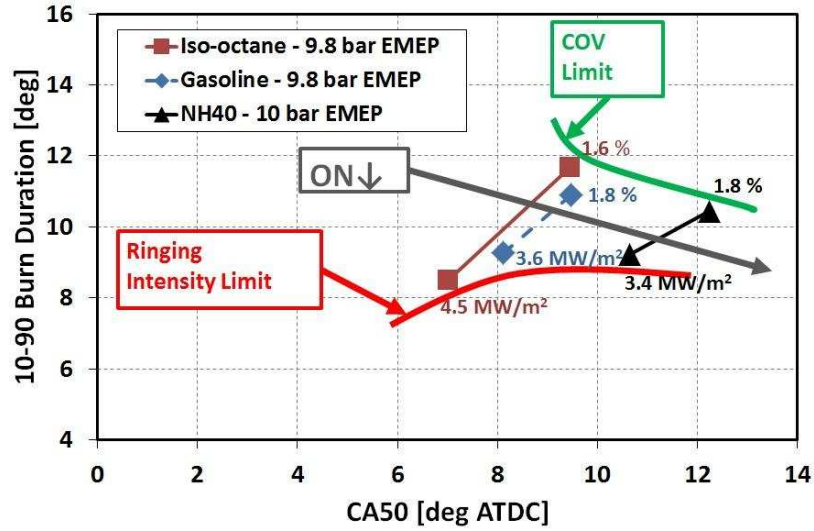
Figure 3.11 Comparison of burn duration at peak load sweeps for the three fuels
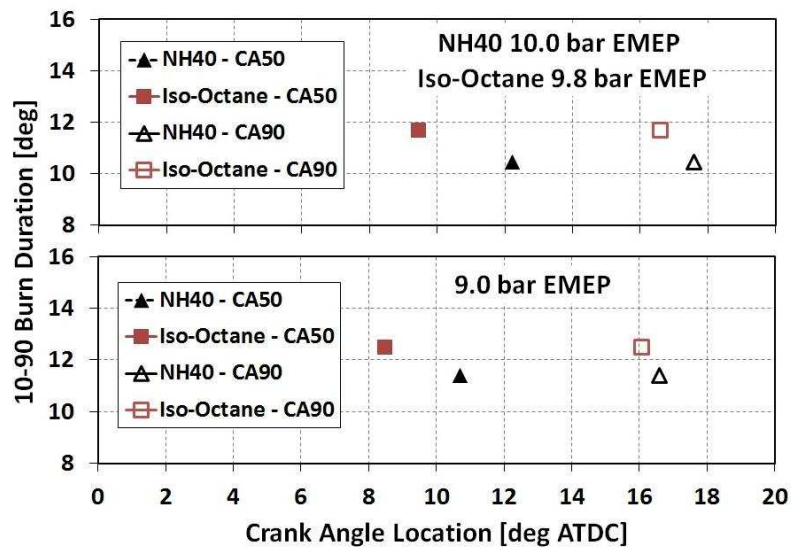
Figure 3.12 Comparison of the 10-90 burn duration to CA50 and CA90 at 9.0 bar EMEP (lower graph) and peak load (upper graph — 9.8 bar for Iso-octane, 10.0 bar for NH40) EMEP for Iso-octane and NH40

3.4 Discussion

3.4.1 Enablers to a Shorter Burn Duration

It has been demonstrated that the fuels with a lower ON exhibited a shorter burn duration, especially the NH40 fuel. This shorter burn duration requires a later phasing for the NH40 at the RI limit, and enables a later phasing at the COV/instability limit, the latter affording higher loads within the RI constraint. So while the NH40 is documented to burn faster and this behavior demonstrates a benefit to combustion load limits for NVO enabled HCCI combustion, the question that remains is what enables the NH40 fuel to have a shorter burn duration than the higher ON fuels.

Several factors could contribute to enabling a shorter burn duration, and will be explored in this section. The most obvious factor to consider is the effect that NVO variation has on the combustion burn duration. Reducing NVO leads to an increase in the amount of fresh charge inducted, increasing the oxygen concentration. The increase in burning speeds in the presence of more oxygen is documented and could lead to a shorter burn duration. Coupled to the oxygen effect is the fact that as NVO decreases, so does the level of EGR in-cylinder. Recycled exhaust gas has a higher specific heat than ambient air (and a lower specific heat ratio, γ) and as such serves to reduce temperature rise, and thus pressure rise rates, which in turn lengthens the burn duration.

Related again to changes in NVO, but separate from the chemical effects of the gas composition, are stratification effects. Reducing the level of required NVO, as NH40 does, tends to reduce both compositional and thermal stratification. Compositional stratification results from poor mixing of the EGR with the fresh charge and fuel spray, with both overly lean and overly rich pockets existing within the cylinder. Thermal stratification, within NVO operation, is to some degree a byproduct of compositional stratification — the internal EGR is very hot compared to the relatively cold fresh incoming mixture, and temperature gradients

58

arise when these hot and cool gases do not have time to fully mix. Both compositional and thermal stratification can serve to increase the length of the burn, so reducing the amount of NVO, and thus internal EGR, serves to reduce stratification and shorten the burn duration.

Lastly, the fuel itself can have properties which impact the burn duration. Different fuel chemistry properties will under certain conditions enable so-called low temperature heat release (LTHR) and intermediate temperature heat release (ITHR). Both are quantifiable net heat release events before the main combustion event. This early burn serves to prepare the mixture for the main event and leads to a faster overall burn.

3.4.2 Oxygen Concentration

A recent study performed at UM by Manofsky Olesky [90] (utilizing the same FFVA engine as in this work) looked at comparing the effect of air versus internal EGR dilution with a recompression strategy. One of the key findings was that the use of air dilution with intake heating, used to reduce the required level of NVO (and thus internal residual) led to a shorter overall burn duration across the sweep for a fixed fueling rate. The increased oxygen concentration that corresponds to operating with a reduced NVO/RGF level with intake heating could impact the burn duration.

Examining how the oxygen concentration changes across an NVO sweep, Figure 3.13 (right axis) shows the estimated oxygen concentration at 9 bar EMEP for the all three fuels. As in-cylinder oxygen concentration is not directly measured, it is inferred from the measured equivalence ratio and the inferred internal residual calculations. The mass based O_2 values presented in Figure 3.13 are estimated as follows. There are two parts to the mixture, unburned (fresh) and burned (residual). For the fresh portion, the O_2 mass fraction can be considered to be that of O_2 in air, 23% (neglecting the fuel, which is a small fraction). For the burned portion, the O_2 concentration is 0.23*(1 - ϕ), where for ϕ = 1 all of the O_2 was consumed in the previous cycle, and for ϕ = 0 there was no O_2 consumed. For the unburned mixture the total O_2 concentration then is (1 - RGF)*0.23, and for the burned it is

(RGF^*O_2). Combining this we arrive at Equation 3.2.

$$O_2 \text{ Fraction} \approx 0.23 \cdot [(1 - RGF) + RGF \cdot (1 - \phi)]$$

(3.2)

$$= 0.23 \cdot (1 - \phi \cdot RGF)$$

Comparing the oxygen values in Figure 3.13, the NH40 has approximately 9% more O_2 than the iso-octane across the sweeps, and ∼4% more than the gasoline. While this difference may seem small, it can bring a significant difference in ignition and burn characteristics. For example, the autoignition correlation developed for HCCI combustion by He [91] demonstrates a dependence on the concentration of O_2. Using the correlation, the 9% difference in O_2 fraction shown between iso-octane and NH40 would bring about a 13% difference in ignition delay. This is not to suggest that burn duration scales with ignition delay, but to note that the magnitude of the difference in O_2 concentration between these fuels, due to the difference in required NVO, is not insignificant with regards to combustion. Furthermore, the magnitude of the difference in O_2 concentration, and the estimated impact on ignition delay, are both of the same magnitude of the observed difference in burn duration for the 9 bar EMEP cases observed in Figure 3.10.

With regards to how the increased oxygen concentration would lead to faster burn rates, it has been hypothesized by Martz [92] that the increased oxygen could have a chemical effect. Specifically, it was speculated that the rate of the $H + O_2 \leftrightarrow OH + O$ chain branching mechanism would be affected by an increase in oxygen concentration in air dilute systems, and this in turn may increase the supply of OH to the primary heat release reaction $CO + OH \leftrightarrow CO_2 + H$, the latter increasing the heat release rate and thus shortening the burn duration.
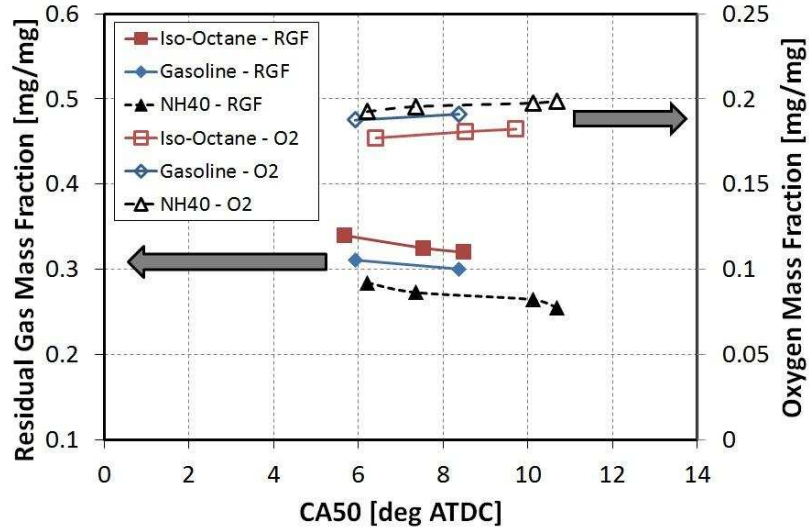
Figure 3.13 Estimated oxygen and residual gas mass fractions for the NVO sweep at 9 bar EMEP

3.4.3 Residual Gas Effect

For this study, as NVO was reduced during a sweep, the residual gas fraction correspondingly decreased, as shown in Figure 3.13. As noted in the Data Analysis section these values are inferred, but nonetheless the trends between fuels hold. From Figure 3.13, comparing the level of RGF between the NH40 and iso-octane shows a difference of 17%, and a difference of 10% between the NH40 and gasoline. This difference in RGF could have an effect on the burn duration. A direct consequence of lowering the RGF with a shorter NVO duration for the NH40 is an increase in the oxygen concentration. Based on the discussion above, lower levels of residual serve to decrease the burn duration due to a greater concentration of O_2.

A second potential consequence of decreasing the RGF with the NH40 fuel is the effect this has on the specific heat, C_P, of the total mixture. A higher specific heat will tend to reduce pressure rise rates, leading to lower peak heat release rates and an overall slower burn.

Unlike previous experiments conducted by Dec, Sjöberg, and Shibata, which utilize "pure" HCCI by means of higher compression ratios and high levels of intake air preheating, the work herein has relied upon high levels of internal RGF to obtain the high temperatures

necessary for HCCI combustion. Introducing high levels of RGF in-cylinder via NVO has been shown by Rothamer [41] to introduce high levels of both thermal and compositional stratification. Sjöberg and Dec have shown that increasing the thermal stratification will lead to an increase in the overall burn duration [50].

3.4.4   Intermediate Temperature Heat Release

In addition to stratification and composition effects, previous work [68–70] has shown that under certain conditions gasoline and other two stage ignition fuels exhibit an intermediate temperature heat release (ITHR) prior to the main ignition event and after low temperature heat release (LTHR). The normalized heat release rates plotted in Figure 3.14 represents the 9 bar EMEP cases shown in Figure 3.10, and HRR plots for the peak EMEP cases in Figure 3.11 are presented in Figure 3.16. As was previously shown by Dec [69], to compensate for the fact that the combustion phasing and peak load differed between the points, the heat release curves were shifted to align the maximum HRR. In addition, the rate of heat release was normalized with the total heat release to compensate for differences in total heat release between points.

For all test cases under the conditions of this study, none of the fuels tested demonstrated a LTHR, which would have been characterized by a small isolated heat release event prior to the main event. Given the high level of normal paraffins 45%) in the NH40 (due to the addition of n-heptane), the lack of observed LTHR is noteworthy given that PRF80 (a fuel with 20% normal paraffins) has repeatedly been demonstrated to exhibit LTHR [64, 68, 93], as well as other lower ON fuels with higher levels of normal paraffins [70]. The authors believe the lack of LTHR is explained due to two reasons: higher engine speed and hotter unburned gas temperatures. Engine speed was maintained at 2000 rpm in this study, a speed high enough that the LTHR reactions do not have time to develop before the main ignition event occurs. The disappearance of LTHR at higher engine speeds for fuels that demonstrate LTHR behavior has previously been shown by Sjöberg [64, 93]. In addition, LTHR is usually

observed with unburned gas temperatures on the order of 760 – 880K [93]. For the cases shown in Figure 3.14 – 3.15 the unburned gas temperatures prior to TDC were ~1100 – 1200K for the three fuels. The high temperatures prior to ignition, resulting from the use of hot internal residual, could potentially bypass the LTHR cool flame chemistry.

While no LTHR was observed for the the test cases, a higher level of ITHR was observed for the NH40 compared to the iso-octane and gasoline. To highlight the ITHR region for both the 9 bar EMEP cases and the peak EMEP/IMEP cases, the vertical axes of Figures 3.14 and 3.16 have been rescaled and are shown in Figures 3.15 and 3.17. In order to align the peak normalized HRR, as described, the heat release traces were shifted, and the magnitude of the required shift is displayed as "TDC Range" in Figures 3.14, 3.15, 3.16, and 3.17. It is clear in both figures that the NH40 exhibits more ITHR than than the other two fuels. This is apparent for both the 9 bar EMEP cases, and the cases at maximum EMEP. The relative difference in ITHR is more pronounced for the peak load cases, shown in Figure 3.17.

Dec [69] has demonstrated that a higher level of ITHR enables a later combustion phasing, and recently Yang [70] demonstrated ITHR behavior with a low octane fuel blend termed Hydrobate. The magnitude of the difference in ITHR between the gasoline and Hydrobate presented by Yang is of the same order of magnitude as the difference between gasoline and NH40 in Figure 3.17. It is possible that one effect of a greater level of ITHR could be to shorten the burn duration by preparing the mixture before the main heat release event. Establishing a relationship between ITHR and burn duration will require a more detailed study.

3.5   Chapter Summary

A study was performed to compare the behavior of HCCI combustion using a lower ON gasoline blended fuel, NH40 (40% n-heptane, 60% gasoline) with regular 87 octane gasoline and iso-octane. HCCI combustion was achieved utilizing a recompression strategy (NVO).
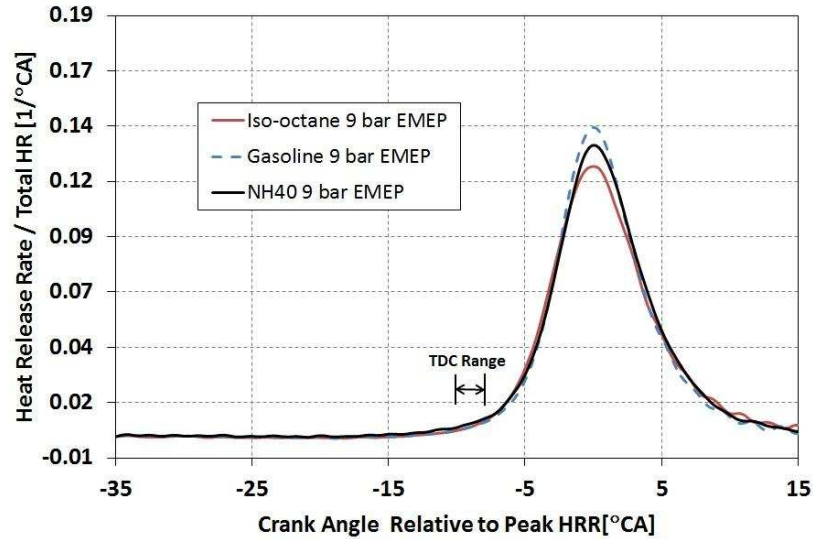
Figure 3.14 Normalized HRR of the highest IMEP$_g$ points at 9 bar EMEP
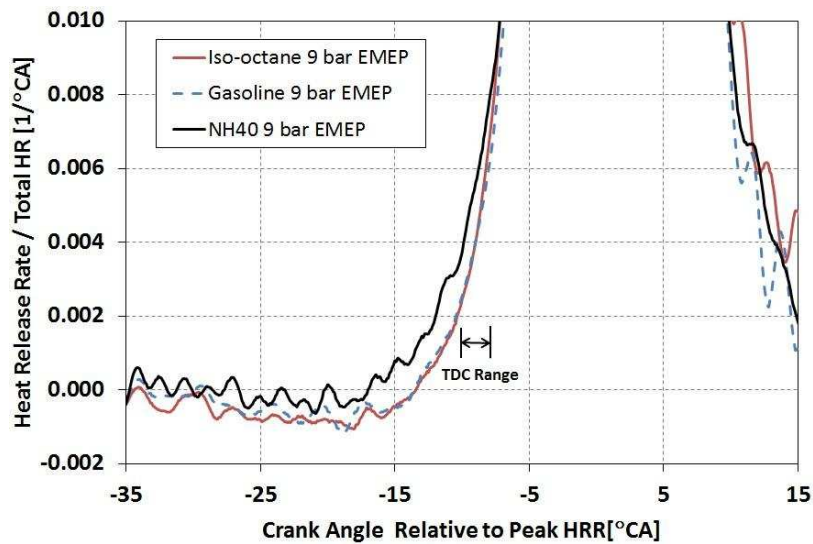
Figure 3.15 Rescaled HRR to highlight ITHR for NH40 at 9 bar EMEP

The engine employed a fully flexible hydraulic valvetrain for symmetrical NVO operation. For comparison, each fuel was run at a fixed fueling rate, with the energy mean effective pressure (EMEP) utilized as a normalized energy addition rate. For each EMEP, the duration of NVO was varied, phasing combustion from the advanced limit dictated by ringing intensity to the retarded limit dictated by COV of IMEP$_g$. For each fuel, the maximum load, in terms of IMEP$_g$, was found by increasing EMEP until there were no longer any stable operating
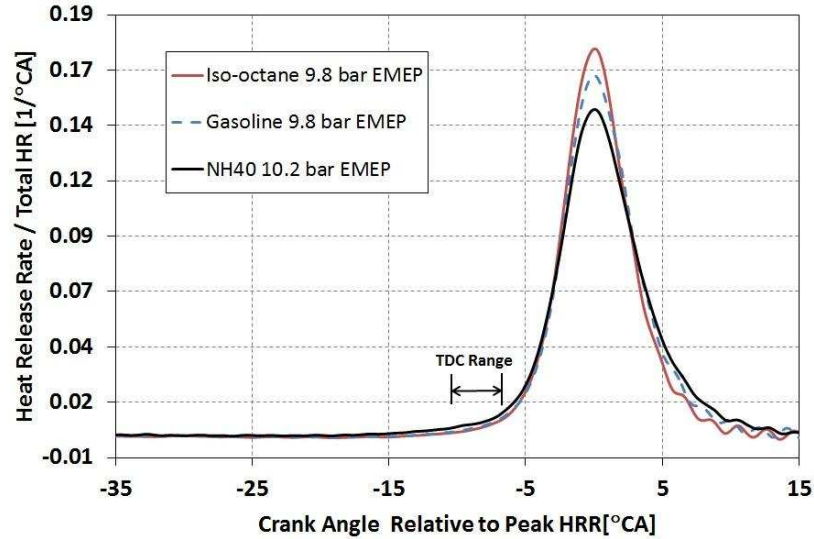
Figure 3.16 Normalized HRR of the highest IMEP$_g$ points at the highest EMEP for three fuels
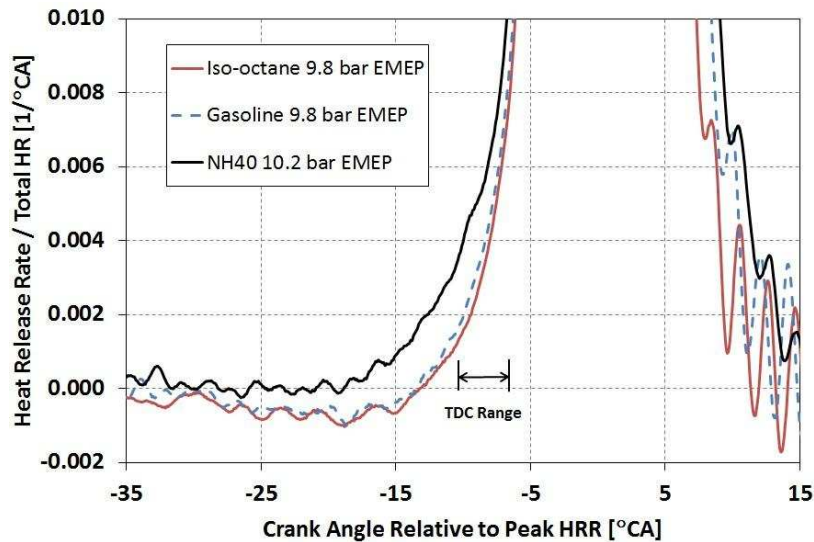
Figure 3.17 Rescaled HRR to highlight ITHR for NH40 at peak IMEP$_g$ & EMEP

points at the next EMEP level. From the results, the following findings were made regarding the NH40 when compared to iso-octane and gasoline:

1. The NH40 was demonstrated to operate at a higher maximum EMEP and IMEP$_g$, at a later combustion phasing.
2. For a sweep at a given EMEP, the NH40 operates at a later combustion phasing for both the advanced RI limit and the retarded COV of IMEP$_g$ limit.
3. For a given CA50 and EMEP, the NH40 has a shorter 10-90 burn duration.
4. For a given EMEP, at the late phasing combustion limit, the NH40 had a later CA50 for a similar CA90, demonstrating that a shorter burn duration allowed later combustion

phasing.

5. Heat release analysis revealed that the NH40 demonstrates increased ITHR.

Based on the above, the higher maximum load attained by the NH40 is attributed to the shorter burn duration for the fuel compared with iso-octane and gasoline. The shorter burn duration could be due in whole or in part to a number of possible factors:

Oxygen Concentration: The reduced level of NVO required to operate the NH40 fuel allows for a larger portion of the charge to be air, increasing the oxygen concentration of the charge and potentially decreasing the burn duration.

EGR level: EGR as a diluent has a higher specific heat than air and tends to reduce pressure rise rates, decreasing the burn rate. The reduced level of internal residual for the NH40 could increase the burn rate due to less EGR and a lower specific heat for the charge.

Stratification: High levels of NVO have been documented to increase both thermal and compositional stratification. Stratification of both temperature and gas composition will reduce the burn rates, so the decrease in NVO required for operation of the NH40 could lead to increased burn rates from less stratification.

Fuel: The NH40 exhibited intermediate temperature heat release (ITHR) to a significantly higher degree than the iso-octane and gasoline. ITHR has been documented to increase burn rates and allow stable operation at late phasing.

While the extent and influence each of the above factors has on burn duration requires future study, this work demonstrated that for NVO enabled HCCI combustion, low octane gasoline-like fuels, especially those demonstrating enhanced ITHR, offer measurable load limit extension and enhanced combustion stability.

66

Chapter 4

A Methodology for HCCI Composition Control

In Chapter 3 it was demonstrated that the lower ON fuel, NH40, had a shorter $10 - 90$ burn duration compared to gasoline and iso-octane at a fixed CA50. Furthermore, the NH40 could be operated at a later phasing than the gasoline and and at a higher load while satisfying the ringing requirements. However, differences in iEGR and composition obfuscated any clear fuel effects on the combustion burn rate. To isolate fuel effects from iEGR and composition effects, a new test procedure was developed to maintain constant composition across varied fuels, engine speed, and duration of NVO.

4.1 The Internal vs External EGR Trade-off

In Chapter 3, as the duration of NVO was varied (corresponding to changing iEGR), the overall equivalence ratio, ϕ, changed in corresponding fashion as shown in Figure 3.5. This raised the question of what is the impact of changing NVO (and thus iEGR) on combustion as opposed to fuel chemistry differences. To quantify the effect of iEGR required changing the NVO while keeping all other conditions the same: composition, combustion phasing, fueling rate and equivalence ratio. By composition, it is meant the sum of the global masses of all constituents. To visualize the constituent masses that make up the charge composition, consider the illustration in Figure 4.1. The injected fuel combined with inducted air fixes the exhaust equivalence ratio, ϕ. The combination of eEGR and iEGR combine to equal the total residual gas fraction (RGF). The injected fuel mass as a fraction of the total charge mass is the fuel/charge equivalence ratio, ϕ', as shown in Equation 3.1. So for composition to remain constant in an NVO sweep, any reduction in iEGR must be met by an increase in
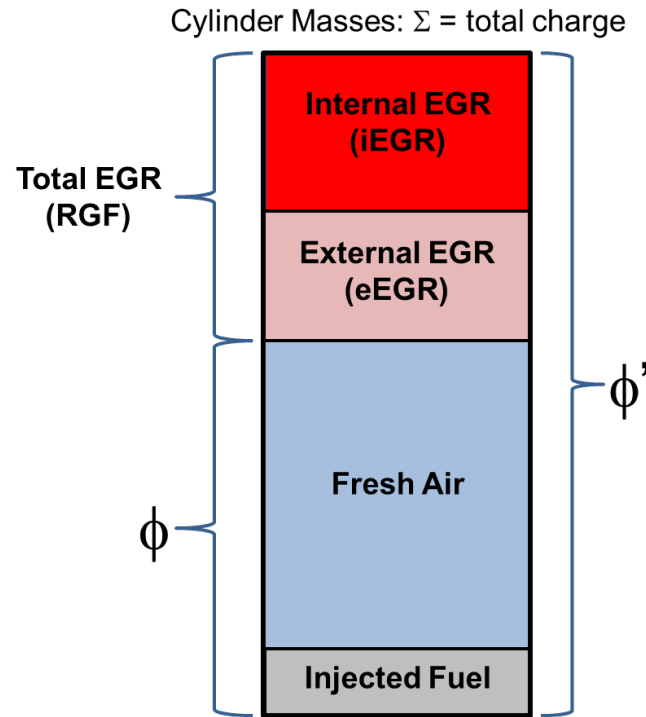
Figure 4.1 Conceptual break-down of distinct in-cylinder constituent masses as they relate to ϕ and ϕ'

eEGR so that the total RGF is constant. The way that this is implemented is to add eternal EGR (eEGR) as iEGR is reduced by reducing NVO. An ideal sweep demonstrating this is illustrated in Figure 4.2.

In Figure 4.2, the idealized approach maintains the following constant: EMEP (fueling rate), engine speed, intake and exhaust pressure, exhaust equivalence ratio (ϕ), the combustion phasing, and total EGR level. From this, ϕ' is fixed, and this approach allows comparison between cases of pure iEGR and pure eEGR, isolating how changes in iEGR affect HCCI burn rates. One variable that will be dependent on iEGR is inlet temperature; as iEGR is reduced and relatively cool eEGR is added, the IVC temperatures will be reduced. For combustion phasing to remain constant the intake temperature then must be increased to maintain a constant IVC temperature, for with a fixed composition charge the IVC temperature determines combustion phasing.

An experiment was performed with gasoline at 2000 rpm with the FFVA engine to
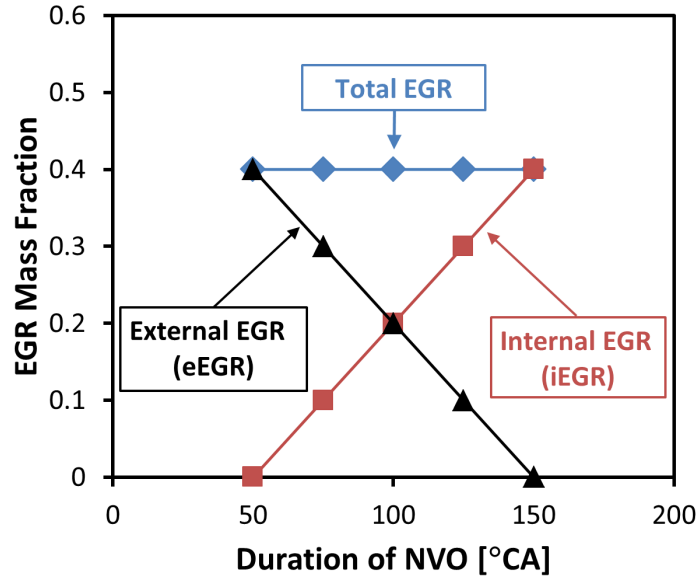
Figure 4.2   Idealized hypothetical NVO sweep exchanging 100% iEGR for 100% eEGR

replicate Figure 4.2. The results of this experiment is shown in Figure 4.3. On the FFVA engine, the inlet temperature has a practical operating range of 50°C – 200°C, and this is the range used for this experiment. The highest iEGR condition is 42% iEGR at 151° of NVO, a condition at which there was very little eEGR and the inlet temperature was 50°C. The lowest iEGR condition is 22% iEGR at 77° of NVO. In order for the complete transition from 100% iEGR to 100% eEGR to have occurred, greater temperature range with the inlet heater would be required; a reduced inlet temperature at the highest iEGR condition, and an increased inlet temperature at the lowest iEGR condition. Nonetheless, a significant variation in NVO/iEGR was demonstrated by increasing the inlet temperature to maintain a near constant IVC temperature at a fixed ϕ and combustion phasing (CA50 = 6° ATDC): this can be observed in Figure 4.4. In Figure 4.4, the inlet temperature is measured from the intake runner, whereas the mean IVC temperature is inferred from the heat release analysis. The reported iEGR is determined by calculations using the Fitzgerald method as detailed in Section 2.2.3.

While the experiment in Figures 4.3 and 4.4 demonstrated trading iEGR for eEGR at fixed combustion phasing and equivalence ratio, it should be noted that the total composition
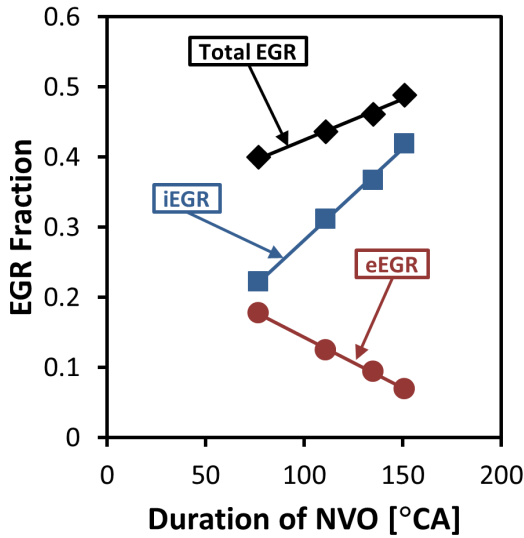
Figure 4.3 Experimental variation of total EGR across NVO sweep with fixed ICV for gasoline at 9.0 bar EMEP, 2000rpm, CA50 fixed at 6° ATDC
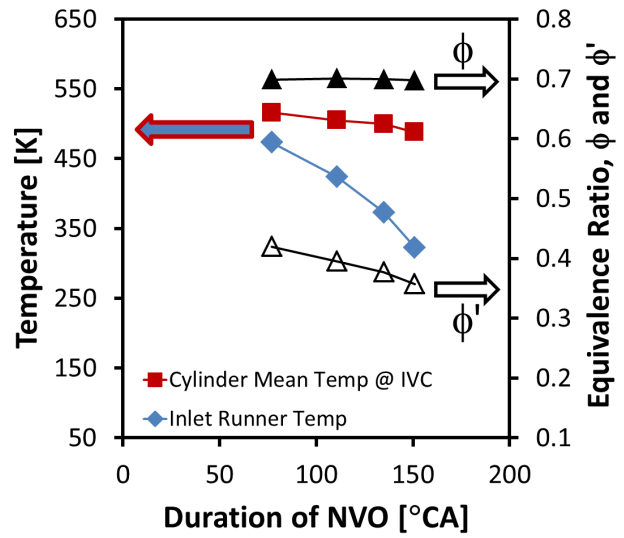
Figure 4.4 Experimental variation of Inlet Temperature to maintain IVC temperature across constant ϕ NVO sweep for gasoline at 9.0 bar EMEP, 2000rpm, CA50 fixed at 6° ATDC

did not remain constant, as can be seen in Figure 4.3 where the total EGR is reduced as NVO/iEGR is reduced. Corresponding to this change in total EGR, the ϕ' can be noted to increase as NVO/iEGR is reduced. This due to the fact that ϕ', as shown in Equation 3.1, is essentially a measure of the fuel to total charge in the cylinder. As the total EGR was reduced, the total charge was reduced (for both the fuel addition and equivalence ratio were constant, so fresh air was constant) and the ϕ' increased. So comparing high and low iEGR cases from this experiment would still present problems with regards to separating iEGR effects from ϕ' effects.

4.2 Sweeping Intake Valve Closing Location

Examination of the experimental results of the first attempt at an NVO sweep revealed that as the NVO/iEGR was reduced, and the inlet temperature increased, the runner dynamics changed, as shown in Figure 4.5(a). In the first experiment, IVC was kept constant, as only EVC and IVO are varied symmetrically as NVO is varied symmetrically. However, as

can be noted in Figure 4.5(a), for a fixed IVC as the NVO was reduced the pressure in the runner at the time of IVC is lower. Examining the cylinder pressure for these cases in Figure 4.5(b) shows that for the cases with lower IVC pressure, the corresponding overall pressure trace along the compression path is lower up to TDC. The lower pressure corresponds to a reduced total charge as the NVO is reduced, as was observed in Figure 4.3.

The reason for this change across the NVO sweep is due to the fact that while operating the engine there is no direct knowledge of total EGR or ϕ'. This can be imagined within the framework of the constituent masses represented in Figure 4.1. During the experiment the method of control is to maintain a constant fueling rate and exhaust equivalence ratio as NVO is reduced. For example, to reduce iEGR from the highest iEGR condition in Figure 4.3, the inlet temperature is first increased by $50°C$[1]. At the higher inlet temperature NVO is reduced to match phasing, and eEGR is gradually increased to match exhaust equivalence ratio. The latter is necessary for reducing NVO advances IVO and allows more fresh charge, so eEGR is added to reduce the amount of fresh air and match the ϕ. This method only fixes the exhaust ϕ and does not guarantee that the amount of eEGR brought in equals the amount that iEGR is reduced, so the total EGR (RGF) in Figure 4.1 can be imagined to decrease as NVO is reduced. In order to match the eEGR to the iEGR it is necessary to shift IVC across the NVO sweep, finding the IVC location that allows the increase in eEGR to match the decrease in iEGR as NVO is reduced.

The NVO sweep for gasoline at 2000 rpm was thus repeated, but this time IVC was not held constant across the NVO sweep. The results of this experiment are presented in Figures 4.5(c), 4.5(d), and 4.6. For the cases where NVO was greater than $\sim 90°$ the IVC was retarded, and for the case where NVO was less than $90°$ the IVC was advanced. This changed the pressure in the runner at IVC (Figure 4.5(c) and the cylinder compression trace demonstrates that for these cases the cylinder pressure is identical across the cases

---

[1]The inlet heaters have a long time constant and slow response, so operation of an NVO sweep is best conducted with predetermined inlet temperatures (essentially an inlet temperature sweep) where then NVO is reduced as the inlet temperature is increased to match phasing
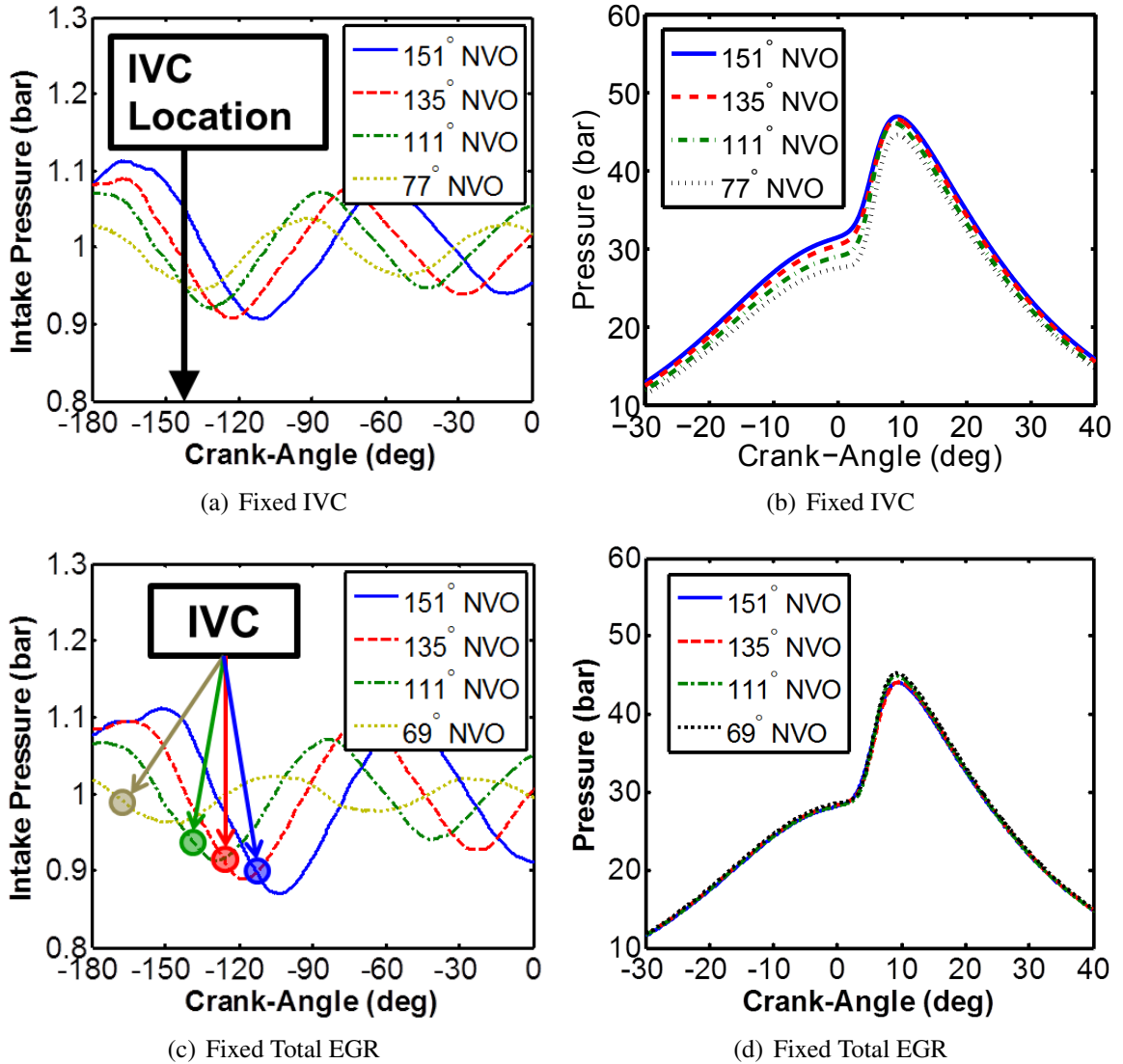
Figure 4.5 Inlet runner pressure dynamics and cylinder pressure traces for fixed IVC and fixed total EGR NVO sweeps for gasoline at 2000rpm, CA50 = 6° ATDC, $\phi = 0.7$

during compression. This now provides essentially constant total EGR, or constant total composition, across the entire NVO sweep as shown in Figure 4.6 compared the fixed IVC cases. Corresponding to the constant composition, ϕ' remains constant across the sweep as well, compared to the case with a fixed IVC.
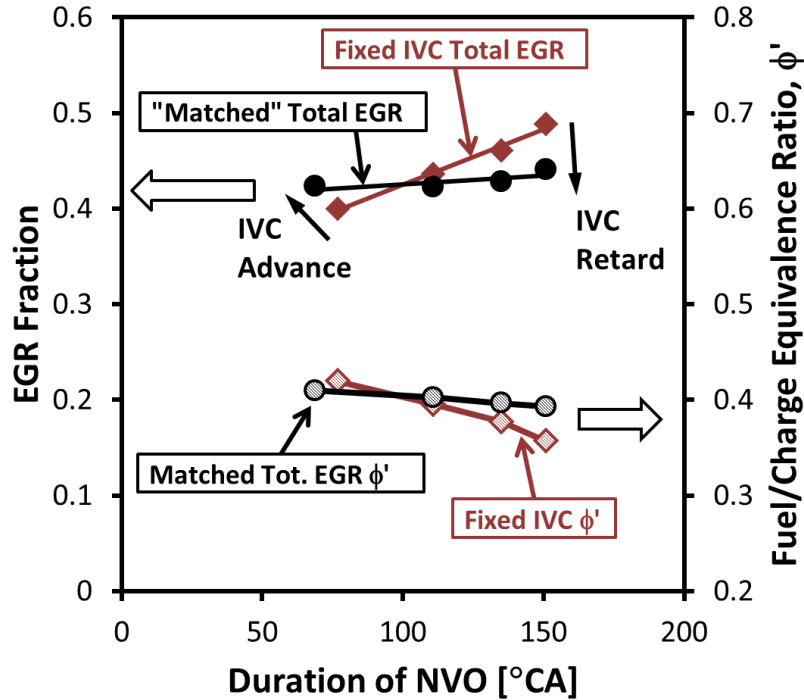
Figure 4.6 Advancing and retarding IVC across NVO sweep to match total EGR and ϕ' for gasoline at 2000rpm

4.3 Intake Throttling

The above method of varying IVC to maintain constant composition worked so long as engine speed was held constant — such as at 2000 rpm in the above cases. Performing the exact same procedure at lower engine speeds, especially for PRF40, was observed to yield higher total EGR fractions (and lower ϕ') as speed was reduced as shown in Figure 4.7. There were only two methods feasible to maintain a constant ϕ' across all engine speeds: throttle the lower engine speed cases, or to increase fueling at the lower engine speed cases. The latter would change the exhaust ϕ while the former would change the pressure. Considering the relative impact of pressure compared to ϕ in the ignition delay correlation proposed by He [91], pressure has an exponent of -1.05, whereas ϕ has an exponent of -0.77, a greater impact. Furthermore it is standard practice to scale for pressure differences in chemical kinetics, but not equivalence ratio so it was decided that the best approach to reducing the total EGR at lower speeds was to throttle slightly.

(a) Fixed Intake Pressure   (b) Throttled Intake at 1000, 1500 rpm
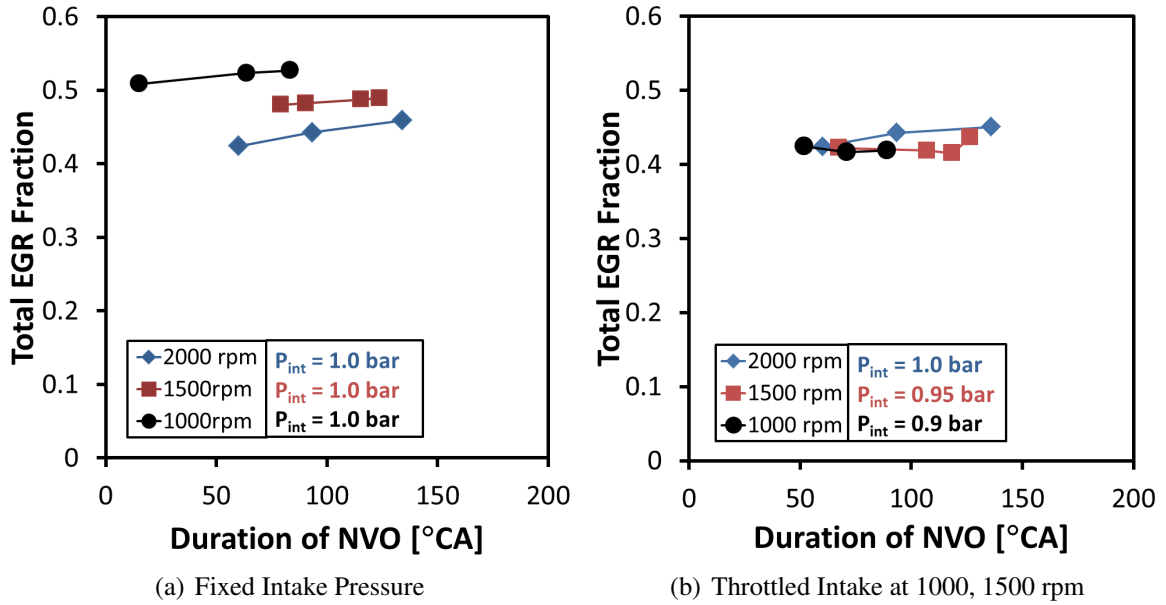
Figure 4.7   Total EGR for PRF40 NVO sweeps with and without intake throttling, 9.0 bar EMEP, Fixed CA50 = 6° ATDC

The result of the throttling is shown in Figure 4.7(b), where at 1500 rpm the intake was throttled to 0.95 bar, and to 0.9 bar at 1000 rpm. The result is that total EGR was brought to an equal level across all three engine speeds.

4.4   Chapter Summary

This study demonstrated that adjusting IVC allowed for constant composition (constant total EGR) across NVO sweeps for a given engine speed. As engine speed is reduced, it is necessary to throttle the inlet to maintain constant composition. These two methods were utilized for all experiments in the remainder of this document. Figure 4.8 represents the ϕ' and total EGR fraction for all data points presented in Chapters 5 and 6, which includes three fuels (PRF40, PRF60, and gasoline) and three engine speeds (1000 rpm, 1500 rpm and 2000 rpm). For all cases, ϕ' was held to 0.40 ± 0.02 ($\pm 5\%$), and total EGR was held to 0.43 ± 0.03 ($\pm 7\%$).
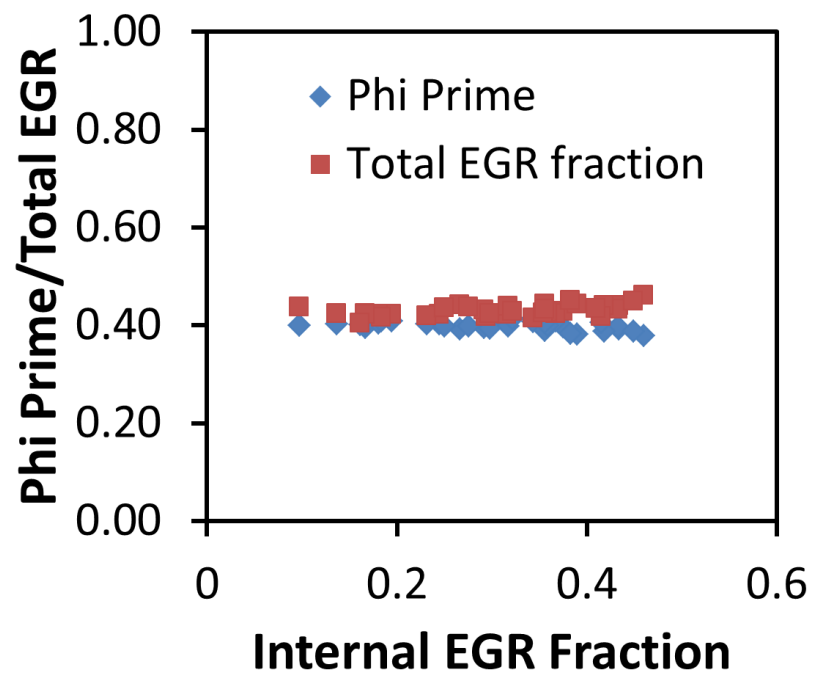
Figure 4.8 Demonstrating control of total EGR and ϕ' for all 9.0 bar EMEP cases presented in Chapters 5 and 6

Chapter 5

Fuel and iEGR Effects on HCCI Burn Rates

To expand upon the finding of Chapter 3, namely the observed trend of faster combustion burn rates and longer burn duration for the NH40 fuel compared to gasoline at fixed combustion phasing, new experiments were undertaken utilizing the constant composition method described in Chapter 4. In Chapter 3 was observed that gasoline and iso-octane had similar burn rates and occupied the same load range, so for the sake of a simplified test matrix iso-octane was omitted from this study, leaving gasoline to represent a higher ON fuel.

For a low ON fuel, PRF40 was selected for this set of experiments. In Chapter 3 the NH40 fuel was utilized to represent a multicomponent fuel of ON rating similar to what could be found in a naptha refinery fuel. For this study a pure PRF was desirable for the kinetic mechanisms are well developed compared the unique blend previously used; from the outset this study anticipated future computational studies would utilize this data. PRF60 would have a RON similar to the NH40 in the original study, but the purpose was to explore fuel effects from operation of low ON fuels exhibiting non-Arrhenius ignition delay behavior, as this behavior is believed to be critical to any observed differences. As such, it was desirable to amplify the amount of n-heptane in the low ON PRF, and PRF40 (RON = 40) was selected as the low ON fuel for comparison with gasoline. Specific fuel properties are listed in Table 5.1.

For this chapter iEGR sweeps are performed at constant composition as described in Chapter 4 while maintaining constant combustion phasing. By constant combustion phasing it is meant that the crank angle location of 50% mass fraction burn (CA50) is held

constant. For all cases described in this chapter, CA50 was held fixed at 6° ATDC. Load was maintained constant at 9.0 bar EMEP, matching energy addition between gasoline and PRF40 as described in Chapter 2. The 9.0 bar EMEP load was selected for this is the highest equal load at which constant phasing comparisons were made in Chapter 3. The one difference is that for these experiments the ringing intensity limit of 5 MW/m^2 was suspended, for it would not have been possible to maintain equal combustion phasing at 9.0 bar EMEP between gasoline and PRF40, as the PRF40 exceeds this limit. So while from a production standpoint some PRF40 data points are unacceptable, for the purpose of extracting fuel chemistry effects they are instructive.

In Chapter 3, all experiments were performed at 2000 rpm. With the knowledge that in HCCI conditions low ON PRFs will likely demonstrate increasing Low Temperature Heat Release (LTHR) as engine speed is decreased [64], the experimental operating space was increased to include sweeps at 1500 rpm and 1000 rpm, in addition to 2000 rpm, to explore the impact of LTHR on combustion burn rates for PRF40 as engine speed is reduced. The engine conditions for these experiments are summarized in Table 5.2.

5.1 Gasoline iEGR Sweeps

The first set of fixed combustion phasing experiments set out to examine the effect of varying iEGR on HCCI combustion. For gasoline, iEGR sweeps were conducted at 1000, 1500, and 2000 rpm. For all three speeds, iEGR sweeps were conducted with iEGR levels ranging from 19% to 46% depending on engine speed. The crank angle based rate of heat release (RoHR) curves for each iEGR at a given speed, for all three speeds, is plotted in Figure 5.1. The observed behavior is nearly identical for each engine, as may be expected for no LTHR is present with the gasoline.

Examining the maximum RoHR across the iEGR sweep at 2000 rpm, it can be noted that at the lowest iEGR level, 19%, the maximum RoHR is 80 J/°CA. Increasing iEGR

77

Table 5.1 Test fuel properties

Property	PRF40	Gasoline
LHV [kJ/kg]	44444	43043
Density [g/mL]	0.687	0.736
MW [g/mol]	105.4	93.0
H/C [molar]	2.272	1.879
RON	40	90.5
MON	40	82.6
AKI [(R+M)/2]	40	87
Paraffins [% WGT]	60	8.1
Iso-Paraffins [% WGT]	40	37.5
Aromatics [% WGT]	0	32.3
Napthenes [% WGT]	0	16.9
Olefins [% WGT]	0	4.5
Boiling Point [°C]	99	N/A
10% Evaporation [°C]	N/A	62
50% Evaporation [°C]	N/A	95
90% Evaporation [°C]	N/A	145

Table 5.2 Experimental parameters

Parameter	Value
Engine Speed [RPM]	1000 – 2000
Fuel Injection Pressure [bar]	≈ 100
Fuel Start of Injection [° BTDC]	330
Intake Temperature [°C]	35 – 200
Abs. Intake Pressure [bar]	0.9 – 1.0
Abs. Exhaust Pressure [bar]	1.05
Coolant Temperature [°C]	90
Oil Temperature [°C]	90
Ringing Intensity [MW/m^2]	< 10.0
COV of IMEP$_g$[%]	< 5.0
Emissions Index NO$_X$ [g/kg-fuel]	<1.0

corresponds to reduced maximum RoHR and at the highest iEGR at 2000 rpm, 43%, the maximum RohR is 69 J/°CA, a decrease of 14% compared to the lowest iEGR case. This trend is consistent across all three engine speeds.

Figure 5.2 is a plot of the 10, 50 and 90% burn locations (CA10, CA50 and CA90 respectively) for the iEGR sweeps for each engine speed. The difference between CA10 and

(a) 1000 rpm

(b) 1500 rpm

(c) 2000 rpm
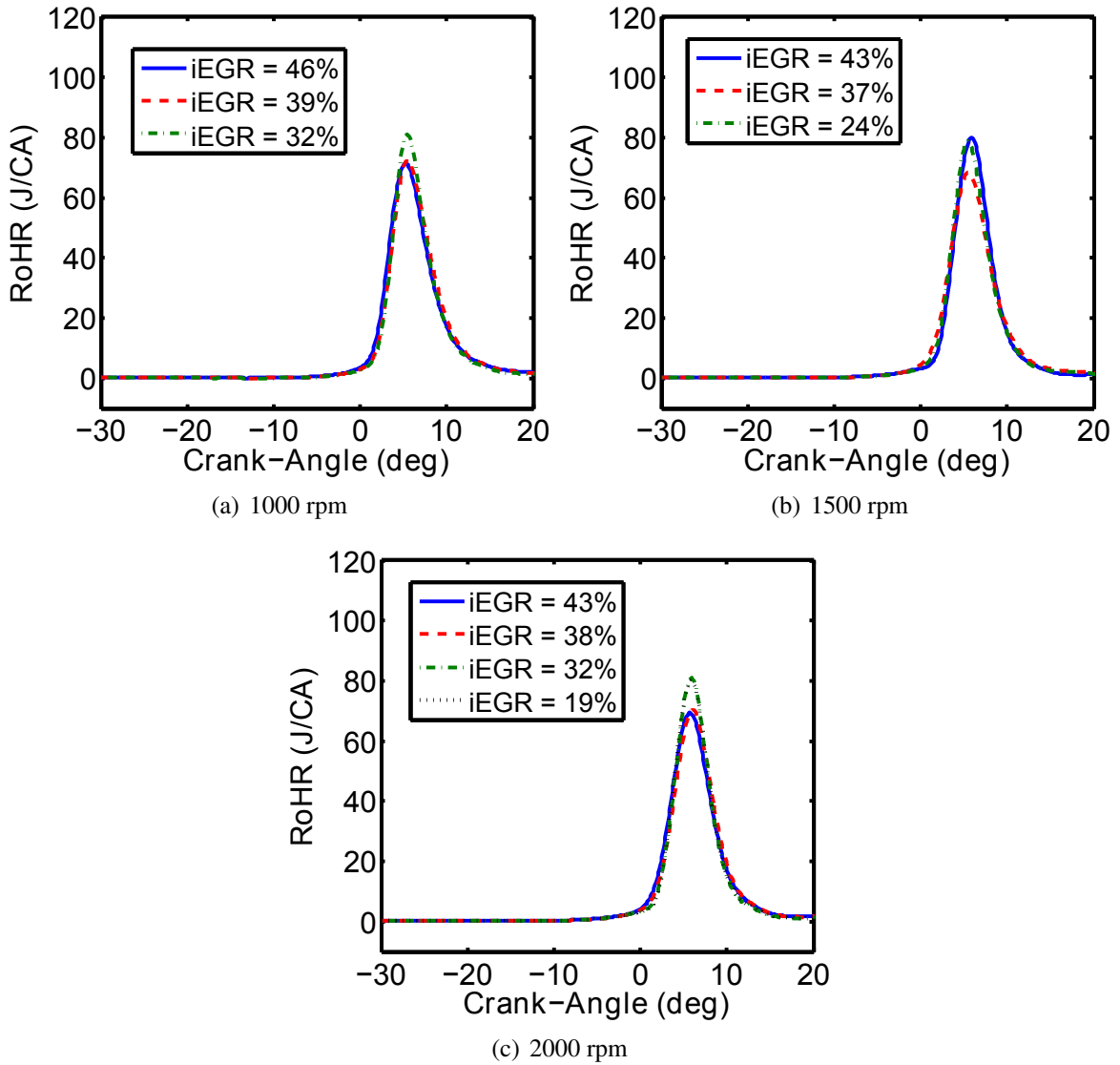
Figure 5.1 Heat Release Curves for Gasoline iEGR Sweeps

CA90, designated the $10-90$ burn duration, is a metric for overall burn duration, and in this document the term burn duration will always refer to the number of crank angle degrees between CA10 and CA90. The difference between CA10 and CA90 for the gasoline at all three engine speeds across iEGR sweeps is shown in Figure 5.3. The burn duration, as it trends with iEGR, is nearly identical between engine speeds, which is consistent with the RoHR having no engine speed dependence. Regarding iEGR dependence, as iEGR is increased there is a noticeable increase in the burn duration above an iEGR of $\sim 30\%$. At
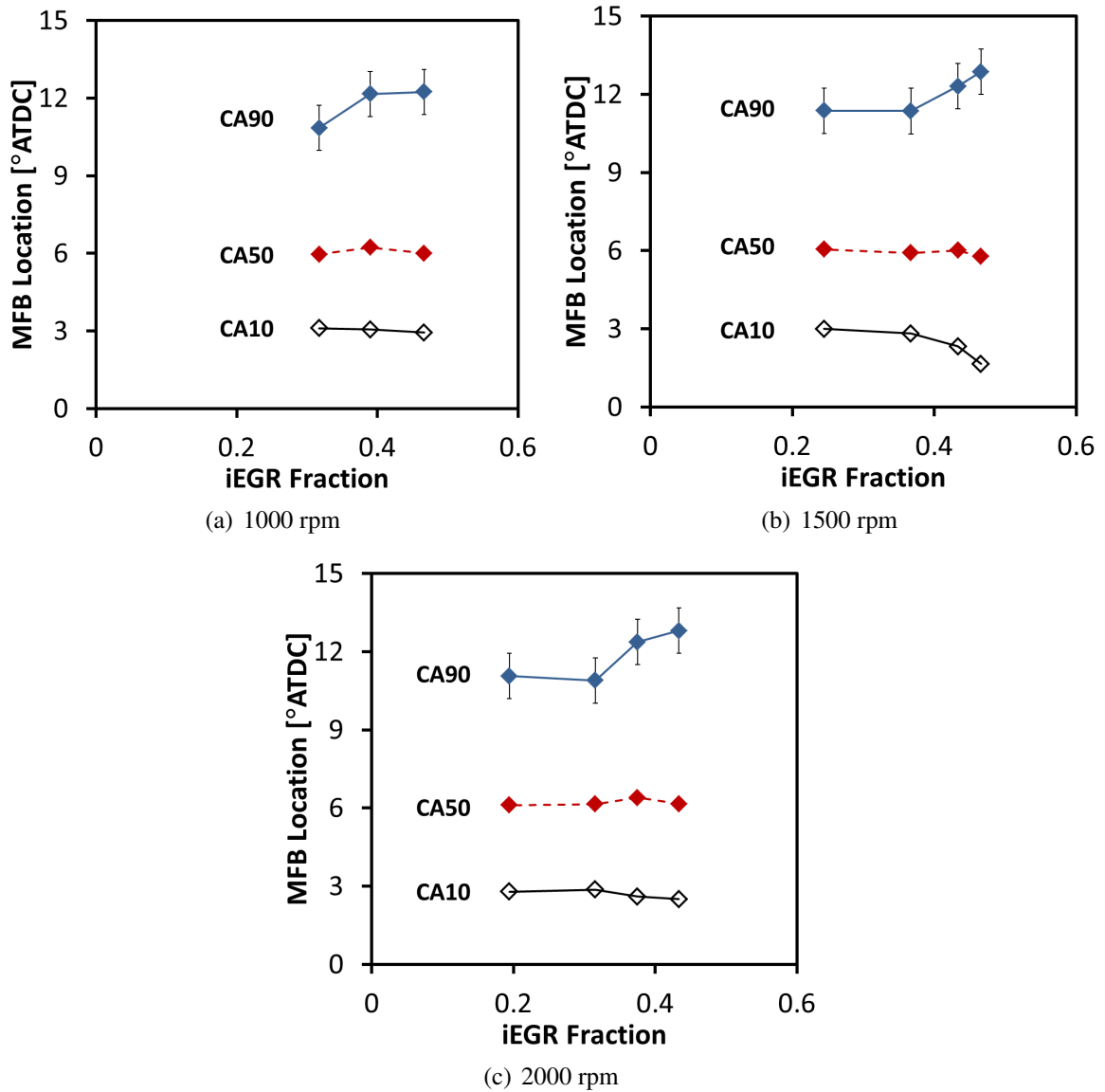
Figure 5.2   Gasoline Mass Fraction Burn Locations for 10, 50, and 90%

2000rpm at the lowest iEGR level (19%) the $10-90$ burn duration is $\sim 8°$, whereas at the highest iEGR (43%) it is $\sim 10°$— an increase of 25%.

The increase in burn duration, and reduction of maximum RoHR, at high levels of iEGR is consistent with the concept of increases in iEGR leading to increases in thermal and compositional stratification, lengthening the burn duration. This would suggest that the highest iEGR cases have larger levels of stratification at the time of auto-ignition, leading to a lengthened burn duration and reduced maximum RoHR. The absolute degree to which
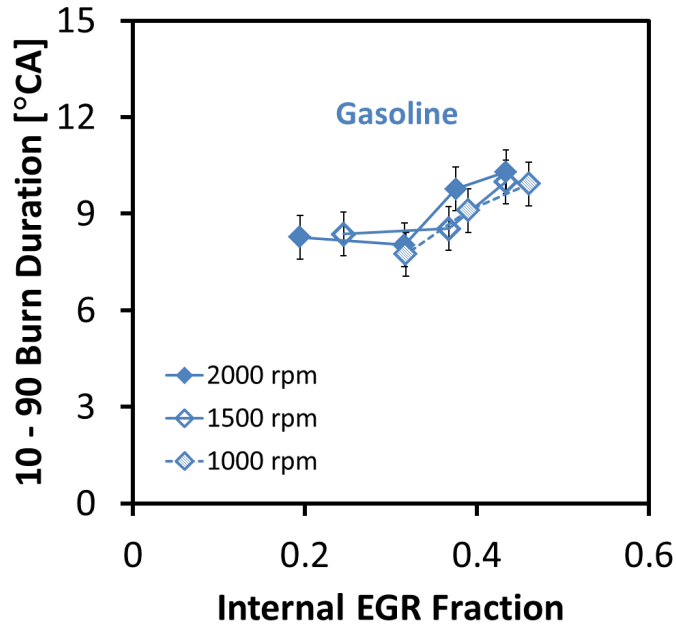
Figure 5.3   10% – 90% Burn Duration of gasoline

stratification is increased for the highest iEGR cases over the lowest can't be quantified from these experiments, nor can the type of stratification (thermal vs. compositional) most responsible for changes in burn rates. Both thermal and compositional stratification is a consequence of increased levels of iEGR, and both could affect burn rates.

5.2   PRF40 iEGR Sweeps

The iEGR sweeps conducted for gasoline in the previous section were repeated for PRF40. As with gasoline, RoHR curves for the iEGR sweep at each engine speed are shown in Figure 5.4. Unlike the gasoline but expected of a low ON PRF, the PRF40 exhibits LTHR which in magnitude increases with decreasing engine speed. The LTHR can be observed as the small "bump" in the RoHR curve prior to the main ignition, and is especially pronounced for the 1000 and 1500 rpm cases, but is present even at 2000 rpm. In contrast to the gasoline, at each engine speed the PRF40 does not show a significant change in the maximum RoHR as iEGR is increased from 17% to 38% at 2000 rpm, or at 1500 and 1000 rpm.

(a) 1000 rpm

(b) 1500 rpm

(c) 2000 rpm
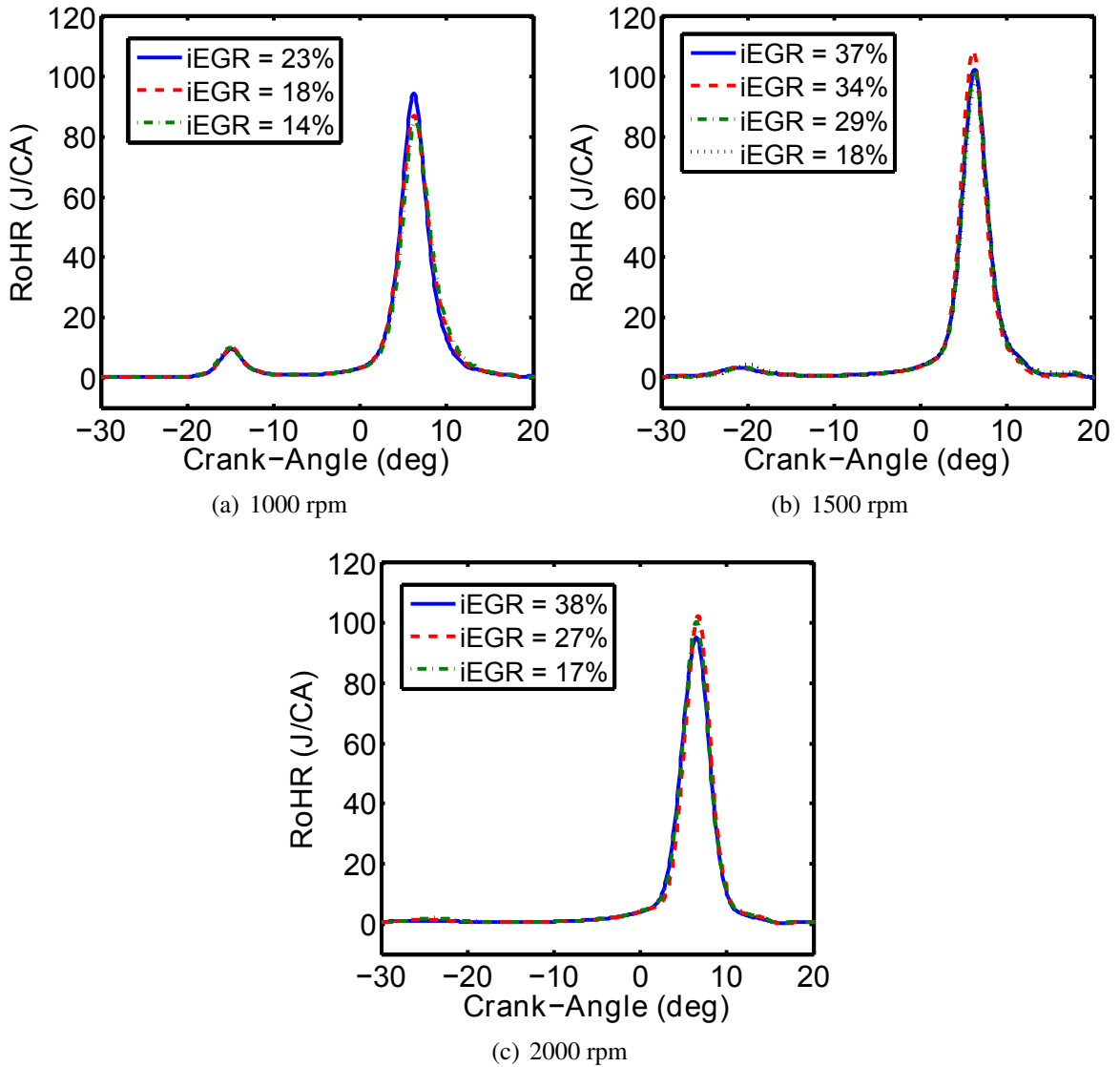
Figure 5.4   Heat Release Curves for PRF40 iEGR Sweeps

To compare the $10 - 90$ burn duration of PRF40 across iEGR and speed sweeps is complicated by the LTHR portion of the MFB curve. The LTHR, especially at 1000 and 1500 rpm, significantly advances the location of CA10. While in terms of the actual cumulative heat release this is correct, what is of primary interest is the $10 - 90$ burn duration of the main combustion event. To examine the $10 - 90$ burn duration of the main event, the MFB curve is truncated and re-scaled, an example of which is demonstrated in Figure 5.5 for PRF40 at 1000 rpm, iEGR = 23%. The the dark (black) dashed line is the original MFB
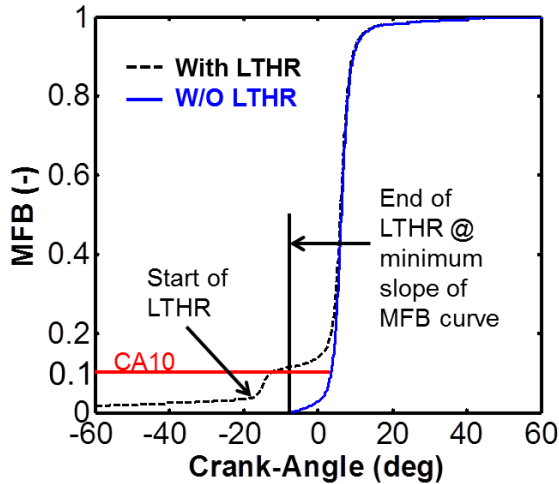
Figure 5.5 Removing LTHR portion of MFB Curve: Example for PRF40 at 1000 rpm
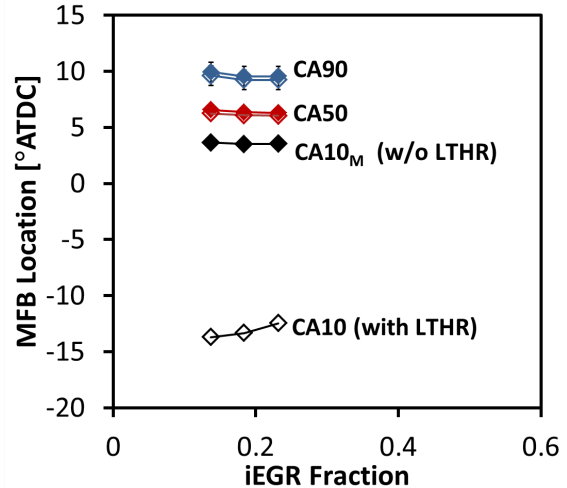
Figure 5.6 CA Burn locations with LTHR portion of MFB removed (PRF40 at 1000 rpm)

curve, and the lighter (blue) solid line is the rescaled MFB curve with the LTHR portion removed. To remove the LTHR from the MFB curve, the portion of lowest slope after the onset of LTHR is determined, and anything prior to this portion of the curve is removed, the remaining MFB curve rescaled from zero to one.

The effect of this rescaling of the MFB curve on CA burn locations is shown in Figure 5.6 where it is observed that only the location of the 10% burn location is significantly modified; the CA50 and CA90 locations are remain practically unchanged (plotted essentially on top of each other), the difference of $0.3°$ being within the error bars. For clarity and completeness in presentation, the CA10 of the main event when the LTHR portion has been removed will be denoted $CA10_M$, and the corresponding burn duration will be designated 10_M–90 with the "M" designating the 10% burn of the "main" combustion event.

Examining the 10_M, 50 and 90 burn locations in Figure 5.7 shows that as with RoHR, there is no apparent dependence of burn location on iEGR level, unlike with gasoline. Similar to gasoline, there is no dependence on engine speed with regards to the burn locations, despite the LTHR increasing significantly at 1000 rpm compared to 2000 rpm. Corresponding to the 10_M, 50 and 90 burn locations, the 10_M–90 burn duration is nearly identical for all iEGR and engine speed cases for PRF40, as shown in Figure 5.8.
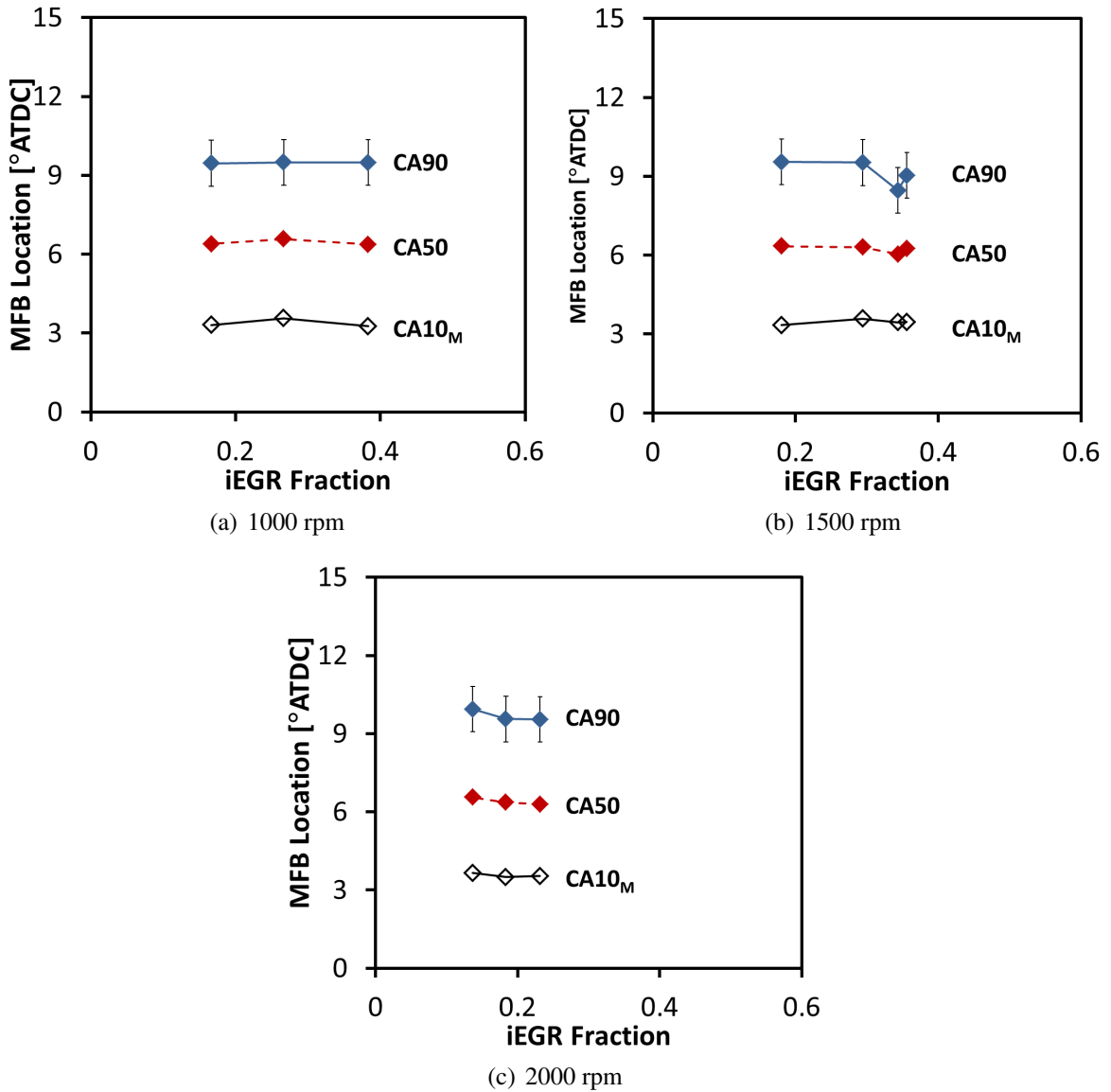
Figure 5.7   PRF40 Mass Fraction Burn Locations for 10, 50, and 90%

5.3   Comparison of Gasoline and PRF40 at Fixed iEGR

There are some noted differences between the behavior of the PRF40 compared with gasoline across the iEGR and engine speed sweeps. To separate the fuel effects, comparisons between PRF40 and gasoline at the same iEGR will be made in this section. PRF40 and gasoline were operated at an iEGR of 37% and 38% at 1500 and 2000 rpm respectively (due to inlet temperature restrictions, there was no overlap with iEGR levels at 1000 rpm), and these four
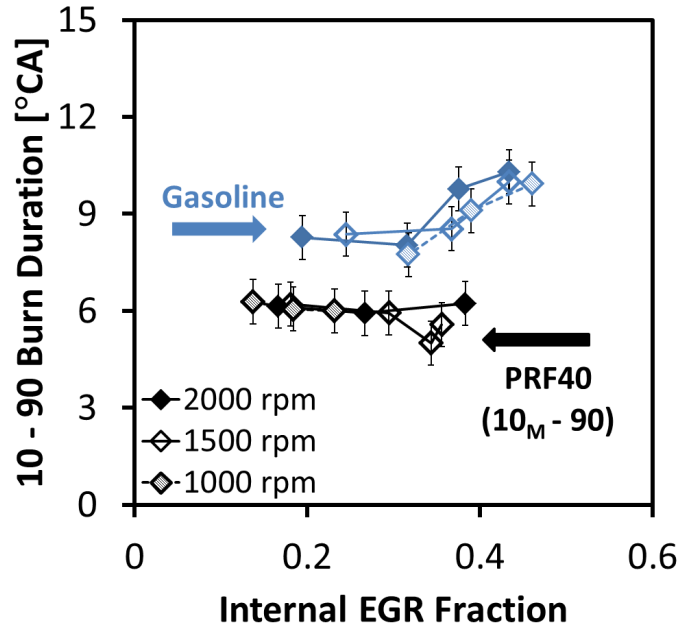
Figure 5.8 10% – 90% Burn Duration of gasoline with 10_M–90 burn duration of PRF40

cases will be examined in detail.

Figure 5.9 shows the RoHR curves for gasoline and PRF40 at 1000 and 1500 rpm. At each speed, the PRF40 demonstrates a maximum RoHR considerably higher than that of gasoline. At 2000 rpm the PRF40 has a maximum RoHR that is 35% higher than gasoline (95 J/°CA vs 70 J/°CA). At 1500 rpm the PRF40 has a maximum RoHR that is 29% higher than gasoline. It is observed that the maximum RoHR curve for both PRF40 and gasoline increased as engine speed decreased from 2000 to 1500 rpm; a 7% increase for PRF40 and a 13% increase for gasoline.

To more closely examine how the early portion of the RoHR differs between the fuels, the RoHR curves in Figure 5.9 were each normalized by the total heat release [J] for each respective curve and shown in Figure 5.10. This normalization allows comparison of heat release rates for the two fuels despite the fact the maximum RoHR varies. As the combustion phasing of the cases in question was already aligned, no shifts were made to align the normalized RoHR curves. The presence of LTHR for the PRF40 is clearly demonstrated here, and the increase of LTHR as engine speed is reduced from 2000 to
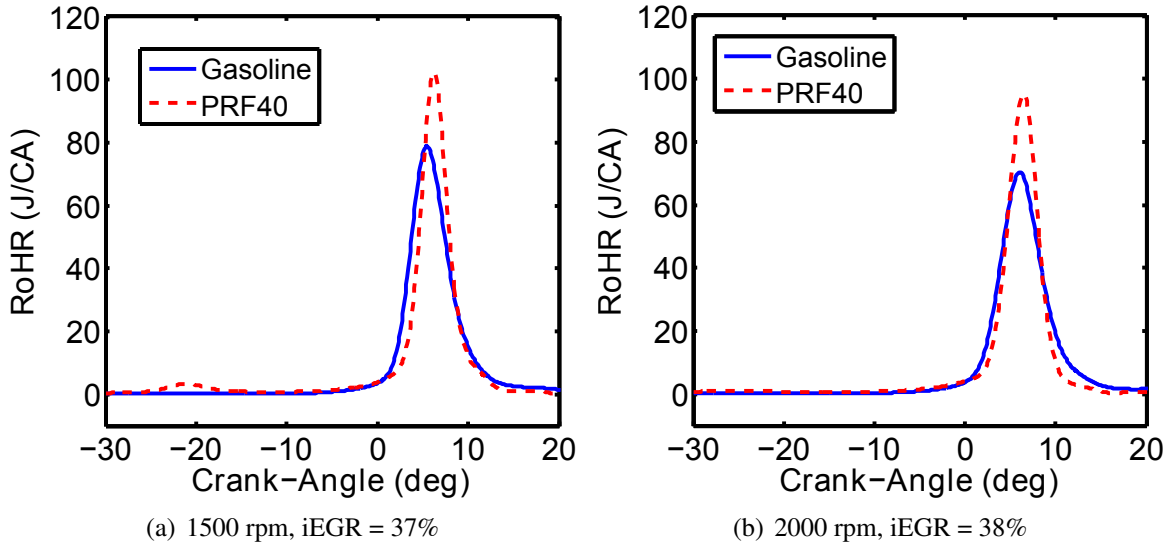
Figure 5.9   Rate of Heat Release Curves Comparing PRF40 and Gasoline

1500 rpm. The PRF40 for both engine speeds demonstrates a progression from LTHR to intermediate temperature heat release (ITHR) before the main ignition event, and this ITHR is elevated above the normalized RoHR for the gasoline. The presence of ITHR has been attributed by Dec [69] to allow for stable retarding of combustion, allowing increased load. In the study in Chapter 3 increased ITHR was observed for the NH40 over gasoline but no LTHR was observed at 2000 rpm, which may be attributable to the lower n-heptane content of NH40 (40% n-heptane) compared to PRF40 (60% n-heptane). The combined LTHR and ITHR for the PRF40 demonstrate a significantly larger portion of burning prior to the main ignition event.

Setting aside for later the discussion on differences in burn rates between fuels, Figures 5.11 and 5.12 show the estimated mean gas temperatures, derived from the the measured pressure traces (Figure 5.12) for both fuels at 1500 and 2000 rpm. For each fuel, the TDC temperature is reduced for the 1500 rpm condition compared to the 2000 rpm condition. This is a function of the ignition delay: at the lower engine speed a lower IVC temperature is required to ignite the fuel at the same phasing, leading to a lower TDC temperature. A lower bulk gas temperature will reduce the thermal gradient between the bulk gas temperature and

(a) 1500 rpm, iEGR = 37%   (b) 2000 rpm, iEGR = 38%
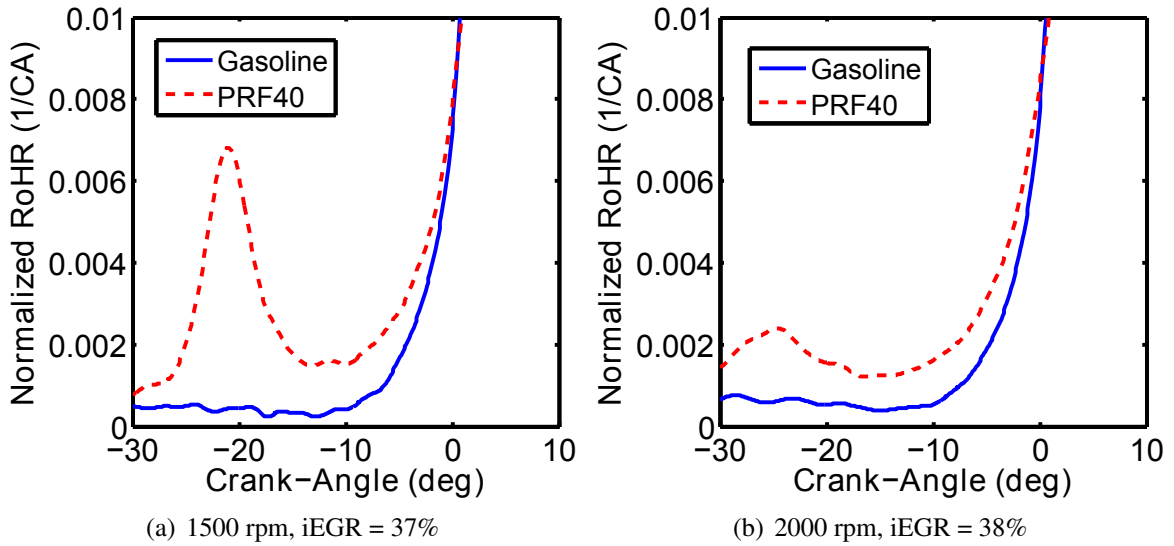
Figure 5.10 Normalized Heat Release Curves Comparing PRF40 and Gasoline

(a) 1500 rpm, iEGR = 37%   (b) 2000 rpm, iEGR = 38%
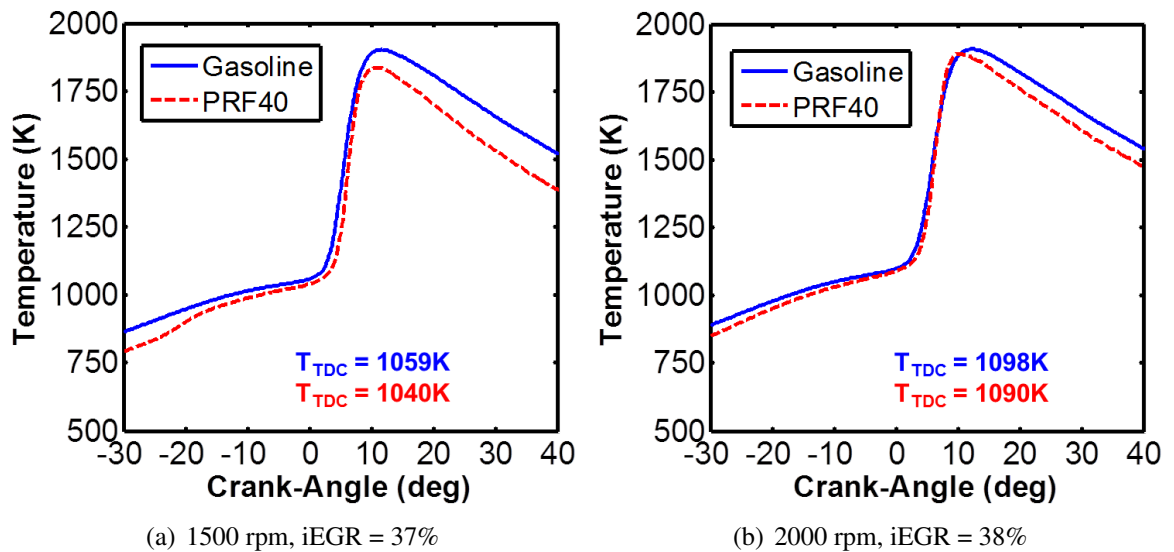
Figure 5.11 Estimated Mean Bulk Gas Temperatures comparing PRF40 and Gasoline

the wall temperature. Such a reduction in thermal gradients could be responsible for the increases in maximum RoHR for both fuels at the reduced engine speed.

Moving from differences in the maximum RoHR to the overall burn duration, Figure 5.8 shows the 10_M–90 burn duration across iEGR sweeps for both PRF40 and gasoline. While the trends with regards to iEGR have been discussed, the focus now is the disparity between the PRF40 and the gasoline. Across all iEGR levels the PRF40 demonstrates a shorter burn

(a) 1500 rpm, iEGR = 37% (b) 2000 rpm, iEGR = 38%
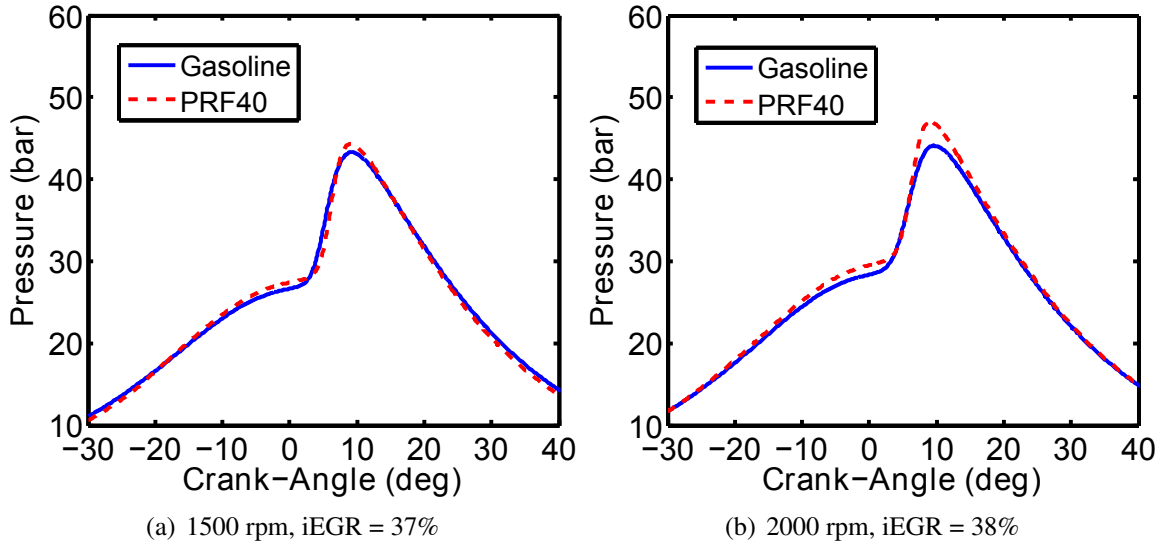
Figure 5.12 Cylinder Pressure Traces comparing PRF40 and Gasoline

duration compared to gasoline. At lower iEGR levels, between 10 and 30%, where gasoline maintains a relatively constant burn duration, the PRF40 has a burn duration ∼29% less than gasoline. This difference increases beyond 30% iEGR as the gasoline begins to exhibit increased burn duration with increasing iEGR. At 2000 rpm the PRF40 has a 10_M–90 burn duration 36% less than gasoline.

5.4   Non-Arrhenius Ignition Delay Effects on Burn Rates

This study has highlighted two primary differences between the PRF40 and gasoline when operated under NVO HCCI conditions. First, whereas gasoline exhibits a trend to have increasing burn duration and reduced maximum RoHR with increased iEGR, PRF40 exhibits no such trend. Second, for a given iEGR, PRF40 demonstrates a significant increase in maximum RoHR and a corresponding decrease in 10_M–90 burn duration. Up to this point the observed differences were noted with no explanation provided. This section provides a discussion on factors which could be responsible for the behavior of the PRF40 in contrast to gasoline.

Section 5.3 clearly demonstrated the differences in heat release rates between PRF40

and gasoline at a fixed iEGR. Let's consider for a moment the factors which could affect the burn rates between the 2000 rpm cases in Figure 5.10 by starting with what could affect burn rates in general. These could be:

1. Equivalence Ratio, ϕ
2. Energy addition/fueling rate
3. Intake Pressure
4. Combustion Phasing
5. Oxygen concentration
6. Dilution/EGR level
7. Turbulence
8. Compositional (local) stratification from NVO
9. Thermal (local) stratification from NVO
10. Thermal stratification due to IVC temperature variation
11. Differences in fuel chemistry characteristics

In the above list, items 1 – 6 were fixed explicitly in the design of the experiments. For item 3 it is noted that we are discussing the 2000 rpm cases, so the inlet pressure is the same (the PRF40 is throttled to 0.95 bar at the 1500 rpm case). For item 7, the engine speed and valve timing is the same between the two cases, there is no reason to believe there is any difference in turbulence. For item 8, the cases selected have the same level of iEGR so any compositional stratification that is due to iEGR will be the same between the cases; the same is true for item 9. This only leaves items 10 and 11 as potential sources for differences that may lead to a difference in burn rates between the fuels.

For item 10, consider Figure 5.16 where the mean TDC temperature is shown as a function of the mean IVC temperature for the experimental data, both calculated from the heat release analysis. All four conditions are for those in Figures 5.11 and 5.12 with the 2000 rpm conditions on the top, and the 1500 rpm conditions on the bottom. Examining Figure 5.16 demonstrates that at 2000 rpm the difference in IVC temperature between PRF40 and gasoline is 16K (505K vs 489K for gasoline and PRF40, respectively). The difference in TDC temperature is 8K (1098 gasoline, 1090 PRF40). So the PRF40 has a slightly cooler temperature both at IVC and TDC, but less of a difference at TDC.

So overall the PRF40 has less of a gradient between the mean bulk gas temperature

and the wall compared to gasoline. Understanding how this might impact the temperature distribution, Figures 5.13 and 5.14 are created to represent an Arrhenius fuel (e.g. PRF40) and a non-Arrhenius fuel (e.g. gasoline), respectively. Here the mean temperature is reduced, as was observed in the experiments. Since the wall temperature is expected to remain the same, the mean is shifted to the left, increasing the occurrence of temperatures near the mean so that the standard deviations from the mean are reduced. Such a reduced thermal gradient at TDC will increase burn rates by means of reducing the amount of deflagrative burning that occurs; with more of the charge at a higher temperature, more of the charge will simultaneously auto-ignite.

It has been shown in a study by Sjöberg [50] that a reduced thermal gradient will lead to a faster burn, as shown in Figure 5.15. In Sjöberg's study this was shown by reducing the coolant temperature, which created larger thermal gradients between the bulk gas and the wall. For this data, it is essentially the inverse condition — cooler bulk gas temperatures are closer to the wall temperature and reduce thermal stratification. So the difference in IVC temperature could have an effect on the burn rate, but the difference in IVC temperature is an indirect fuel chemistry effect. A question then, is what is the source of the different required IVC and TDC temperatures for the PRF40 compared to gasoline?

Considering item 11 on the above list, since the HCCI combustion event is auto-ignited the ignition delay is the fuel chemistry-dependent variable of interest. PRF40 has an ignition delay curve that under these TDC conditions demonstrates non-Arrhenius and NTC behavior [23]. The question then is how does the non-Arrhenius behavior and fit in with other possible effects in the NVO/iEGR environment.

A paper by Babajimopoulos [94] demonstrated that at the top dead center conditions (pressure, temperature) relevant to NVO HCCI combustion, the corresponding ignition delay was equivalent to the time taken to travel 10 crank-angle degrees, and this was found to scale with engine speed - higher engine speeds had a higher TDC temperature and shorter ignition delay, still corresponding to $10°$. So the time available for a fuel to ignite in-cylinder can be
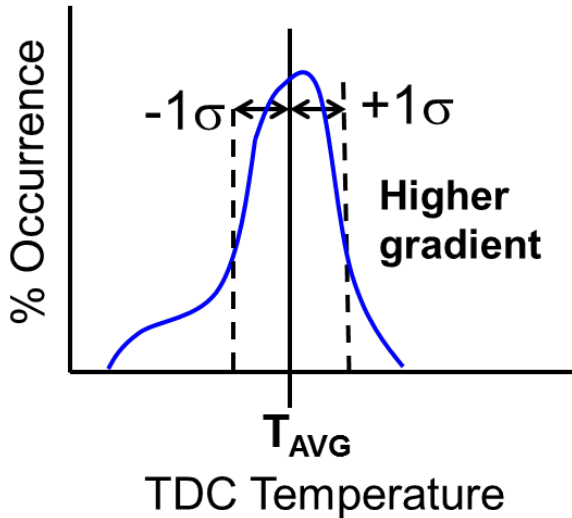
Figure 5.13 Conceptual TDC Temperature probability with greater thermal stratification for higher bulk gas temperature
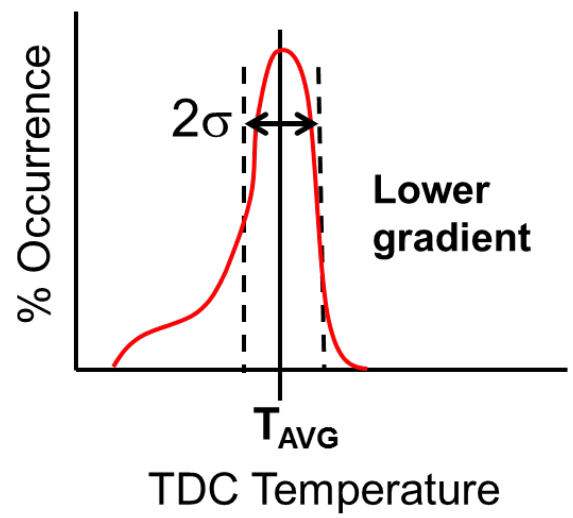
Figure 5.14 Conceptual TDC Temperature probability with reduced thermal stratification for lower bulk gas temperature
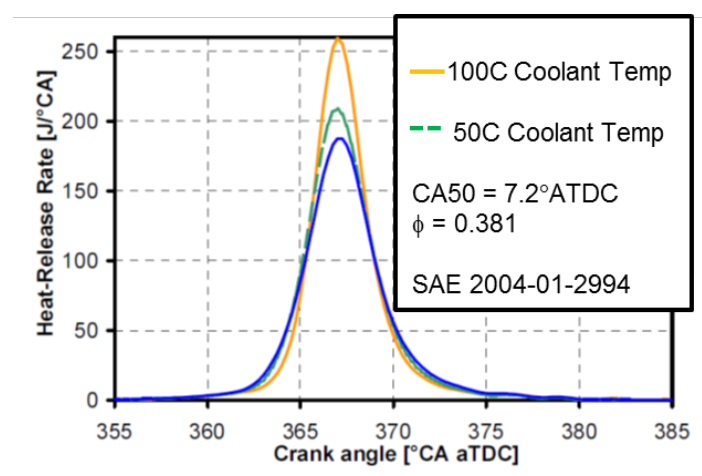
Figure 5.15 Demonstration of reduced HCCI burn rates for higher thermal stratification due to reduced coolant temperature (Sjöberg, 2004). The inverse conditions apply for the PRF40 — cooler gas temperatures serve to reduced thermal stratification between the gas and wall, increasing burn rates.

thought of in terms of fundamental ignition delay, keeping in mind this simple correlation visually represented in Figure 5.17.

A practical engine is significantly stratified in-cylinder and we can imagine a temperature distribution within the cylinder of the engine at TDC as shown in Figure 5.18, similar to what was discussed in Figures 5.13 and 5.14. Again the interactions of the bulk gas with the

91
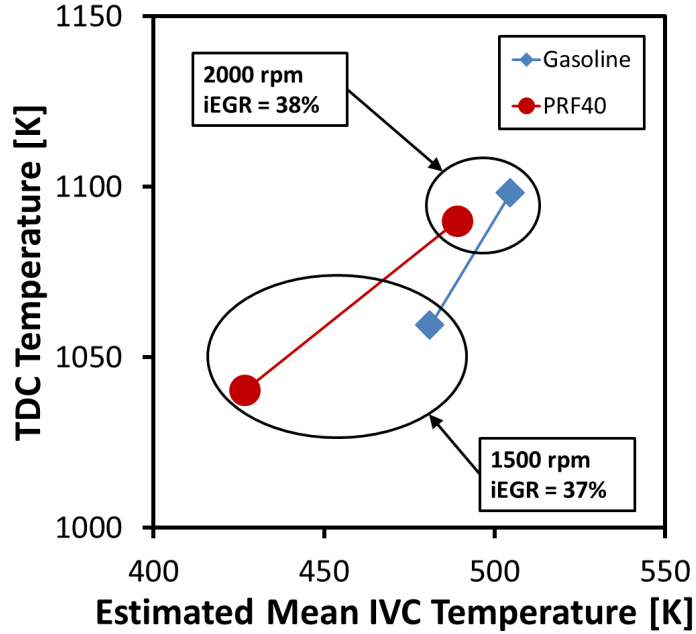
Figure 5.16 Inferred Mean TDC temperature as a function of IVC temperature at 9.0 bar EMEP, CA50 = 6° ATDC

cold wall temperature are considered to skew the distribution towards cooler temperatures. For this distribution there is a mean gas temperature with a standard deviation (σ) around the mean. For now, let us assume this temperature distribution is constant between a high ON fuel that does not exhibit non-Arrhenius behavior, and a low ON fuel that does exhibit non-Arrhenius behavior.

Applying the mean and standard deviation of the bulk gas equally to the two fuels, consider the conceptual ignition delay curves for the high and low ON fuels as shown in Figure 5.19. Assume that the mean gas temperature is down in the region for both fuels where no NTC behavior is present, which in a real engine is a temperature greater than 1000 Kelvin. At the mean temperature, for identical pressure histories in the engine, both fuels share the same ignition delay and will ignite at the same time. Considering the standard deviation in the temperature probability, temperatures at 1σ higher than the mean will still share the same ignition delay, as these will be to the left of the mean where the curves are identical. Now consider the gas at a temperature 1σ less than mean, for which the low ON
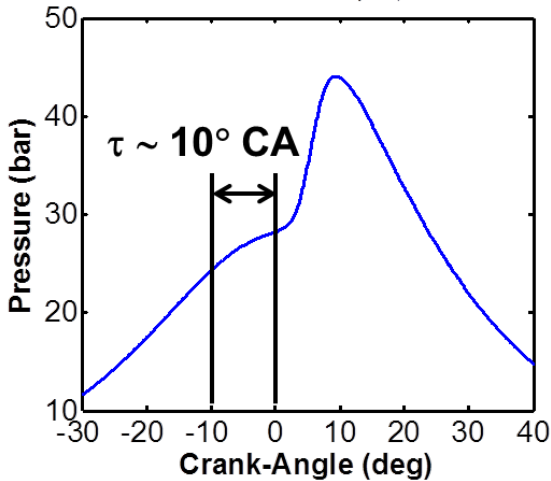
Figure 5.17 Representation of 10°CA window to auto-ignite in HCCI
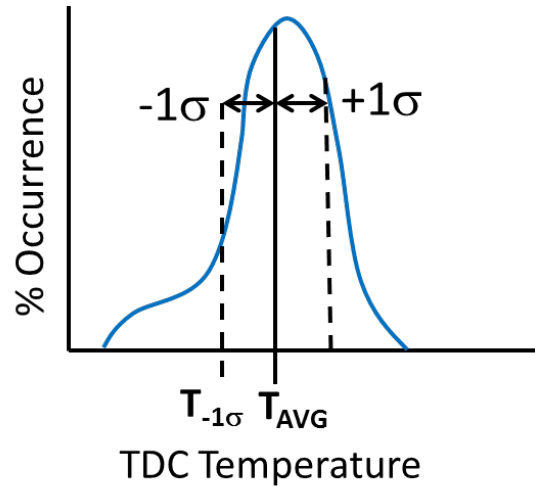
Figure 5.18 Conceptual cylinder temperature probability at TDC
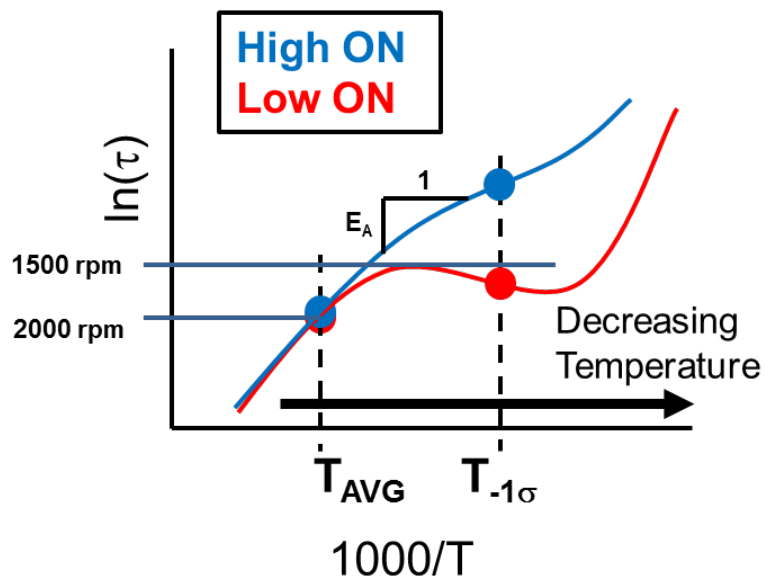
Figure 5.19 Conceptual ignition delay curves for a high ON fuel and a low ON fuel

fuel and high ON no longer behave the same. A temperature of 1σ lower for the low ON fuel puts it in the non-Arrhenius region in this illustration, where the ignition delay is close to that of the mean.

The result is that the gas at a 1σ lower temperature for the low ON fuel will ignite sooner than gas at the same 1σ lower temperature for the high ON fuel as combustion progresses. This is a function of the activation energy [28], which is related to the slope of the ignition

delay curve in Equation 5.1, which can be simplified and re-arranged as Equation 5.2 from which it is noted that the ignition delay is proportional to the activation energy of the fuel. So as combustion progresses, less work energy is required to ignite cooler regions for the low ON fuel than the high ON fuel, and the lower ON fuel completes combustion faster with a shorter burn duration.

$$\tau_{id} = \frac{A}{p^n} exp \left(\frac{E_A}{\tilde{R}T} \right) \tag{5.1}$$

$$ln(\tau_{id}) \propto E_A \frac{1}{T} \tag{5.2}$$

Having discussed potential differences in fuel chemistry leading to the faster burn rate for PRF40, it is now appropriate to revisit the earlier observation of different required IVC and TDC temperatures for the PRF40 compared to gasoline. The reason for the larger disparity in IVC temperature going from 2000 to 1500 rpm is likely do to changes in the ignition delay curve of the fuel. From Figure 5.19, consider reducing speed from 2000 rpm to 1500 rpm. The reduction in speed increases the gas residence in-cylinder in the time domain, lengthening the ignition delay which shifts the ignition delay curve to a lower temperature. For a low ON fuel this can also shift the ignition delay into non-Arrhenius and/or NTC regions, as illustrated by the blue line at 1500 rpm for a fixed ignition delay. Here the required temperature for a given ignition timing is less, which matches what was experimentally observed for the PRF40 compared to gasoline. Also important is that the LTHR is increased at the 1500 rpm condition, requiring less IVC temperature for the required ignition at TDC due to the heating that occurs prior to TDC, raising the bulk gas temperature prior to the main combustion event.

While the lower required bulk gas temperature for PRF40 could explain the faster burn rate for PRF40 compared to gasoline at a fixed iEGR, it does not explain why PRF40 exhibits no sensitivity to increases in iEGR. However, the ignition delay concept allows us to

94

understand how a non-Arrhenius fuel could be less sensitive to changes in iEGR. Assuming a condition with high iEGR has more thermal stratification, as the literature supports, it could be envisioned to have a TDC temperature profile as shown in Figure 5.21. This is compared to a lower iEGR condition with a temperature distribution less spread out due to reduced thermal stratification, and is illustrated in Figure 5.20. For the low iEGR case the standard deviation is lower than for the high iEGR case, and when we put these standard deviations on the ignition delay chart we've shown previously, Figure 5.22 is the result. Here it is clear that for the high ON fuel such as gasoline changes in stratification will have a noticeable effect on the ignition delay of the local mixture at that temperature compared to the bulk gas temperature. For the low ON fuel, in the non-Arrhenius region, changes in the temperature due to stratification have less impact (if any at all) on the ignition delay when compared to the high ON fuel.

As was discussed before, the high ON fuel will have a longer burn duration at high iEGR cases with a wide temperature distribution due to the higher activation energy required to ignite the cooler regions which leads to a slower progress of combustion. For the low ON fuel, the increased change in temperature due to stratification, if within the non-Arrhenius region, will not exhibit significant change in ignition delay and combustion will progress similarly between the high and low iEGR cases. This is what was experimentally observed, supporting this understanding of the fuel chemistry effect being tied to the ignition delay behavior.

Another possible scenario for a fuel that exhibits not just non-Arrhenius behavior but true NTC behavior is the potential for "multiple-ignition" sources to increase the burn rate. Examining Figure 5.19 again, consider that if the 1σ lower temperature is in the NTC region at an ignition delay equal to the mean, these cooler regions would ignite simultaneously with the regions at the mean temperature. Couple this with a lower activation energy, and the combustion rate of progress for the low ON fuel would be faster than the high ON fuel.
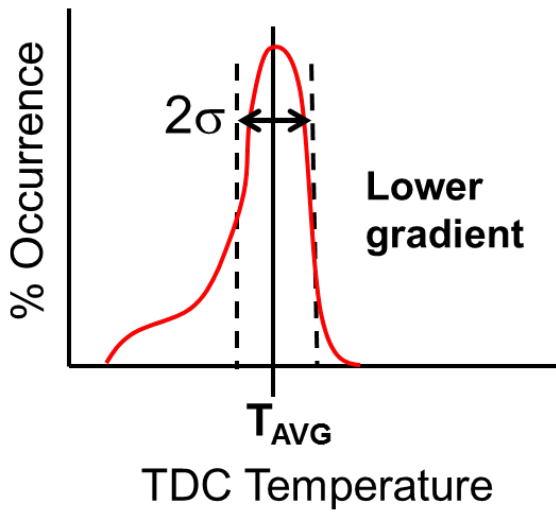
Figure 5.20 Conceptual TDC Temperature probability with reduced thermal stratification at lower iEGR level
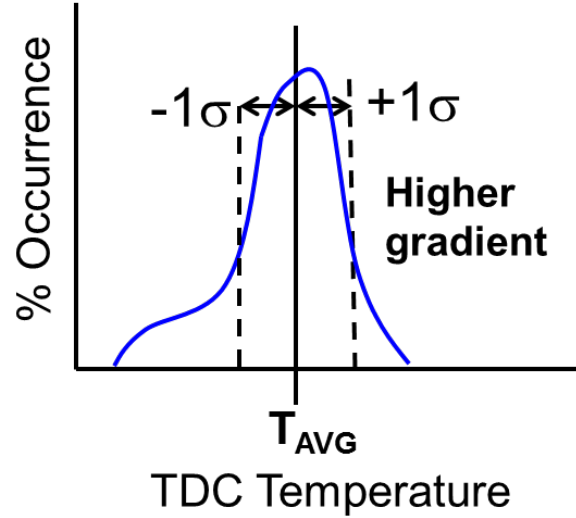
Figure 5.21 Conceptual TDC Temperature probability with greater thermal stratification at higher iEGR level
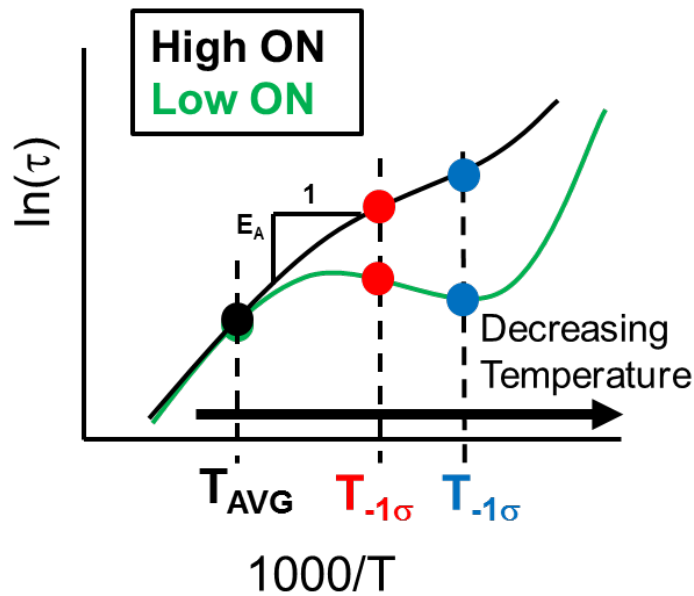
Figure 5.22 Conceptual ignition delay curves and the impact of reducing thermal stratification with reduced iEGR. The blue 1σ on the right corresponds to the blue colored higher gradient profile, the red 1σ on the left corresponds to the red colored lower gradient temperature profile, highlighting how a non-Arrhenius fuel is less sensitive to gradient changes which could be attributed to changes in iEGR.

5.5   Discussion and Summary

Several key findings were made in this chapter with regards to the behavior of PRF40 as compared to gasoline. A follow up to the study in Chapter 3, this chapter applied the newly developed constant composition control method detailed in Chapter 4 to clearly separate fuel effects from iEGR effects on HCCI burn rates in the NVO engine.

In performing iEGR (trading iEGR for eEGR) sweeps at constant phasing and composition, it was demonstrated that gasoline exhibits a sensitivity to iEGR with respect to burn rates — increased levels of iEGR decreased burn rates and lengthened combustion duration. This trend was not observed for the PRF40 undergoing similar iEGR sweeps, where no dependence on burn rates to iEGR was found. Furthermore, for a given iEGR level, PRF40 exhibited a significant increase in burn rates, and a correspondingly shorter burn duration, compared to gasoline. The PRF40 demonstrated LTHR, present at all engine speeds an increasing in magnitude as engine speed decreased.

Three methods have been proposed by which PRF40 could use non-Arrhenius behavior to increase burn rates in the NVO HCCI environment. First, it was observed that the IVC temperature required for a fixed combustion phasing for PR40 is less than for gasoline. While LTHR was shown to increase temperatures prior to TDC, for PRF40 they are still below the TDC temperatures for gasoline. This suggests that there is reduced thermal stratification for the PRF40, due to the reduced bulk gas temperature compared to wall temperature, and this will lead to increased burn rates. The required temperature is a function of the fuel chemistry as understood through a shallower ignition delay slope, characteristic of a non-Arrhenius fuel. The fact that for a fixed iEGR the PRF40 has a lower TDC temperature supports this concept, as it must be on a lower slope to ignite at the same time at a lower temperature compared to gasoline.

Second, the faster burn for PRF40 was interpreted by means of considering the temperature distribution in-cylinder and how that relates with the activation energy of the fuel, a function of the slope of the ignition delay curve. If auto-ignition occurs in or near

the non-Arrhenius region due to temperature stratification, a non-Arrhenius lower ON fuel such as PRF40 would then burn faster compared to a higher ON fuel exhibiting Arrhenius behavior (such as gasoline).

Last, it is possible that there are "multiple ignition temperatures" for a non-Arrhenius fuel such as PRF40, which means that different portions of the charge at different temperatures can auto-ignite simultaneously or very closely together, compared to an Arrhenius behaving fuel such as gasoline which must "ride the curve" of the ignition delay, waiting longer for cooler regions to ignite.

The lack of dependence of PRF40 on iEGR in terms of burn rates is understood to be a function of PRF40 exhibiting non-Arrhenius ignition delay behavior. With this, increases in thermal stratification in-cylinder fall within the non-Arrhenius region of the ignition delay curve where the slope of the ignition delay curve is very low and not sensitive to changes in temperature. This results in burn rates for the PRF40 remaining constant as iEGR is increased. This is in contrast to gasoline which is understood to demonstrate an ignition delay curve more closely resembling an Arrhenius curve, and sensitive to changes in temperature, which increases sensitivity to iEGR.

Chapter 6

Fuel and iEGR Effects on HCCI Stability Limits

In the first study in Chapter 3 it was observed that at the load limit, the NH40 fuel was operated at higher load at a later combustion phasing. Due to the nature of the experiment it was not clear which factors enabled this later phasing. The NH40 was operated with less iEGR than the gasoline, which could could contribute to the later phasing, as discussed in Section 1.2.3. However in Section 5.2 it was observed that PRF40 exhibited no dependence on iEGR for burn rates, so it is not immediately clear which effect is more important to phasing limits for a low octane fuel: iEGR level or fuel chemistry. The purpose of this chapter is to explore both iEGR (NVO) and fuel chemistry effects as it relates to HCCI phasing limits.

Previous studies [51] with "pure" HCCI have demonstrated that HCCI can be subject to cycle to cycle variability, and it is hypothesized here that increasing the level of iEGR could lead to increased cyclic feedback, increasing the COV of IMEP$_g$. The highest iEGR cases in Chapter 5 had the total iEGR equal to 43% of the charge. This is a significant level of iEGR and creates a dependency on any given cycle to the cycle previous to it; a late burning cycle will have higher exhaust temperatures (and potentially more unburned fuel) leading the next cycle to be advanced; an advanced cycle will lower exhaust temperatures leading to a late burning cycle following, so setting up a "see-saw" effect on the combustion phasing, leading to a higher COV of IMEP$_g$. The preceding is the theory that led to this study.

The experiments of this chapter will again follow the method outlined in Chapter 4, maintaining constant charge composition across all fuels, iEGR levels and engine speeds. Instead of maintaining a fixed combustion phasing (CA50), for each test condition

combustion was retarded until the combustion stability limit was reached. The combustion stability limit was chosen to be a COV of IMEP$_g$ equal to 3%. This was selected for COV of IMEP$_g$ is a common stability limit criteria and easily measured real-time while operating the engine. For this study only two engine speeds were examined, 1000 rpm and 2000 rpm, with strong LTHR expected at 1000 rpm and little to no LTHR at 2000 rpm. The engine conditions for these experiments are summarized in Table 6.2.

For this study, as with Chapter 5, a pure PRF was compared with gasoline. For the Chapter 5 study, PRF40 was selected to provide a significant difference in ON and LTHR behavior between it and gasoline. When the PRF40 was phased at CA50 = 6° ATDC, as was the case for that study, it was possible to operate within a wide range of iEGR and engine speed conditions. As was noted in Section 5.4, the onset of LTHR at lower engine speeds required reduction of the inlet temperature for the PRF40. It was found that retarding combustion of PRF40 to the stability limit at 1000 rpm would require an inlet temperature below the ambient test cell temperature and as such was not possible. To increase the required inlet temperature to operable levels yet retain a low ON, PRF60 was selected for these experiments. PRF60 allowed the desired retarding of combustion phasing down to 1000 rpm at a sufficient range of iEGR levels. Specific fuel properties are listed in Table 6.1.

6.1   iEGR Effects on Gasoline Stability Limits

As a precursor to running this series of experiments, high and low iEGR cases for gasoline were examined to determine if a difference existed in the COV of IMEP$_g$ at a fixed phasing. For this comparison two gasoline cases at 2000 rpm from Chapter 5 were selected: a high iEGR case (iEGR = 43%) and a low iEGR case (iEGR = 19%). The pressure traces and MFB curves for all 200 cycles are plotted in Figure 6.1. The numerical difference in the COV of IMEP$_g$ for these two cases is small, 1.3% vs 1.5% for the low and high iEGR cases respectively. Despite this, there is a noticeable visual spread in the pressure and MFB curves

Table 6.1 Test fuel properties

Property	PRF60	Gasoline
LHV [kJ/kg]	44401	43043
Density [g/mL]	0.689	0.736
MW [g/mol]	108.2	93.0
H/C [molar]	2.265	1.879
RON	60	90.5
MON	60	82.6
AKI [(R+M)/2]	60	87
Paraffins [% WGT]	40	8.1
Iso-Paraffins [% WGT]	60	37.5
Aromatics [% WGT]	0	32.3
Napthenes [% WGT]	0	16.9
Olefins [% WGT]	0	4.5
Boiling Point [°C]	99	N/A
10% Evaporation [°C]	N/A	62
50% Evaporation [°C]	N/A	95
90% Evaporation [°C]	N/A	145

Table 6.2 Experimental parameters

Parameter	Value
Engine Speed [RPM]	1000 – 2000
Fuel Injection Pressure [bar]	≈ 100
Fuel Start of Injection [° BTDC]	330
Intake Temperature [°C]	35 – 200
Abs. Intake Pressure [bar]	0.9 – 1.0
Abs. Exhaust Pressure [bar]	1.05
Coolant Temperature [°C]	90
Oil Temperature [°C]	90
Ringing Intensity [MW/m^2]	< 3.0
COV of IMEP$_g$[%]	3.0
Emissions Index NO$_X$ [g/kg-fuel]	<1.0

for the high iEGR case compared to the low iEGR case.

To examine the sequence of the cycles as it relates to combustion phasing, all 200 recorded cycles are plotted in Figure 6.2 for both the low and high iEGR cases. Examining the CA50 histories demonstrates that despite the fact the two different cases have the same mean CA50, the individual cycles have a much larger spread around the mean for the high
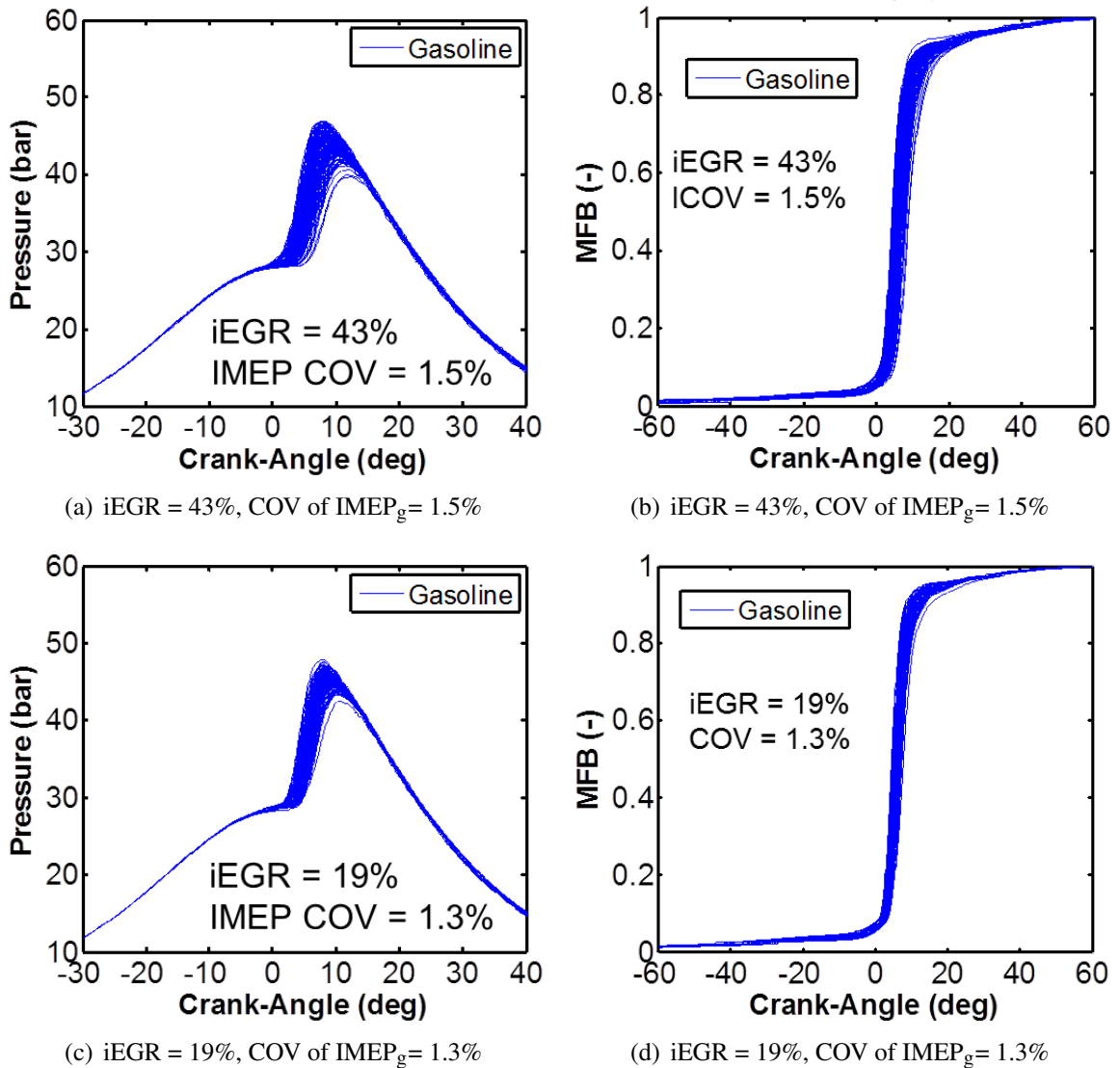
Figure 6.1 Comparing gasoline pressure and mass fraction burn histories for 200 cycles at 2000 rpm for fixed mean CA50 = 6° ATDC at high iEGR (43%) and low iEGR (19%) conditions

iEGR case. It is not clear from these plots if the larger spread is due to the cyclic feedback theory discussed at the beginning of this chapter.

In order to examine the relationship between cycles, plots referred to as "first return plots" were made for each of the cases, and are shown in Figure 6.3. First return plots are based in chaos and nonlinear dynamics theory [95, 96] and have previously been used by Wagner [97] in examining cyclic variability in SACI combustion cases. In the plots, each point represents a single recorded cycle, with the abscissa representing the CA50 of the
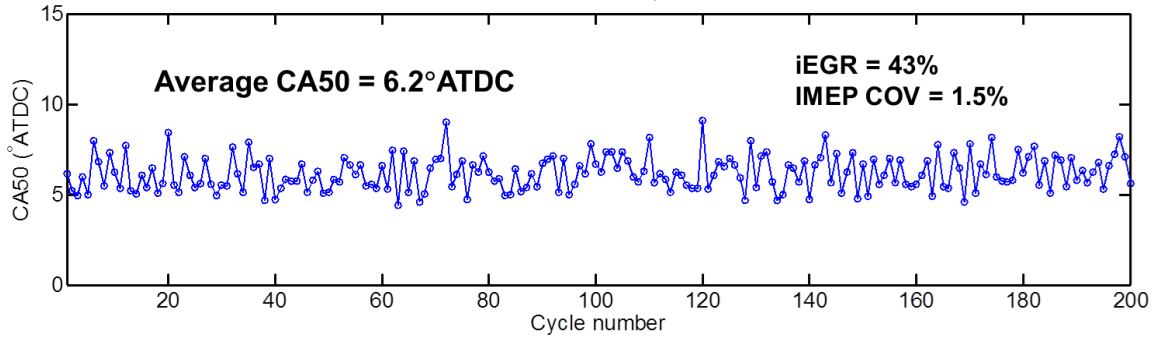
(a) iEGR = 43%, COV of IMEP$_g$= 1.5%
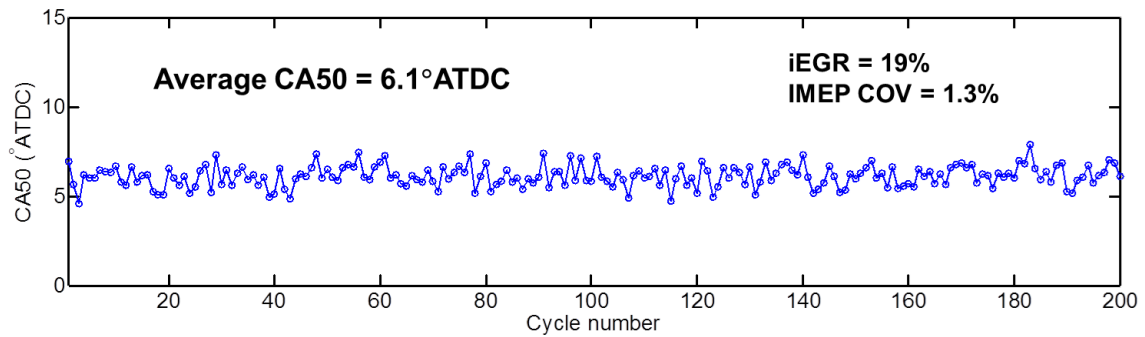
(b) iEGR = 19%, COV of IMEP$_g$= 1.3%

Figure 6.2 Comparing gasoline location of CA50 history for 200 cycles at 2000 rpm for fixed mean CA50 = 6° ATDC at high iEGR (43%) and low iEGR (19%) conditions

selected cycle and the ordinate representing the CA50 of the immediately following cycle. The solid line plotted is the line of equal phasing — that is the cycle following has an equal CA50 to the current cycle. A distribution along this line or equally clustered around this line represents a random distribution of phasing. Conversely, data points spreading out perpendicular or away from the line represent what is called "anti-correlated" behavior, where the CA50 of the current cycle is either advanced or retarded, and followed by a cycle with a phasing shift in the opposite direction.

Examining the first return plots for the two cases provides no dramatic differences but the overall spread of CA50 data points for the high iEGR case in Figure 6.3(a) is greater than that of the low iEGR case in Figure 6.3(b), and exhibits slightly more anti-correlated behavior within the spread. These plots suggest a small decrease in cyclic variability as the iEGR was decreased, despite the actual difference in COV of IMEP$_g$ being small; these

(a) iEGR = 43%, COV of IMEP$_g$= 1.5%   (b) iEGR = 19%, COV of IMEP$_g$= 1.3%
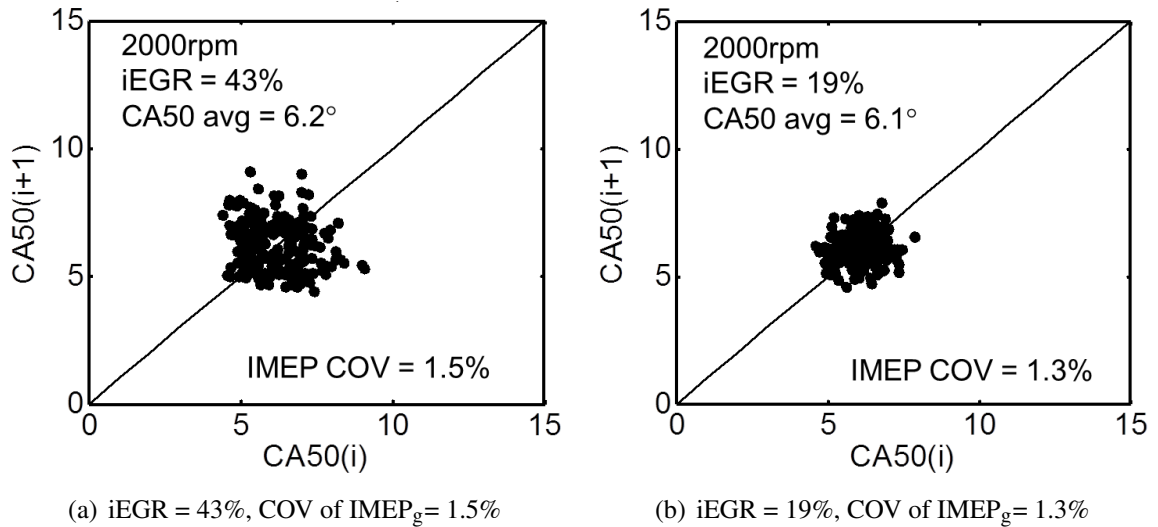
Figure 6.3   Comparing gasoline first return map plots of CA50 location for 200 cycles at 2000 rpm for fixed mean CA50 = 6° ATDC at high iEGR (43%) and low iEGR (19%) conditions

cases are at a relatively early fixed combustion phasing and very stable. Nevertheless, a sufficient difference existed to perform a study at fixed combustion stability to examine the effect of iEGR on phasing limits at a fixed stability. The hypothesis being that if low iEGR produces less cyclic feedback, then for a given stability limit, a low iEGR case should be able to operate at a later combustion phasing than a high iEGR case, all other things being equal.

Resulting from this new experiment, a phasing map of the iEGR sweeps is shown in Figure 6.4, demonstrating that as iEGR is reduced, the allowable late phasing limit for the fixed COV of IMEP$_g$ is retarded. The spread of iEGR was from $17\% - 45\%$ between the two engine speeds of 1000 and 2000 rpm. With regards to engine speed, no discernible difference is observed trend-wise between iEGR and the CA50 limit: the overlap of iEGR between engine speeds shows an identical trend of increasing the CA50 retard limit at the fixed COV of IMEP$_g$. Both engine speeds are clear in the trend with increasing iEGR advancing the CA50 limit for the fixed COV of IMEP$_g$ condition. For the 2000 rpm sweep, increasing the iEGR from a low of 17% to a high of 42% retarded CA50 from 8.5° ATDC to 12.8° ATDC, not an insignificant difference. The question that remains then, is how the
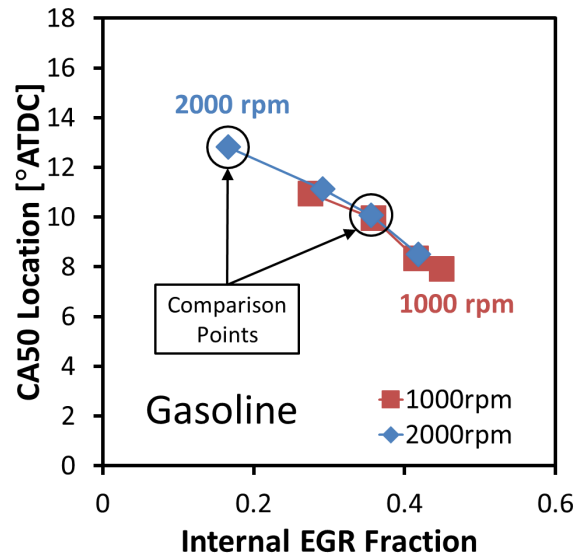
Figure 6.4   Gasoline iEGR sweeps at COV of IMEP$_g$ = 3%

increase in iEGR is related to reducing combustion phasing limits.

To answer the question of how iEGR relates to phasing limits, comparison points of high and low iEGR were selected from the 2000 rpm iEGR sweep; a "high" EGR case of 36% iEGR and a "low" EGR case of 17% iEGR as highlighted in Figure **??**. The pressure and MFB history for all 200 cycles of these cases are plotted in Figure 6.5. There is significant difference in the range of peak pressure and combustion phasing comparing the 36% iEGR condition to the 17% iEGR condition, and the difference is noticeably greater than the difference between high and low iEGR fixed CA50 cases in Figure 6.1. Examining the history of CA50 across the 200 cycles in Figure 6.6 the increase in the spread of CA50 for the 36% iEGR case is evident, and it appears that a significantly retarded CA50 case is usually followed by a significantly advanced case.

To clearly demonstrate the relationship between early and late cycles, first return plots are presented for the 2000rpm 17% and 36% iEGR cases in Figure 6.7. Here the contrast between the high and low iEGR cases is quite apparent, with the 36% iEGR case demonstrating marked "anti-correlated" behavior. Whereas the 17% iEGR case has an essentially random distribution clustered around the mean CA50 of 12.8°ATDC, the

(a) Pressure history, iEGR = 36%

(b) MFB history, iEGR = 36%

(c) Pressure history, iEGR = 17%

(d) MFB history, iEGR = 19%
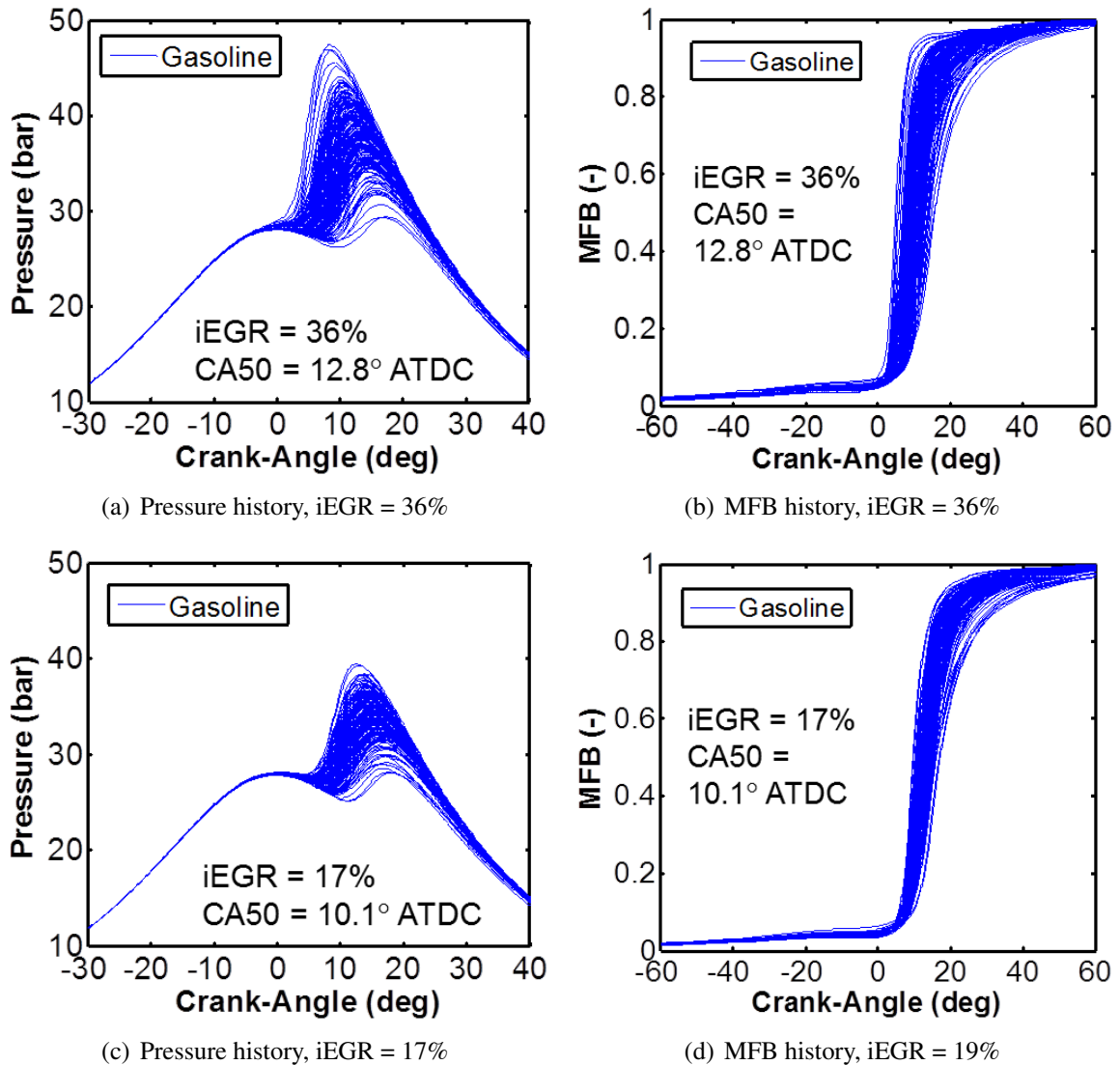
Figure 6.5 Comparing gasoline pressure and mass fraction burn histories for 200 cycles at 2000 rpm for a fixed COV of $IMEP_g$ = 3% at high iEGR (36%) and low iEGR (17%) conditions

36% iEGR case resembles more of a "band shaped" distribution, spreading out almost perpendicular to the line of equal return phasing. Aside from the shape of the distribution, spread of CA50 across 200 cycles is shown to be higher for the 37% iEGR case compared to the comparatively narrower spread in CA50 for the 17% iEGR case. The narrower spread of CA50 is required for a later phasing at a fixed COV of $IMEP_g$. This can be thought of in terms of how spark timing effects brake torque (BMEP) as spark retards from MBT [28]. Small variations in spark timing make little difference in BMEP near MBT but as spark is

106
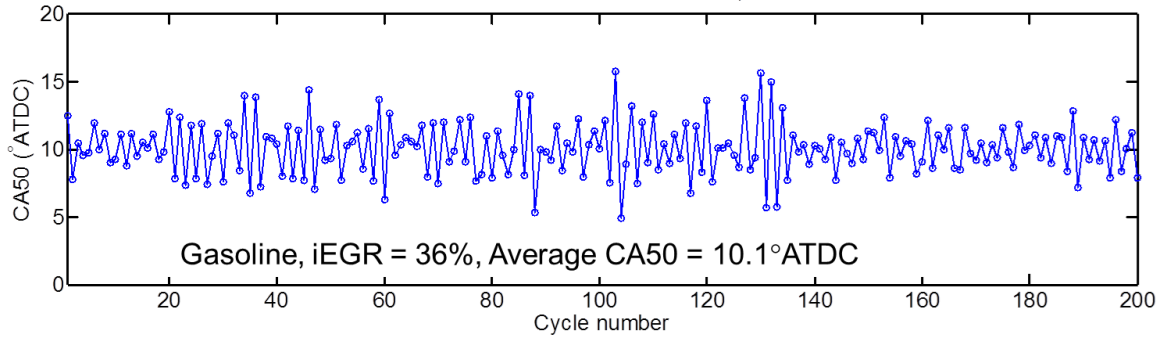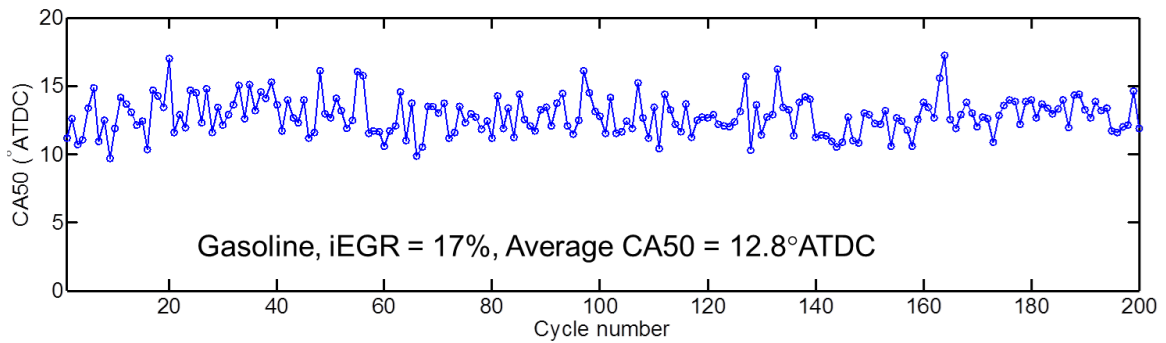
(a) Gasoline, iEGR = 36%

(b) Gasoline, iEGR = 17%

Figure 6.6   Comparing gasoline location of CA50 history for 200 cycles at 2000 rpm for a fixed COV of $IMEP_g$ = 3% at high iEGR (36%) and low iEGR (17%) conditions

retarded away from MBT the slope of BMEP drop increases as spark is retarded further and combustion retards farther into the expansion stroke. In the same way, the further CA50 is retarded from maximum IMEP, the greater a change in CA50 will have on IMEP. So a later phasing requires less change in CA50 than an earlier phasing for a given COV of $IMEP_g$.

The first return plot showing a high level of anti-correlated behavior for the high iEGR case is a clear demonstration that increases in iEGR not only leads to greater variation in CA50, but the variation is coupled to a cyclic dependency. This agrees with the hypothesis that a larger level of iEGR increases the dependence of the current cycle on the one previous to it, and for the first time quantifies to what degree the effect is on phasing limits.
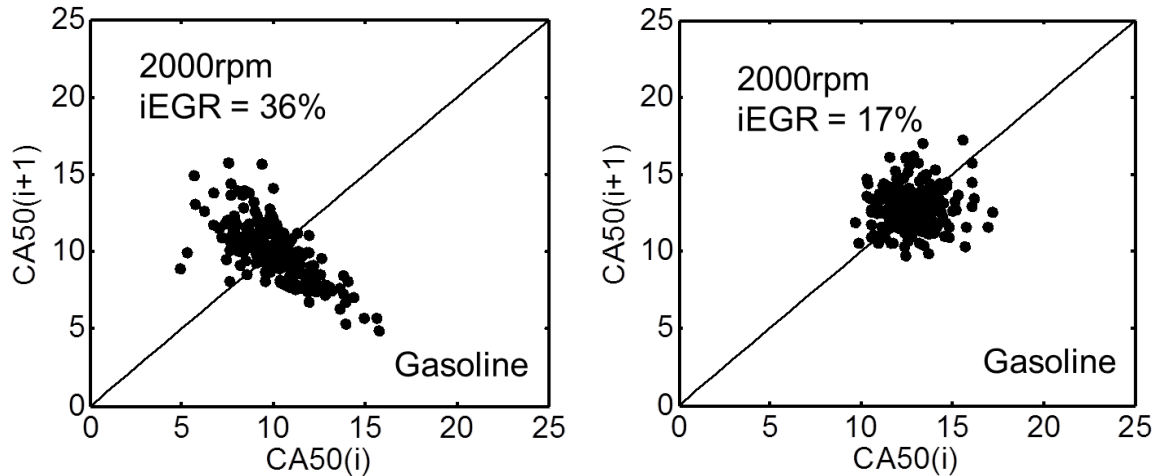
(a) Gasoline, iEGR = 36%, avg. CA50 = 10.1° ATDC   (b) Gasoline, iEGR = 17%, avg. CA50 = 12.8° ATDC

Figure 6.7   Comparing gasoline first return map plots of CA50 location for 200 cycles at 2000 rpm for fixed COV of IMEP$_g$ = 3% at high iEGR (36%) and low iEGR (17%) conditions. The high iEGR case has a reduced CA50 limit and demonstrates a wider spread in CA50.

6.2   Comparison of Gasoline and PRF60 Stability Limits

With the knowledge that increased levels of iEGR will reduce the phasing limit for gasoline, the study now investigates the effect of a low ON fuel on phasing limits, and to what impact, if any, LTHR and ITHR may play in the ability to retard combustion phasing limits over gasoline. Figure 6.8 contains the iEGR sweeps for PRF60 at 1000 rpm and 2000 rpm, with the respective gasoline sweeps. For both PRF60 and gasoline, a condition was operated at 36% (*pm*1 percentage point) for each engine speed, and these four cases will be examined in detail.

Starting first with the 1000 rpm iEGR sweep, it is observed that the PRF60 does not exhibit a strong trend with iEGR, in fact for most of the sweep the CA50 at the COV limit remains constant, which is an obvious departure from the gasoline. This is reminiscent of the behavior that was observed in Chapter 5 where the PRF40 did not show a dependence on iEGR for burn rates or burn duration, but the gasoline did. To examine this, the cases at 36% will be examined.

First, to relate the fuel effects to iEGR effects, the first return plots for gasoline and
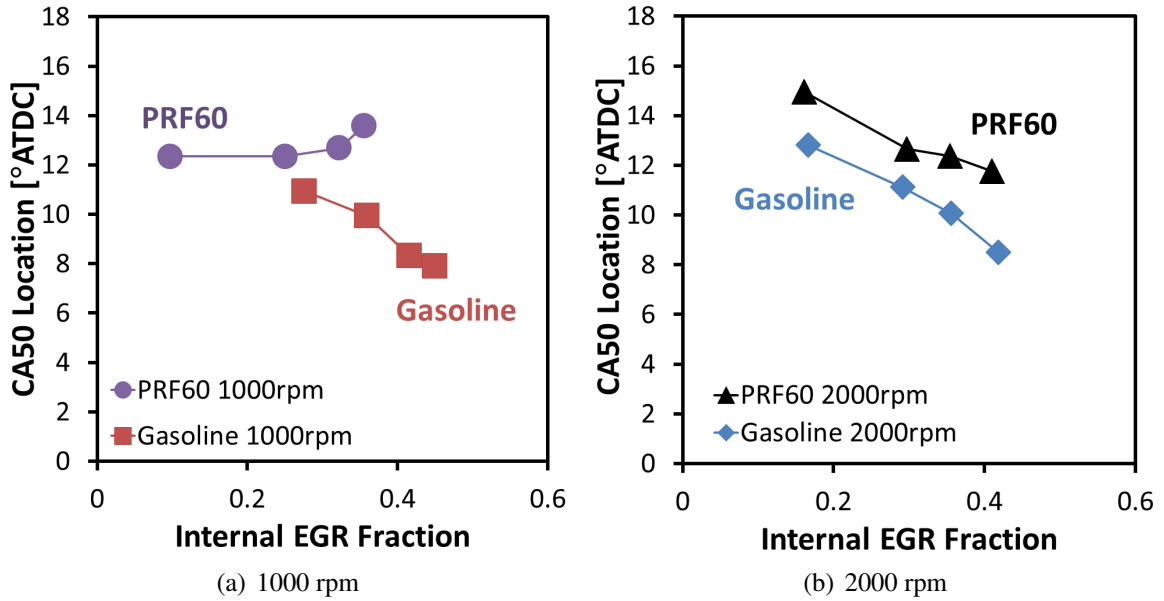
Figure 6.8 CA50 location of gasoline and PRF60 for iEGR sweeps at 1000 and 2000 rpm, COV of $IMEP_g = 3\%$. Gasoline CA50 data is repeated from Figure 6.4

PRF60 at 1000 rpm are given in Figures 6.9(a) and 6.9(b) respectively. Here the gasoline again demonstrates "anti-correlated" behavior corresponding to the cyclic feedback of this relatively high iEGR condition, similar to what was observed in at 2000 rpm as shown in Figure 6.9(c) (in fact, Figure 6.9(c) for gasoline at 2000 rpm is the same plot as Figure 6.7(a) but repeated for convenience to the reader). In a noticeable departure from the gasoline the PRF60 exhibits no "anti-correlated" behavior at the same iEGR level, instead the CA50 distribution for PRF60 is randomly clustered in a circular manner around the mean. Furthermore, for the same iEGR (36%), the PRF60 can be operated at a later combustion phasing compared to the gasoline — 13.6° ATDC CA50 for the PRF60 compared to 9.9° ATDC for gasoline.

To explore how the PRF60 is able to operate independently of the "anti-correlated" iEGR effects exhibited by the gasoline, and to operate at a later combustion phasing, the RoHR and normalized RoHR curves for the 36% iEGR cases at 1000 rpm are shown in Figures 6.10(a) and 6.10(b) respectively. Note that for the normalized RoHR curves the PRF60 curve was advanced by 3.6° to align it with the gasoline for a comparison of ITHR occurring

(a) Gasoline, 1000 rpm, avg. CA50 = 9.9° ATDC   (b) PRF60, 1000 rpm, avg. CA50 = 13.6° ATDC

(c) Gasoline, 2000 rpm, avg. CA50 = 10.1° ATDC   (d) PRF60, 2000 rpm, avg. CA50 = 12.4° ATDC
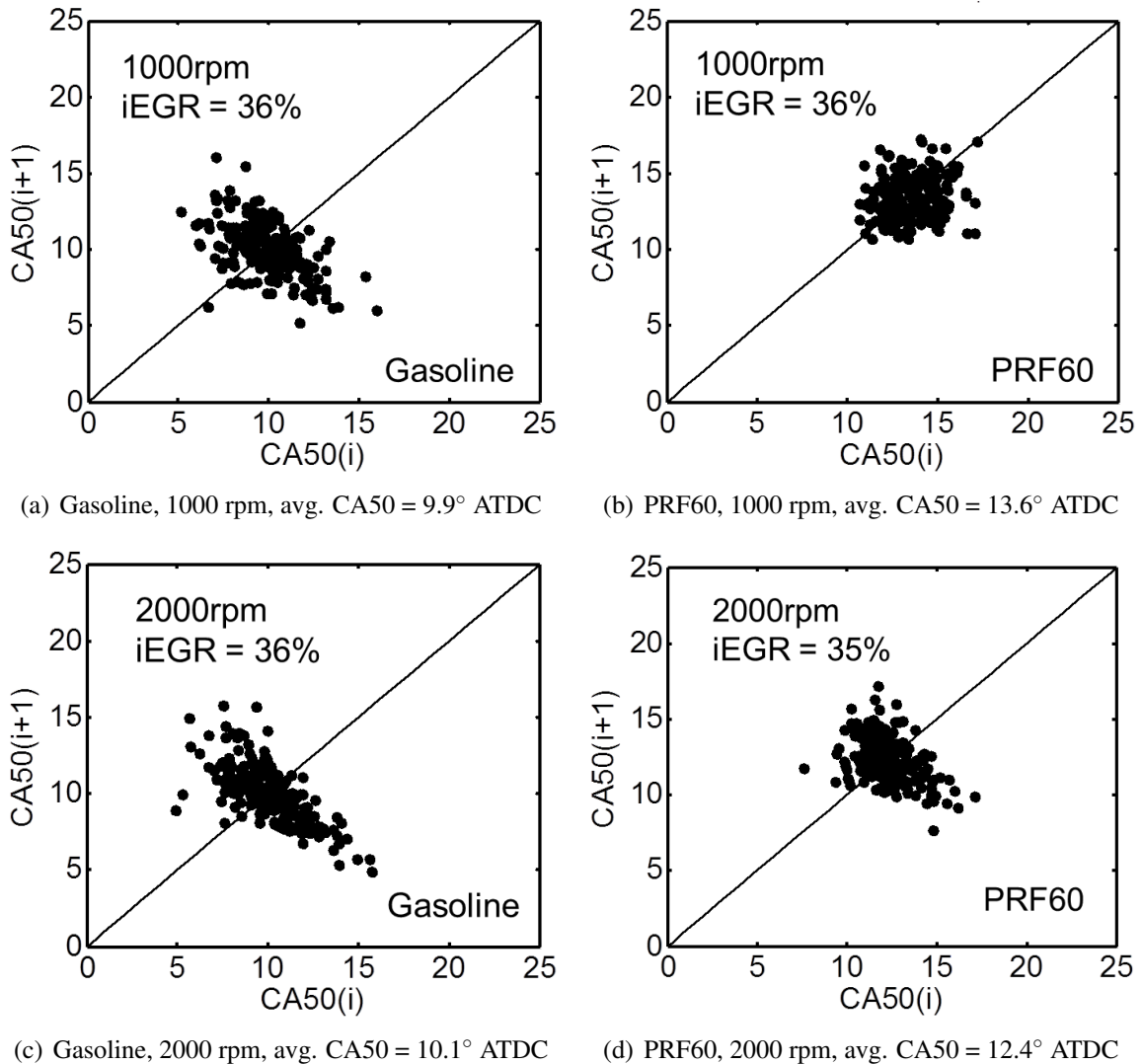
Figure 6.9   Comparing gasoline and PRF60 first return map plots of CA50 location for 200 cycles fixed COV of $IMEP_g$ = 3% at a fixed iEGR = 36%

before main ignition. For the PRF60, there is a noticeable LTHR event centered around 20° ATDC followed by the main combustion event. The main combustion event for the PRF60 is phased later corresponding to the later CA50 observed in Figure 6.8(a). Note that while the combustion phasing is later, the PRF60 had a maximum RoHR equal to that of gasoline.

The 10_M–90 burn duration for the 1000 rpm cases is shown in Figure 6.11(a), and while at 36% iEGR the burn duration is not equal between fuels, the general trend is that the 10_M–90 burn duration for both PRF60 and gasoline remains relatively constant as the iEGR

is reduced. When taking into account the error bars, there is in fact no statistical difference for the burn duration between fuels or across the iEGR sweep. Figure 5.8 in Chapter 5 demonstrated that the PRF40 showed no influence of iEGR on burn duration at 1000 rpm, whereas gasoline demonstrated an increase in burn duration above $\sim 30\%$ iEGR. This demonstrates the trade-off that is occurring for gasoline as iEGR is reduced and CA50 retarded for the fixed COV of $IMEP_g$ study. Whereas at a fixed combustion phasing reducing iEGR reduced the overall burn duration, since the phasing was retarded to maintain the COV of $IMEP_g$ the burn duration remains constant as retarding combustion phasing will slow the burn and increase the burn duration, which in this case is counter-acted by the reduction of iEGR for gasoline.

For the PRF60 at 1000 rpm, it was shown that the maximum RoHR matches that of gasoline, and overall the 10_M–90 burn duration between the fuels is again statistically the same across the sweep. The ability of the PRF60 to burn at the same rate as the gasoline at retarded phasing is believed to be related to the difference in the ignition delay curves of the fuels. As described in Section 5.4 the PRF60, similar to PRF40, is understood to have a shallower slope to the ignition delay curve compared with gasoline. This concept, with regards to phasing limits, will be developed in a later section.

Now examining the 2000 rpm cases for and gasoline and PRF60 for 36% iEGR, the first return plots in Figures 6.9(c) and 6.9(d) for gasoline and PRF60 respectively show that here PRF40 appears to exhibit some "anti-correlated" behavior, but to a lesser degree than the gasoline. Further examining the cases, Figure 6.8(b) illustrates the CA50 location as a function of iEGR for both fuels. Here both PRF60 and gasoline demonstrate a similar trend of retarding CA50 at the COV of $IMEP_g$ limit as iEGR decreases. The slopes of the lines appear in fact to be very similar, with the PRF60 shifted by a couple of degrees. Comparing the RoHR and normalized RoHR (here with PRF60 shifted 2.3°to align maximum RoHR for comparison) curves in Figures 6.10(c) and 6.10(d) there are several observations. First, the PRF60 exhibits no LTHR at 2000 rpm. This agrees with the findings of Chapter 3, where
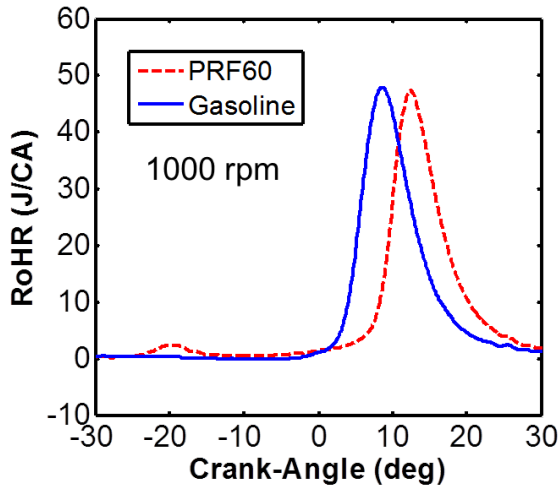
(a) 1000 rpm, Rate of Heat Release
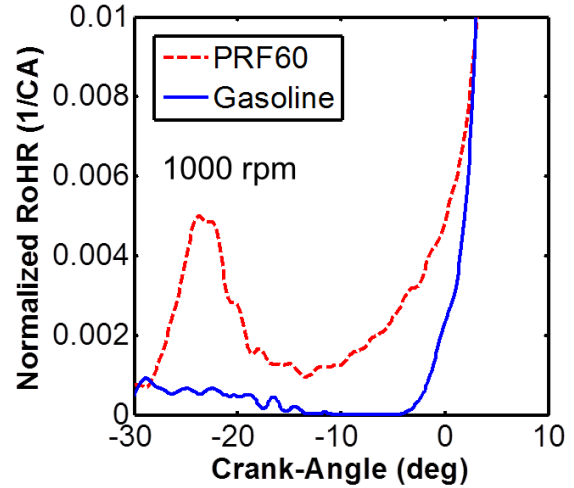
(b) 1000 rpm, Normalized RoHR, shifted to align maximum RoHR
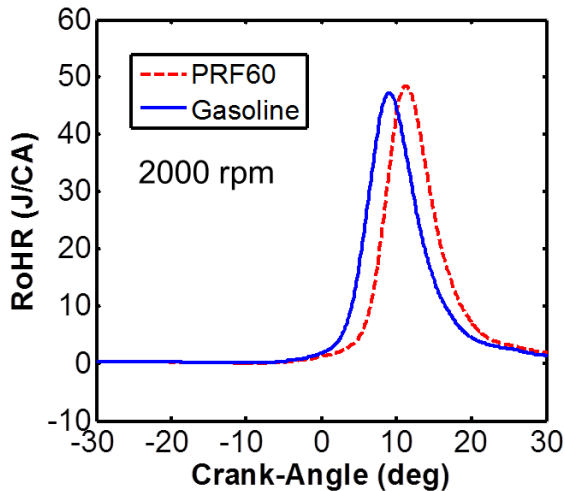
(c) 2000 rpm, Rate of Heat Release
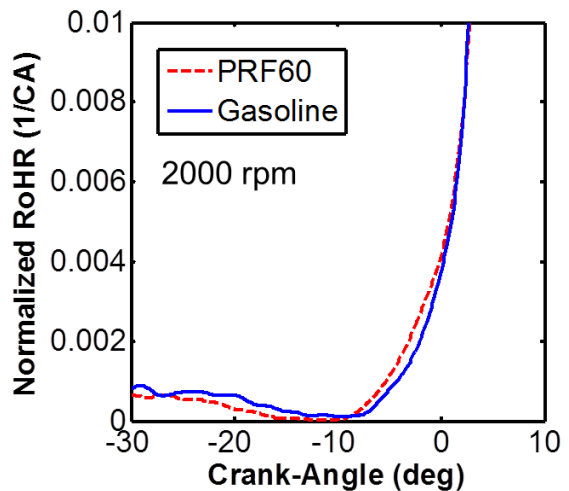
(d) 2000 rpm, Normalized RoHR, shifted to align maximum RoHR

Figure 6.10   Gasoline and PRF60 RoHR and Normalized RoHR at 1000, 2000 rpm for iEGR = 36%, COV of $IMEP_g$ = 3%

the NH40 fuel has similar n-heptane content and does not exhibit LTHR behavior. Despite the lack of LTHR, PRF60 still exhibits a CA50 that is 2.4°more retarded than gasoline. The absence of LTHR for PRF60 at 2000 rpm is understood to explain the iEGR dependency present for PRF60 at 2000 rpm that is not there for the 1000 rpm condition.

To determine what may allow the PRF60 a later phasing at the COV of $IMEP_g$ limit despite a lack of LTHR, examining Figure 6.10(d) demonstrates that the PRF60 does exhibit
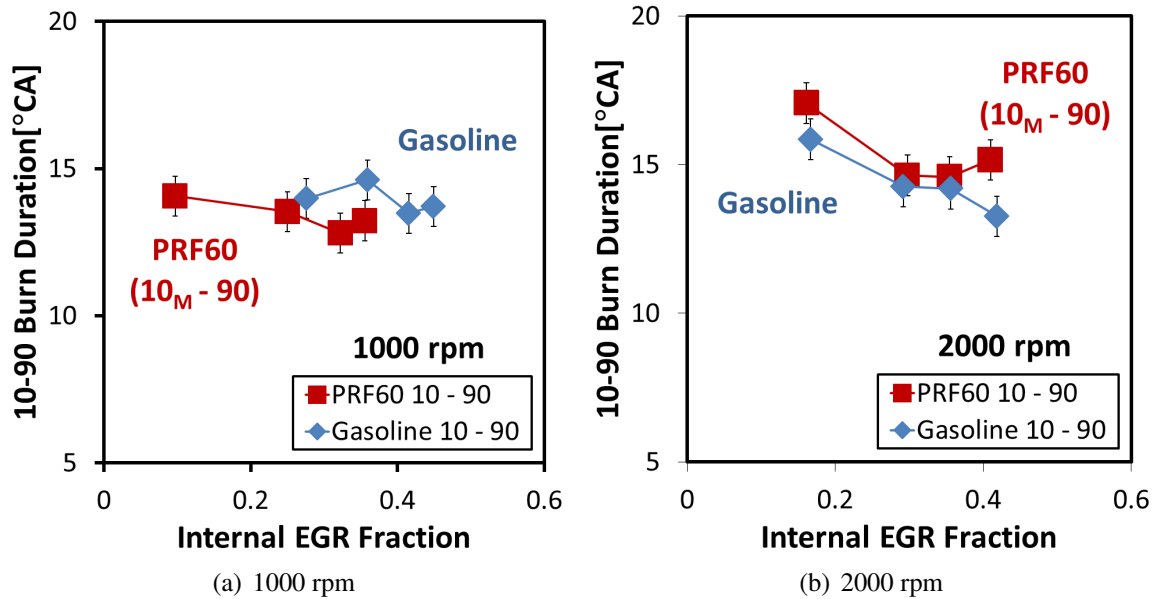
(a) 1000 rpm   (b) 2000 rpm

Figure 6.11 Gasoline and PRF60 10 – 90 burn duration for 1000 rpm and 2000 rpm iEGR sweeps at COV of $IMEP_g = 3\%$

increased ITHR over the gasoline, although the difference is slight. The ITHR is understood to be essentially an early heat release due to the fact that the PRF60, despite not exhibiting LTHR, has different fuel chemistry and a different ignition delay slope that the gasoline. This allows the later phasing in the same what that was described for the 1000rpm cases.

Up until this point the PRF60 has been compared to gasoline at relatively high iEGR levels. To examine the effects of PRF60 where very little iEGR is present, the fuels are now compared at 2000 rpm for iEGR = 17% (± 1 percentage point). Examining the first return plots in Figure 6.13 demonstrates that neither the gasoline or PRF60 demonstrate "anti-correlated" behavior, due to the fact that this is a low iEGR condition. Just from a visual inspection of the first return plots it is not clear how the distribution varies, only that both exhibit a random distribution around the mean. Despite this fact both fuels show no "anti correlated" behavior, the PRF60 still is operated at a phasing 2.2° later than the gasoline(15.0° ATDC vs 12.8° ATDC).

Examining the heat release curves in Figure 6.13 shows that the PRF60 again shows no LTHR in the RoHR curve (Figure 6.13(a)) at the 2000 rpm condition. Also like the 36%

113
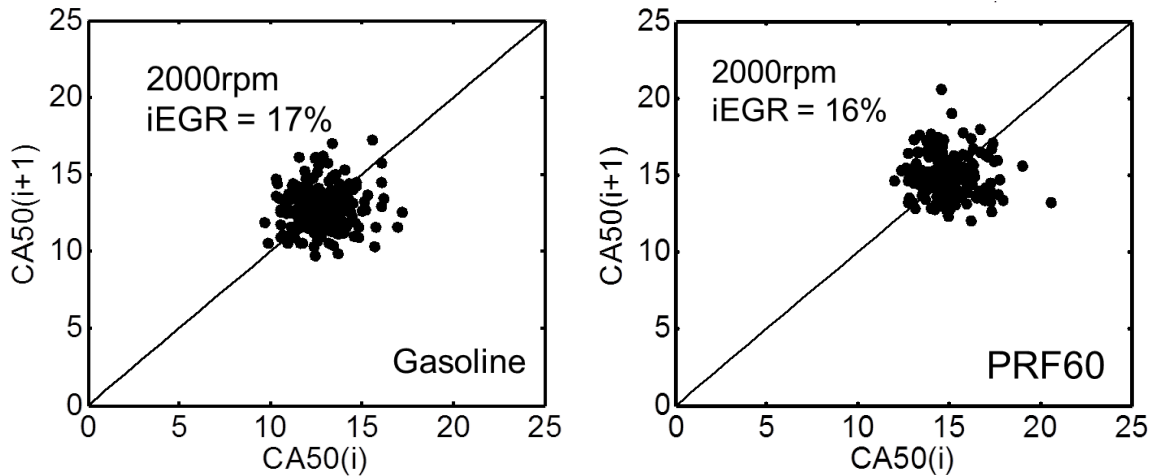
(a) Gasoline, 2000 rpm, avg. CA50 = 12.8° ATDC   (b) PRF60, 2000 rpm, avg. CA50 = 15.0° ATDC

Figure 6.12   Gasoline and PRF60 first return map plots of CA50 location for 200 cycles fixed COV of $IMEP_g$ = 3% at a fixed iEGR = 17%

(a) Rate of Heat Release   (b) Normalized RoHR, shifted to align maximum RoHR
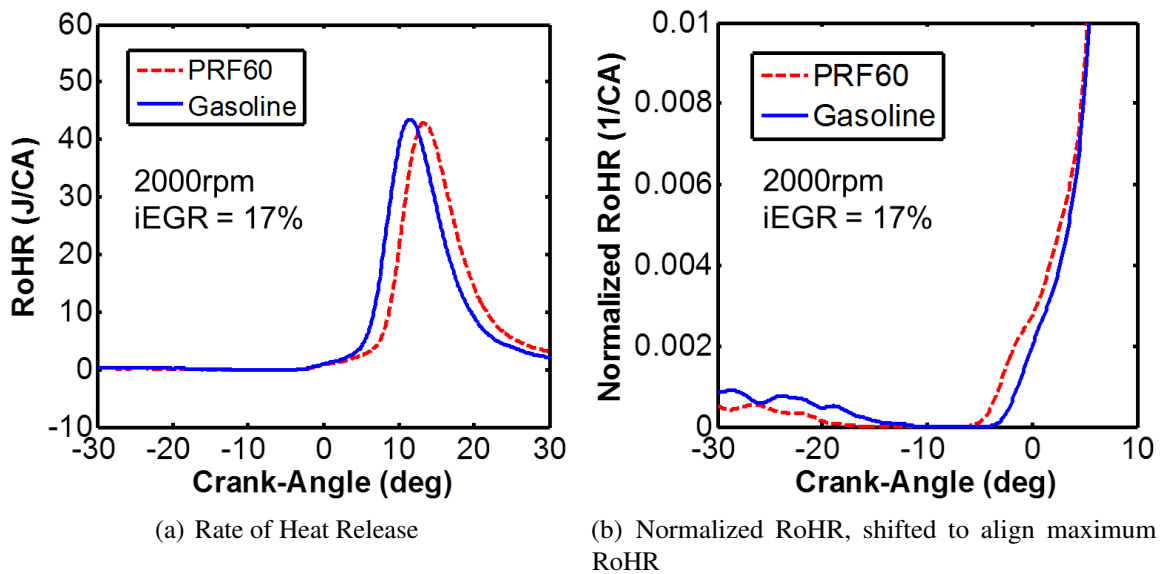
Figure 6.13   Heat Release Rates for Gasoline and PRF60 at 2000 rpm, iEGR = 17%

iEGR cases, the maximum RoHR for both gasoline and PRF60 is nearly identical with the PRF60 phased later as noted. The normalized RoHR plot in Figure 6.13(b) (again shifted to align the maximum RoHR) demonstrates a slight increase in ITHR for the PRF60 over the gasoline. From the 10 − 90 curves in Figure 6.11(b) the 17% iEGR cases are the points farthest left. The PRF60 actually has a slightly longer burn duration than the gasoline despite a later phasing at the same stability limit.
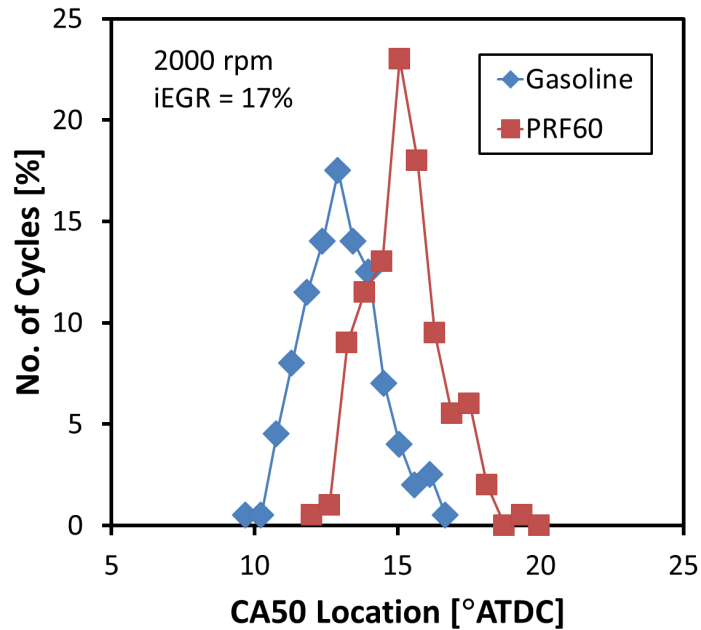
Figure 6.14 Probability distribution for CA50 location in 200 cycles for Gasoline and PRF60

Since the first return maps were inconclusive on the change in distribution of CA50, for these two cases a probability distribution is presented for the number of cases that fall within a certain CA50 range, and this is presented in Figure 6.14. Here it is observed that the PRF60 has a narrower distribution with a higher percentage of cycles closer to the mean CA50, clearly showing more stable combustion for the PRF60.

6.3   Non-Arrhenius Ignition Delay Effects on Stability

Within this study it was observed that for a given iEGR level, PRF60 could be phased later than gasoline. Up until this point a thorough explanation for this behavior has not been provided. As with the fixed phasing study in Chapter 5, the only potential differences between the cases comparing PRF40 to gasoline at fixed iEGR are that of bulk gas temperature and the fuel chemistry.

The 2000 rpm cases for gasoline and PRF60 at 17% iEGR (Figure 6.13) are unique in that for these conditions not only was the intake pressure the same, but intake temperature was identical (200°C) between the fuels as well, and the IVC and TDC temperatures were

115
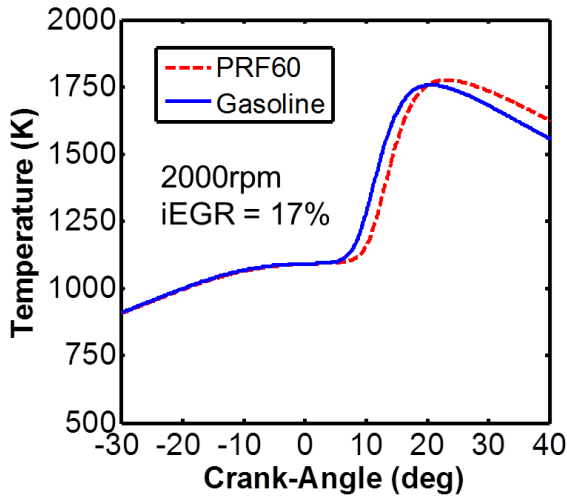
Figure 6.15 Inferred mean temperature for Gasoline and PRF60 at 2000 rpm, COV of IMEP$_g$ = 3%, iEGR = 17%
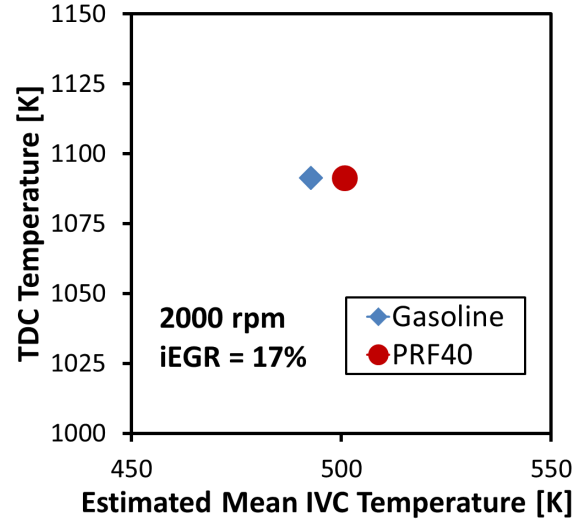
Figure 6.16 Inferred IVC and TDC temperature for gasoline and PRF60 at 2000rpm, COV of IMEP$_g$ = 3%, iEGR = 17%

within 8 Kelvin and 1 Kelvin respectively as shown in Figures 6.16 and 6.15. For these conditions the only difference is fuel: temperature and composition are as identical as possible for an NVO HCCI engine experiment.

As the temperatures between these cases are nearly identical, a difference in temperature stratification is not the explanation for the fact that the PRF60 is phased later than the gasoline for a given iEGR. From this it can only be concluded that differences in fuel chemistry enable the PRF40 to be phased later for a given stability limit. In Section 5.4 the reduced impact of thermal stratification in-cylinder on PRF40 was explained with the non-Arrhenius behavior of the ignition delay curve. Now, instead of differences in thermal stratification, let's consider differences in thermal feedback.

Figure 6.17 is the estimated temperature trace for 200 cycles operated at a COV of IMEP$_g$ = 3%. As illustrated, there is a noticeable band in the temperatures between the cycles during the expansion process. This is a function of cyclic variation in phasing leading to differences in expansion temperatures. So for a relatively unstable, there is range of exhaust temperatures, ΔT_e.

Consider now the ignition delay curve which was described in Section 5.4 and is again
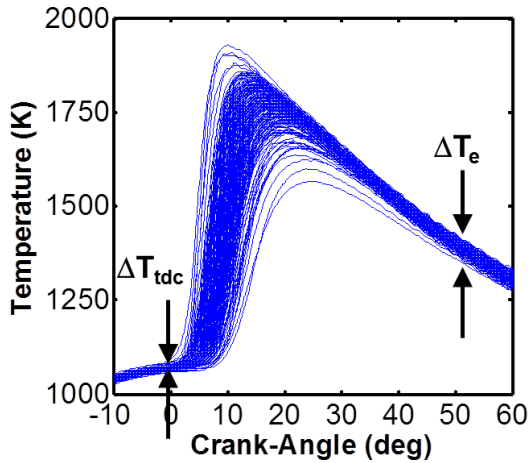
Figure 6.17 Spread in expansion temperatures for 200 cycles at 3% COV limit
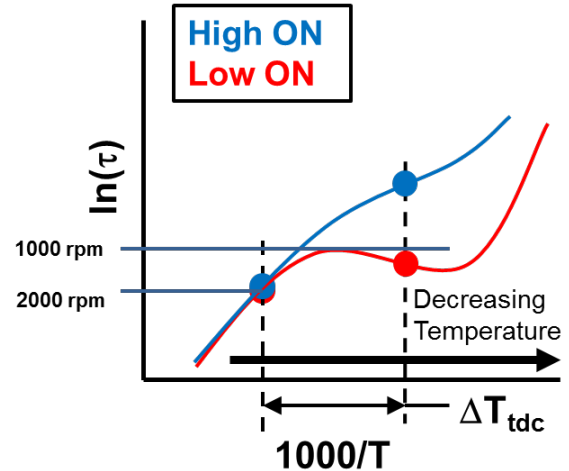
Figure 6.18 Effect of cyclic temperature variations on ignition delay

displayed here. But instead of considering the temperature distribution in-cylinder, consider the effect of cyclic temperature fluctuations. In NVO HCCI operation with sufficient levels of iEGR, the cyclic fluctuations in exhaust temperature, ΔT_e, will cause cyclic fluctuations in bulk temperature approaching TDC, denoted ΔT_{tdc}.

Now take consider ΔT_{tdc} as it impacts the ignition delay of the fuel at TDC, as illustrated in Figure 6.18. For the high ON fuel, such as gasoline, the cyclic changes in bulk gas temperature will significantly impact the ignition delay; a cooler exhaust temperature fed back to create a cooler inlet charge will lengthen the ignition delay and retard the entire combustion event. This is the behavior that was observed experimentally on the first return plots for gasoline. For a non-Arrhenius fuel, the same change in IVC temperature will have significantly less effect on the ignition delay and the corresponding combustion phasing for the next cycle, which matches the observed behavior for PRF60 when we compare it to gasoline for a fixed iEGR level. As the non-Arrhenius fuel has less cyclic variation in CA50 due to this effect, it can be phased later while maintaining the same COV of IMEP$_g$.

Taking this conceptual model one step further, it was observed (Figure 6.9) that the PRF60 could be operated at a later phasing for the same iEGR as engine speed was decreased from 2000 to 1000 rpm, whereas gasoline exhibited no speed effect on the phasing limit. If

we overlay how reducing engine speed lengthens the ignition delay (based on time domain residence), it can be seen that the slope of the ignition delay curve for the high ON fuel is still the same, and from this the sensitivity to iEGR as speed is changed will remain about the same. For the non-Arrhenius low ON fuel, the slope decreases significantly moving from 2000 rpm to 1000 rpm, and this will serve *reduce* the sensitivity to cyclic temperature changes in the bulk gas. Consider that if the ΔT_{tdc} is the same for a given iEGR between speeds, the lower speed will have more temperature regions at the same ignition delay than the higher engine speed, and combustion will ignite (and thus be phased) near the same time every cycle.

6.4   Discussion and Summary

A study was conducted with the purpose of investigation and separating iEGR and fuel effects on the combustion stability limits of HCCI. The effect of iEGR was observed to reduce phasing limits for a given COV of IMEP$_g$, as the cyclic feedback is increased, producing "anti-correlated" behavior where more late CA50 cycles are followed by early CA50 cycles, increasing the overall spread of CA50. For gasoline at 2000 rpm, decreasing iEGR from 42% to 17% allowed the CA50 to be retarded by 51% at the COV of IMEP$_g$ = 3% limit.

PRF60 was compared to gasoline at 1000 rpm and 2000 rpm. At 1000 rpm, conditions where LTHR is present, PRF60 does not exhibit "anti-correlated" cyclic feedback behavior. This led to a the PRF60 operating at a more retarded CA50 than gasoline at the COV of IMEP$_g$ = 3% limit. Additionally, the PRF60 exhibited little dependence of CA50 to iEGR at the stability limit. At 2000 rpm the PRF60 did not exhibit LTHR and was found to exhibit "anti-correlated" cyclic feedback in the CA50 history of 200 cycles, though to a lesser degree than gasoline at the same iEGR level.

It is worthy of note that the difference in phasing between PRF60 and gasoline was

greater at 1000 rpm than at 2000 rpm, yet the difference is still less than that between high and low iEGR cases for gasoline. So the effect of fuel properties on HCCI phasing limits is less than the effects of iEGR (through thermal and compositional stratification), but they are on the same order of magnitude.

The conceptual model of different ignition delay curves for a non-Arrhenius low ON fuel and a high ON fuel with a more Arrhenius shape (higher slope) has been demonstrated to explain the observed effects in this experiment as it relates to phasing limits at a fixed COV of $IMEP_g$.Namely, the sensitivity of gasoline (high ON) to changes in iEGR and the lack thereof for PRF60 (low ON), as well as the speed effect observed for PRF60.

The findings in this Chapter support those of Chapter 3, where it was found that the NH40 could be phased later at a lower iEGR and maintain the same burn duration as gasoline. In this chapter it was shown that both a lower iEGR (NVO) level and a lower ON fuel allow a later phasing limit. In the study in Chapter 3, as iEGR was not held constant, both effects contributed to allow the NH40 to operate at a higher load at a later phasing and matched burn duration.

Chapter 7

Summary of Contributions with Implications and Recommendations for Future Work

7.1   Summary of Results

The overarching goal of this work was to examine the impact of low octane fuels on the burn rates and phasing limits of HCCI combustion, as it pertained to enabling extension of the HCCI load limit in a NVO engine. To accomplish this, a new method was developed to maintain constant composition across a wide range of iEGR, engine speed, and fuels. This allowed independent comparison of the effects of both fuel and iEGR on burn rates and stability limits, the findings of which are summarized below.

7.1.1   HCCI Load Limits

A study previously published by the author, and represented herein, demonstrated that a lower octane blended gasoline, NH40, offered a 7% increase in load (IMEP$_g$) over gasoline and iso-octane. This increased load occurred at a later phasing compared to regular gasoline and iso-octane, where the NH40 had a burn duration similar to that of iso-octane despite the later phasing. This was related to the observation that the NH40, for a given combustion phasing, had a shorter overall burn duration.

The nature of the experiment varied NVO (and thus iEGR) across phasing sweeps, and between fuels for a given phasing. The latter is due to the fact that the lower octane fuel requires a lower cylinder temperature at IVC for a given phasing, and the phasing control in the experiment was the use of NVO (higher NVO = higher iEGR = higher cylinder

temperature at IVC). Different levels of iEGR between fuels of a given combustion phasing changes the cylinder charge composition, in terms of ϕ and ϕ', as well as the thermal and compositional stratification. These differences made it impossible to separate fuel effects from compositional effects, requiring additional studies. To be able determine fuel effects at fixed combustion phasing, the composition must also be maintained constant.

7.1.2 Maintaining Constant Composition

The composition in an NVO HCCI engine is comprised of injected fuel, fresh air, internal residual gas, recycled external residual gas, and a small amount of unburned fuel in the residual gas; changing any one of these changes the composition. To maintain constant composition, to a first approximation, is achieved by keeping the injection amount of fuel (EMEP) constant, and keeping the exhaust ϕ constant. This keeps the mass of fuel and fresh air constant but is not sufficient to maintain constant composition across wide variations in NVO and engine speed. It was shown that in order to maintain constant total EGR across a wide iEGR sweep, IVC timing must be varied as well to compensate for changes in intake runner dynamics. Additionally as engine speed is decreased it is necessary to apply part throttle at lower engine speeds for the total EGR to be kept constant.

Utilizing the fully flexible valves with the FFVA engine to adjust IVC timing independent of NVO timing, and making small adjustments with inlet pressure, a method to maintain constant composition with NVO HCCI across a wide range of iEGR ($16\% - 43\%$) and engine speed (1000 - 2000 rpm) has been demonstrated. These methods are utilized to conduct experiments which expand the knowledge of HCCI combustion in terms of iEGR and fuel effects on burn rates.

7.1.3 Fixed Combustion Phasing Study

Utilizing the constant composition method described above, PRF40 and gasoline were compared at a fixed CA50 across iEGR sweeps at engine speeds of 1000, 1500, and 2000 rpm. The purpose of the experiments was to quantify the effect of both fuel and iEGR on HCCI burn rates at fixed phasing and composition.

The results show that for gasoline there is a sensitivity to iEGR on burn rate and 10 – 90 burn duration. It was observed that increasing iEGR from 19% to 43% reduced the maximum RoHR by 14% while increasing the 10-90 burn duration by 35%. This trend with iEGR was consistent at 1500 and 1000rpm. The reduction in burn rates at higher iEGR levels is attributed to increased thermal stratification.

Comparing the PRF40 to gasoline at a given phasing and iEGR, PRF40 has a higher maximum RoHR (35% at iEGR = 38% at 2000 rpm). This trend was consistent across all iEGR levels and all engine speeds. Corresponding to the increased RoHR, PRF40 exhibited a shorter 10 – 90 burn duration compared to gasoline. Since the iEGR, phasing and EMEP are maintained constant, the only factors which could contribute to the observed differences in burn rate and duration are fuel chemistry and differences in thermal stratification separate from that of iEGR.

For a given iEGR the PRF40 demonstrated a lower required IVC temperature compared to gasoline, which is due to both differences in fuel chemistry and the presence of LTHR providing heat release during the compression stroke to attain the required TDC temperature. This has the potential to reduce thermal stratification between the bulk gas mean temperature and the wall temperature, leading to faster burn rates for an NTC fuel exhibiting LTHR.

In addition to bulk temperature differences, a conceptual analysis demonstrated how a non-Arrhenius fuel with a ignition delay curve slope, reducing the activation energy, allows a faster burn compared to higher ON fuel for a given temperature distribution. It also demonstrated how the slope of the ignition delay curve relates to the sensitivity to changes in iEGR for a high ON fuel such a gasoline, and the lack of sensitivity to a low ON fuel

such as PRF40.

This study is the first to quantify the impact iEGR on HCCI burn rates for a gasoline fuel and a low RON PRF. This study is also the first to consider how different fuel chemistry and the corresponding ignition delay curve relates to differences in burn rates and sensitivity to iEGR.

7.1.4 Fixed Combustion Stability Study

Utilizing the constant composition method, gasoline and PRF60 were both compared at a fixed combustion stability criteria, COV of $IMEP_g$ = 3%, across iEGR sweeps at 1000 and 2000 rpm. The purpose of the experiments was to quantify the effect of iEGR and fuel chemistry effects on NVO HCCI combustion stability limits.

Gasoline showed a significant trend with regards to iEGR level and CA50 retard limit. Reducing iEGR at 2000 rpm from 42% to 17% iEGR increased the CA50 retard limit by 4.3°CA. Examining first return plots of CA50 demonstrated that while the low iEGR case has a random distribution, the high iEGR case is highly anti-correlated; many extra-late CA50 cycles are followed by extra-early CA50 cycles, and vice-versa. Furthermore the high iEGR case has a much wider variation in CA50 from the mean, causing the advanced CA50 limit at a fixed COV of $IMEP_g$. The higher variation in CA50 for the higher iEGR case is attributed to the increased dependency on combustion phasing to the previous cycle, with increasing sensitivity to fluctuations in the exhaust temperatures of individual cycles.

Comparing between gasoline and PRF40 at high iEGR levels demonstrated "anti-correlated" behavior for the gasoline but not for the PRF60, and the PRF60 could operate at a CA50 more retarded at the stability limit. Additionally, reducing engine speed demonstrated an additional retarding in the phasing limit for PRF60, but not for gasoline. This was explained by the conceptual model of different ignition delay slopes between the fuels, with enhanced non-Arrhenius behavior for the PRF60 understood to reduce sensitivity to cyclic changes in temperature as it relates to ignition delay, a trait not present for a high ON

fuel like gasoline. Reducing engine speed serves to shift the location of the ignition delay into the non-Arrhenius region, further reducing sensitivity to fluctuations in temperature, supporting the experimental results for PRF60 demonstrating further retarded limits at 1000 rpm compared to 2000 rpm.

This study is the first to quantify the impact of iEGR level as it relates to the phasing limit of HCCI combustion. This study also demonstrated for the first time that a low RON PRF fuel will extend the phasing limit over gasoline, and this is attributed fuel chemistry differences presented in the form of differences in the slope of the ignition delay curve.

7.2   Key Contributions of the Work

The focus of this work was to separate fuel chemistry effects from compositional effects in HCCI combustion, for the purpose of determining the fuel characteristics which allow a low octane fuel to achieve a higher load. The key contributions of this work are as follows:

1. Utilizing the unique and specialized capabilities of the UM FFVA engine, a new method was developed to isolate iEGR effects independent of fuel chemistry effects

2. For the first time, demonstrated experimentally that high levels of iEGR slow combustion and advance phasing limits for gasoline

3. Low octane PRFs exhibit reduced sensitivity to iEGR, and exhibit faster burn rates and later phasing limits compared to gasoline

4. The disparity in behavior between gasoline and low RON PRFs is attributed to: a shallower ignition delay slope providing less sensitivity to both spatial and cyclic temperature variation; a reduction in required IVC temperature (less thermal stratification).

As an extension of item four, it was hypothesized that the reduced slope of the ignition delay curve of a non-Arrhenius fuel will have a lower activation energy, which would provide another method for which a low ON fuel could be understood to have a faster burn rate at a fixed combustion phasing, and a later combustion phasing at a fixed stability limit.

Item two is the key enabler to allowing a LTHR fuel to operate in HCCI at a higher load than a non-LTHR fuel, for the later combustion phasing allows load to be increased within

the ringing constraint.

7.3 Concluding Thoughts and Recommendations for Future Work

At the outset of this work, the goal was to ascertain to what benefit, if any, a lower octane refinery blend could offer to HCCI combustion. With detailed experiments having provided new insight into how both iEGR and low octane PRF fuels behave in NVO HCCI engines, some insights can be made.

A LTHR fuel will be able to be retarded more than a non-LTHR fuel for a given combustion criteria. This allows a higher load to achieved for a fixed ringing intensity. So for a pure HCCI engine, a fuel exhibiting LTHR will be able to provide an increase in load or BMEP. A good application for this might be stationary power generation in a region where low ON fuel is prevalent.

Within this work, several experiments demonstrated a disparity between the behavior of a low ON PRF fuel compared to gasoline. The PRFs required a lower IVC temperature for a given combustion phasing than gasoline, which is believe to reduce thermal gradients in-cylinder. Furthermore, it was hypothesized that the PRFs benefited from the reduced slope of the ignition delay curves, leading to reduction in the activation energy. To test these observations, a logical next step would be to computationally examine how PRFs behave in HCCI combustion. A practical approach would be to extend the work of Kodavasal [98] to an LTHR fuel using an appropriate kinetics mechanism. Such an approach would enable a direct comparison of required IVC and TDC temperatures, and provide an estimation of the degree of thermal stratification which a lower IVC temperature brings.

Extending the study, the same temperature stratification found for the LTHR fuel could be imposed on a non-LTHR fuel to determine if the observed experimental effects are purely a function of thermal gradients imposed by bulk gas temperatures. If they are not, then some

of the difference in burn characteristics is a function of fuel chemistry, such as characterized by the ignition delay curves.

Extending this work further, a practical implementation of HCCI will also require SACI and SI operating conditions to meed load requirements. While a low ON fuel may not be desirable for SACI and SI conditions, it would be of interest to investigate what hydrocarbon blends are available meeting the RON requirements of SI and SACI conditions that may also exhibit non-Arrhenius behavior under boosted SACI and SI conditions. Tailoring of the blends could yield a fuel which lowers the required temperatures for SACI and SI conditions, reducing conditions where the onset of knock occurs and improving thermal efficiency.

References

[1] Voorhees, Josh. U.S. Vehicle Fleet Shrank 2% Last Year, Biggest Decline in Decades – Report. Retrieved from `http://www.eenews.net/public/Greenwire/2010/01/06/3`, January 6, 2010. *Greenwire*.

[2] Davis Jr., David E. *Thus Spake David E.: The Collected Wit and Wisdom of the Most Influential Automotive Journalist of Our Time*. Momentum Books Ltd, Troy, Michigan, 1999.

[3] Obama, Barack. 2011 State of the Union Address, January 25, 2011. Transcript retrieved 08/10/2011 from `http://www.nytimes.com/2011/01/26/us/politics/26obama-text.html?pagewanted=all`.

[4] U.S. Department of Energy. *EV Everywhere*, 2013. Retrieved 12-09-2013 from `http://www1.eere.energy.gov/vehiclesandfuels/electric_vehicles/pdfs/eveverywhere_blueprint.pdf`.

[5] Mondt, Robert J. *Cleaner Cars: The History and Technology of Emission Control Since the 1960s*. Society of Automotive Engineers, Inc., Warrendale, PA, 2000.

[6] A.J. Haagen-Smit. Chemistry and Physiology of Los Angeles Smog. *Ind. Eng. Chem.*, 44(6):1342–1346, 1952.

[7] U.S. Environmental Protection Agency. *Light-Duty Vehicle, Light-Duty Truck, and Medium-Duty Passenger Vehicle — Tier 2 Exhaust Emission Standards*. Retrieved 10-13-2011 from `http://www.epa.gov/otaq/standards/light-duty/tier2stds.htm`.

[8] U.S. Environmental Protection Agency. *EPA Proposes Tier 3 Motor Vehicle Emission and Fuel Standards*, 2013. Retrieved 12-09-2013 from `http://www.epa.gov/otaq/documents/tier3/420f13016a.pdf`.

[9] Timothy Johnson. Vehicular Emissions in Review. *SAE Int. J. Engines*, 6(2):699–715, April 2013. SAE Paper 2013-01-0538.

[10] Annual Energy Review 2009, 2009. Report no. DOE/EIA–0384.

[11] U.S. Energy Information Administration. *Short-Term Energy Outlook — Real Energy Prices*. Retrieved 08/10/2011 from `http://www.eia.gov/emeu/steo/realprices/`.

[12] Michael Lamm. Driving the 1978 Chevrolets, Pontiacs, Buicks, Oldsmobiles, and Cadillacs. *Popular Mechanics*, Oct. 1977.

[13] Mass, Peter. The Breaking Point. *The New York Times Magazine*, Aug. 21 2005. Retrieved from `http://www.nytimes.com/2005/08/21/magazine/21OIL.html`.

[14] Asjylyn Loder. Fracking Moves U.S. Crude Output to Highest Level Since 1989. *Bloomberg News*, September 13, 2013.

[15] Ayesha Rascoe. UPDATE 1 - U.S. oil demand in 2012 was lowest in 16 years - EIA. *Reuters*, 2013. Retrieved 12-09-2013 from `http://www.reuters.com/article/2013/02/27/usa-eia-monthly-idUSL1N0BRBG620130227`.

[16] ExxonMobil Corporation. *The Outlook for Energy: A View to 2040*, 2013. Retrieved 12-09-2013 from `http://www.esso.co.th/Thailand-English/PA/Files/2013_eo_eng.PDF`.

[17] United Nations Framework Convention on Climate Change. *Report of the Conference of the Parties on its thirteenth session, held in Bali from 3 to 15 December 2007*, December 2007.

[18] Barack Obama. Presidential Memorandum Regarding Fuel Efficiency Standards, May 21, 2010. Retrieved 10-11-2011 from `http://www.whitehouse.gov/the-press-office/presidential-memorandum-regarding-fuel-efficiency-standards`.

[19] EPA and NHTSA Set Standards to Reduce Greenhouse Gases and Improve Fuel Economy for Model Years 2017-2025 Cars and Light Trucks , Aug 2012. Retrieved 12-09-2013 from `http://www.epa.gov/otaq/climate/documents/420f12051.pdf`.

[20] Guatam Kalghatgi. *Fuel/Engine Interactions*. SAE International, Warrendale, PA, 2014.

[21] ASTM International. *Standard Test Method for Research Octane Number of Spark-Ignition Engine Fuel*, 2011. Standard D2699-11.

[22] ASTM International. *Standard Test Method for Motor Octane Number of Spark-Ignition Engine Fuel*, 2011. Standard D2700-11.

[23] K. Fieweger, R. Blumenthal, and G. Adomeit. Self-ignition of S.I. engine model fuels: A shock tube investigation at high pressure. *Combustion and Flame*, 109(4):599–619, June 1997.

[24] William R. Leppard. The chemical origin of fuel octane sensitivity, 1990. SAE Paper 902137.

[25] ASTM International. *Standard Test Method for Cetane Number of Diesel Fuel Oil*, 2010. Standard D2613-10a.

[26] Sandia National Laboratories. *Constant-Volume Diesel Combustion: Fuels*. Sandia Engine Combustion Network, retrieved 12-11-2013 from `http://www.sandia.gov/ecn/cvdata/sandiaCV/fuels.php`.

[27] J.N. Bowden, A.A. Johnston, and J.A. Russell. *Octane-Cetane Relationship*. Southwest Research Institute, 1974. AFLRL Report No. 33.

[28] John B. Heywood. *Internal Combustion Engine Fundamentals*. McGraw-Hill, New York, 1988.

[29] Shigeru Onishi, Hong Souk Jo, Katsuji Shoda, Pan Do Jo, and Satoshi Kato. Active Thermo-Atmoshphere Combustion (ATAC) — A New Combustion Processs for Internal Combustion Engines, 1979. SAE Paper 790501.

[30] Masaaki Noguchi, Yukiyasu Tanaka, Taro Tanaka, and Yukihisa Takeuchi. A Study of Gasoline Engine Combustion by Observation of Intermediate Reactive Products during Combustion, 1979. SAE Paper 790840.

[31] Paul M. Najt and David E. Foster. Compression-Ignited Homogeneous Charge Combustion, 1983. SAE Paper 830264.

[32] R.H. Thring. Homogeneous-Charge Compression-Ignition (HCCI) Engines, 1989. SAE Paper 892068.

[33] Thomas W. Ryan and Timothy J. Callahan. Homogeneous charge compression ignition of diesel fuel, 1996". SAE Paper 961160.

[34] Hiromichi Yanagihara and Yasuo Sato. A study of DI diesel combustion under uniform higher-dispersed mixture formation. *JSAE Review*, 18(2):361–367, 1997.

[35] Yoshinaka Takeda, Nakagome Keiichi, and Niimura Keiichi. Emission characteristics of premixed lean diesel combustion with extremely early staged fuel injection, 1996. SAE Paper 961163.

[36] Kazuhiro Akihama, Yoshiki Takatori, Kazuhisa Inagaki, Shizuo Sasaki, and Anthony M. Dean. Mechanism of the smokeless rich diesel combustion by reducing temperature, 2001. SAE Paper 2001-01-0655.

[37] Shuji Kimura, Osamu Aoki, Hiroshi Ogawa, and Shigeo Muranaka. New Combustion Concept for Ultra-Clean and High-Efficiency Small DI Diesel Engines, 1999. SAE Paper 1999-01-3681.

[38] Timothy John Jacobs. *Simultaneous Reduction of Nitric Oxide and Particulate Matter Emissions from a Light-Duty Diesel Engine Using Combustion Development and Diesel Oxidation Catalyst*. PhD thesis, University of Michigan, 2005.

[39] Sanghoon Kook, Choongsik Bae, Paul C Miles, Dae Choi, and Lyle M Pickett. The Influence of Charge Dilution and Injection Timing on Low-Temperature Diesel Combustion and Emissions, 2005. SAE Paper 2005-01-0655.

[40] A. Babajimopoulos, V.S.S.P. Challa, G.A. Lavoie, and D.N. Assanis. Model-Based Assessment of Two Variable CAM Timing Strategies for HCCI Engines: Recompression vs. Rebreathing. In *Proceedings of the ASME Internal Combustion Engine Division 2009 Spring Technical Conference, ICES2009-76103*, 2009.

[41] David A Rothamer, Jordan A Snyder, Ronald K Hanson, Richard R Steeper, and Russell P Fitzgerald. Simultaneous imaging of exhaust gas residuals and temperature during HCCI combustion. *Proceedings of the Combustion Institute*, 32(2):2869–2876, 2009.

[42] Ramanan Sankaran, Hong G. Im, Evatt R. Hawkes, and Jacqueline H. Chen. The effects of non-uniform temperature distribution on the ignition of a lean homogeneous hydrogenair mixture. *Proceedings of the Combustion Institute*, 30(1):875–882, January 2005.

[43] Jacqueline H. Chen, Evatt R. Hawkes, Ramanan Sankaran, Scott D. Mason, and Hong G. Im. Direct numerical simulation of ignition front propagation in a constant volume with temperature inhomogeneities. *Combustion and Flame*, 145(1-2):128–144, April 2006.

[44] Evatt R. Hawkes, Ramanan Sankaran, Philippe P. Pébay, and Jacqueline H. Chen. Direct numerical simulation of ignition front propagation in a constant volume with temperature inhomogeneities. *Combustion and Flame*, 145(1-2):145–159, April 2006.

[45] Gaurav Bansal and Hong G. Im. Autoignition and front propagation in low temperature combustion engine environments. *Combustion and Flame*, 158(11):2105–2112, November 2011.

[46] Magnus Sjöberg, John E. Dec, and Nicholas P Cernansky. Potential of Thermal Stratification and Combustion Retard for Reducing Pressure-Rise Rates in HCCI Engines , Based on Multi-Zone Modeling and Experiments, 2005. SAE Paper 2005-01-0113.

[47] Chun Sang Yoo, Tianfeng Lu, Jacqueline H. Chen, and Chung K. Law. Direct numerical simulations of ignition of a lean n-heptane/air mixture with temperature inhomogeneities at constant volume: Parametric study. *Combustion and Flame*, 158(9):1727–1741, September 2011.

[48] Chun Sang Yoo, Zhaoyu Luo, Tianfeng Lu, Hongjip Kim, and Jacqueline H. Chen. A DNS study of ignition characteristics of a lean iso-octane/air mixture under HCCI and SACI conditions. *Proceedings of the Combustion Institute*, 34(2):2985–2993, January 2013.

[49] Magnus Sjöberg and John E Dec. Smoothing HCCI Heat-Release Rates Using Partial Fuel Stratification with Two-Stage Ignition Fuels, 2006. SAE Paper 2006-01-0629.

[50] Magnus Sjöberg and John E Dec. Comparing Enhanced Natural Thermal Stratification Against Retarded Combustion Phasing for Smoothing of HCCI Heat-Release Rates, 2004. SAE Paper 2004-01-2994.

[51] Mahdi Shahbakhti and C R Koch. Characterizing the cyclic variability of ignition timing in a homogeneous charge compression ignition engine fuelled with ¡i¿n¡/i¿-heptane/iso-octane blend fuels. *International Journal of Engine Research*, 9(5):361–397, May 2008.

[52] Lu Xingcai, Ji Libin, Ma Junjun, and Huang Zhen. Experimental study on the cycle-by-cycle variations of homogeneous charge compression ignition combustion using primary reference fuels and their mixtures. *Proceedings of the Institution of Mechanical Engineers, Part D: Journal of Automobile Engineering*, 221(7):859–866, January 2007.

[53] Laura Manofsky, Jiri Vavra, and A. Babajimopoulos. Bridging the Gap between HCCI and SI: Spark-Assisted Compression Ignition, 2011. SAE Paper 2011-01-1179.

[54] Leif Hildingsson, Gautam Kalghatgi, Nigel Tait, Bengt Johansson, and Andrew Harrison. Fuel Octane Effects in the Partially Premixed Combustion Regime in Compression Ignition Engines, 2009. SAE Paper 2009-01-2648.

[55] William L. Leffler. *Petroleum Refining in Nontechnical Language*. PennWell Corporation, Tulsa, OK, fourth edition, 2008.

[56] Gautam Kalghatgi. Auto-Ignition Quality of Practical Fuels and Implications for Fuel Requirements of Future SI and HCCI Engines, 2005. SAE Paper 2005-01-0239.

[57] Gen Shibata and Tomonori Urushihara. Auto-Ignition Characteristics of Hydrocarbons and Development of HCCI Fuel Index, 2007. SAE Paper 2007-01-0220.

[58] Peter L. Perez and André L. Boehman. Experimental Investigation of the Autoignition Behavior of Surrogate Gasoline Fuels in a Constant-Volume Combustion Bomb Apparatus and Its Relevance to HCCI Combustion. *Energy & Fuels*, 26(10):6106–6117, October 2012.

[59] Vi H. Rapp, William Cannella, J.-Y. Chen, and Robert W. Dibble. Predicting Fuel Performance for Future HCCI Engines. *Combustion Science and Technology*, 185(5):735–748, May 2013.

[60] Andy D B Yates, André Swarts, and Carl L Viljoen. Correlating Auto-Ignition Delays and Knock-Limited Spark- Advance Data For Different Types Of Fuel, 2005. SAE Paper 2005-01-2083.

[61] H.K. Ciezki and G. Adomeit. Shock-tube investigation of self-ignition of n-heptane-air mixtures under engine relevant conditions. *Combustion and Flame*, 93(4):421–433, June 1993.

[62] Ida Truedsson, Martin Tuner, Bengt Johansson, and William Cannella. Pressure Sensitivity of HCCI Auto-Ignition Temperature for Primary Reference Fuels, 2012. SAE Paper 2012-01-1128.

[63] Vahid Hosseini, W Stuart Neill, and Wallace L Chippior. Influence of Engine Speed on HCCI Combustion Characteristics using Dual-Stage Autoignition Fuels, 2009. SAE Paper 2009-01-1107.

[64] Magnus Sjöberg and John E Dec. Combined Effects of Fuel-Type and Engine Speed on Intake Temperature Requirements and Completeness of Bulk-Gas Reactions for HCCI Combustion, 2003. SAE Paper 2003-01-3173.

[65] Magnus Sjöberg and John E. Dec. Comparing late-cycle autoignition stability for single- and two-stage ignition fuels in HCCI engines. *Proceedings of the Combustion Institute*, 31(2):2895–2902, 2007.

[66] Gen Shibata and Tomonori Urushihara. Dual Phase High Temperature Heat Release Combustion, 2008. SAE Paper 2008-01-0007.

[67] J.-S. Chen, T.a Litzinger, and H.J Curran. The Lean Oxidation of Iso-Octane in the Intermediate Temperature Regime at Elevated Pressures. *Combustion Science and Technology*, 156(1):49–79, July 2000.

[68] W Hwang, J Dec, and M Sjöberg. Spectroscopic and chemical-kinetic analysis of the phases of HCCI autoignition and combustion for single- and two-stage ignition fuels. *Combustion and Flame*, 154(3):387–409, 2008.

[69] John E. Dec and Yi Yang. Boosted HCCI for High Power without Engine Knock and with Ultra-Low NO_X Emissions - using Conventional Gasoline, 2010. SAE Paper 2010-01-1086.

[70] Yi Yang, John Dec, and Nicolas Dronniou. Boosted HCCI Combustion Using Low-Octane Gasoline with Fully Premixed and Partially Stratified Charges, 2012. SAE Paper 2012-01-1120.

[71] Yi Yang, John Dec, Nicolas Dronniou, Magnus Sjöberg, and William Cannella. Partial Fuel Stratification to Control HCCI Heat Release Rates : Fuel Composition and Other Factors Affecting Pre-Ignition Reactions of Two-Stage Ignition Fuels, 2011. SAE Paper 2011-01-1359.

[72] Kevin Cedrone, Wai K Cheng, John Williams, and Brad Vanderwege. Fuel Effects on HCCI Operation in a Spark Assisted Direct Injection Gasoline Engine, 2011. SAE Paper 2011-01-1763.

[73] Adam J. Weall and James P. Szybist. The Effects of Fuel Characteristics on Stoichiometric Spark-Assisted HCCI. *Journal of Engineering for Gas Turbines and Power*, 134(7), 2012.

[74] Luke M. Hagen, Laura Manofsky Olesky, Stanislav V. Bohac, George Lavoie, and Dennis Assanis. Effects of a Low Octane Gasoline Blended Fuel on Negative Valve Overlap Enabled HCCI Load Limit , Combustion Phasing and Burn Duration. *Journal of Engineering for Gas Turbines and Power*, 135(7), 2013.

[75] Donald L. Stivender. Development of a Fuel-Based Mass Emission Measurement Procedure, 1971. SAE Paper 710604.

[76] William M. Silvis. The algorithmic structure of the air/fuel ratio calculation. *Readout: Horiba Technical Reports*, 15:17–24, September 1997.

[77] G. Woschni. A Universally Applicable Equation for the Instantaneous Heat Transfer Coefficient in the Internal Combustion Engine, 1967. SAE Paper 670931.

[78] Junseok Chang, Orgun Güralp, Zoran Filipi, Dennis Assanis, Tang-Wie Kuo, Paul Najt, and Rod Rask. New Heat Transfer Correlation for an HCCI Engine Derived from Measurments of Instantaneous Surface Heat Flux, 2004. SAE Paper 2004-01-2996.

[79] Elliott Ortiz-Sota. *Combustion Modeling of Spark Assisted Compression Ignition for Experimental Analysis and Engine System Simulations*. PhD thesis, University of Michigan, 2013.

[80] Russell P Fitzgerald, Richard Steeper, Jordan Snyder, Ronald Hanson, and Randy Hessel. Determination of Cycle Temperatures and Residual Gas Fraction for HCCI Negative Valve Overlap Operation, 2010. SAE Paper 2010-01-0343.

[81] Elliott A Ortiz-Soto, Jiri Vavra, and Aristotelis Babajimopoulos. Assessment of Residual Mass Estimation Methods for Cylinder Pressure Heat Release Analysis of HCCI Engines with Negative Valve Overlap. In *Proceedings of the ASME 2011 Internal Combustion Engine Division Fall Technical Conference, ICES2011-60167*, 2011.

[82] Jan-ola Olsson, Per Tunestå L, Jonas Ulfvik, and Bengt Johansson. The Effect of Cooled EGR on Emissions and Performance of a Turbocharged HCCI Engine, 2003. SAE Paper 2003-01-0743.

[83] Charles Fayette Taylor. *The Internal-Combustion Engine in Theory and Practice*. The M.I.T. Press, Cambridge, Massachusetts, revised edition, 1985.

[84] J.A. Eng. Characterization of Pressure Waves in HCCI Combustion, 2002. SAE Paper 2002-01-2859.

[85] Jiri Vavra, Stanislav V. Bohac, Laura Manofsky, George Lavoie, and Dennis Assanis. Knock in Various Combustion Modes in a Gasoline-Fueled Automotive Engine. In *Proceedings of the ASME 2012 Internal Combustion Engine Division Spring Technical Conference, ICES2011-60124*, Morgantown, WV USA, Oct 2 – 5 2011.

[86] Gen Shibata and Tomonori Urushihara. Realization of Dual Phase High Temperature Heat Release Combustion of Base Gasoline Blends from Oil Refineries and a Study of HCCI Combustion Processes, 2009. SAE Paper 2009-01-0298.

[87] Luke M. Hagen, Laura Manofsky-Olesky, Stanislav V. Bohac, George Lavoie, and Dennis N. Assanis. Effects of a Low Octane Gasoline Blended Fuel on NVO Enabled HCCI Load Limit, Combustion Phasing and Burn Duration. In *ASME 2012 Internal Combustion Engine Division Fall Technical Conference, ICEF2012-92155*, Vancouver, BC, Canada, 2012.

[88] George A. Lavoie, J. Martz, M. Wooldridge, and D. Assanis. A multi-mode combustion diagram for spark assisted compression ignition. *Combustion and Flame*, 157(6):1106–1110, 2010.

[89] Magnus Sjöberg and John E. Dec. An investigation into lowest acceptable combustion temperatures for hydrocarbon fuels in HCCI engines. *Proceedings of the Combustion Institute*, 30(2):2719–2726, 2005.

[90] Laura Manofsky-Olesky, Jiri Vavra, Aristotelis Babajimopoulos, and Dennis Assanis. Effects of Charge Preheating Methods on the Combustion Phasing Limitations of an HCCI Engine with Negative Valve Overlap. *ASME Journal of Engineering for Gas Turbines and Power*, 134, 2012.

[91] X He, M Donovan, B Zigler, T Palmer, S Walton, M Wooldridge, and A Atreya. An experimental and modeling study of iso-octane ignition delay times under homogeneous charge compression ignition conditions. *Combustion and Flame*, 142(3):266–275, 2005.

[92] Jason B Martz. *Simulation and model development for auto-ignition and reaction front propagation in low-temperature high-pressure lean-burn engines*. PhD thesis, University of Michigan, 2010.

[93] Magnus Sjöberg and John E Dec. EGR and Intake Boost for Managing HCCI Low-Temperature Heat Release over Wide Ranges of Engine Speed, 2007. SAE Paper 2007-01-0051.

[94] Aristotelis Babajimopoulos, George A. Lavoie, and Dennis N. Assanis. On the Role of Top Dead Center Conditions in the Combustion Phasing of Homogeneous Charge Compression Ignition Engines. *Combustion Science and Technology*, 179(9):2039–2063, 2007.

[95] C. Moon, Francis. *Chaotic and Fractal Dynamics*. John Wiley and Sons, New York, 1992.

[96] Steven H. Strogatz. *Nonlinear Dynamics and Chaos*. Addison - Wesley, Reading, MA, 1994.

[97] Robert M Wagner, K Dean Edwards, C Stuart Daw, Johnny B. Green Jr., and Bruce G Bunting. On the Nature of Cyclic Dispersion in Spark Assisted HCCI Combustion, 2006. SAE Paper 2006-01-0418.

[98] J. Kodavasal, M. J. McNenly, a. Babajimopoulos, S. M. Aceves, D. N. Assanis, M. a. Havstad, and D. L. Flowers. An accelerated multi-zone model for engine cycle simulation of homogeneous charge compression ignition combustion. *International Journal of Engine Research*, 14(5):416–433, June 2013.